1987

Adsorption of ferrous iron on synthesized [gamma]-FeOOH

Suingill Choi
Iowa State University

Order Number 9020181

Adsorption of ferrous iron on synthesized γ-FeOOH

Choi, Suingill, Ph.D.

Iowa State University, 1987

U·M·I
300 N. Zeeb Rd.
Ann Arbor, MI 48106

Adsorption of ferrous iron on synthesized γ-FeOOH

by

Suingill Choi

A Dissertation Submitted to the
Graduate Faculty in Partial Fulfillment of the
Requirements for the Degree of
DOCTOR OF PHILOSOPHY

Department: Civil and Construction Engineering
Major: Sanitary Engineering

Approved:

Members of the Committee:

Signature was redacted for privacy.

In Charge of Major Work

Signature was redacted for privacy.

For the Major Department

Signature was redacted for privacy.

For the Graduate College

Iowa State University
Ames, Iowa

1987

TABLE OF CONTENTS

LIST OF FIGURES

LIST OF TABLES

NOMENCLATURE AND ABBREVIATIONS

Nomenclature

(I)	ionic strength
K	equilibrium constant for the adsorption of ferrous iron in ferric iron surface, mol/mg
k_{Cl}	rate constant of homogeneous iron oxidation reflecting the effect of chloride ion in solution
k_{ClO4}	rate constant of homogeneous iron oxidation reflecting the effect of perchloric ion in solution
k_o	rate constant of homogeneous oxygenation, $M^{-3}s^{-1}$
k_s	overall kinetic constant of heterogeneous oxygenation, s^{-1}
$k_{s,o}$	real rate constant of heterogeneous oxygenation, $M^{-1}s^{-1}$
L	mean dimension normal to the diffracting plane, angstroms
$_{aq}M^{m+}$	metal ion in solution phase
$M(OH)_n^{m-n+}$	hydrolyzed metal ion in solution
q_a	amount of solute adsorbed on a unit surface area of the adsorbent, mg/m^2 or mol/m^2

q_e	amount of solute adsorbed per unit weight of adsorbent at the equilibrium, mg/g or mol/g
S	bare solid surface
SH	protonated solid surface
S_nM^{m-n}	solid surface with adsorbed metal ion
SM^{m+}	solid surface with adsorbed metal ion
$SM(OH)_n^{m-n}$	solid surface with adsorbed hydrolyzed metal ions
β	diffraction line broadening at half maximum intensity, radian
$[\beta]$	buffer intensity, eq./pH
λ	wavelength of the X-ray, nm
θ	diffracting angle with respect to the plane, degree

Abbreviations

cm	centimeter
^oC	degree Celsius
c.c.	cubic centimeter
eq.	one equilibrium
g	gram
hr	hour
l	liter
M	one mole per liter
m	meter

m^2 or sq.m	square meters
ml	milliliter
mol.	one mole
mg	milligram
nm	nanometer, 10^{-9} cm
s or sec	second

CHAPTER I. INTRODUCTION

Iron and Environmental Engineering

Iron, which is the fourth most abundant element in the earth's crust, has been a research subject in many fields, including mineralogy, corrosion science, metallurgy, chemistry, and environmental engineering.

Each field has its own interest in iron. In environmental engineering, iron is not classified as a hazardous substance, but rather as a nuisance in water. Iron is a common constituent in water derived from ground sources. The presence of dissolved iron in water imparts color and a bitter, astringent taste detectable by some people at levels above 1 or 2 mg/l. The deposition of precipitated iron causes staining of laundry and plumbing fixtures. Thus, the United States Environmental Protection Agency has established a secondary drinking water maximum contaminant level of 0.3 mg/l, in other words iron should be present in potable water at levels less than 0.3 mg/l.

Present Practice of Iron Removal

Iron, which is a element of the first transition series in the periodic table, can exist at II(ferrous) and III(ferric) oxidation states. Ferrous iron, whether it is in equilibrium with ferrous hydroxide or ferrous carbonate, is so soluble in water that its concentration can easily

exceed several mg/l and cause trouble in water supplies. However, the solubility of ferric iron is less than 10^{-7} mole/l in a water pH range between 5 and 12. This thermodynamic information leads to the conclusion that most dissolved iron in water is ferrous iron, and if ferrous iron is oxidized to ferric iron in the pH range of 5 and 12, it will be precipitated out of water.

As a result, the main concern in environmental engineering has been the oxidation rate of ferrous iron. After Just (1908) proposed qualitative oxidation kinetics for ferrous iron, many researchers determined the kinetic constants applicable for various water quality conditions and confirmed the homogeneous rate law, which stated that the oxidation rate of ferrous iron was proportional to the concentrations of both dissolved oxygen and dissolved iron, and to the square of the hydroxide ion concentration. In mathematical form, it is:

$$-d[Fe(II)]/dt = k_o[Fe(II)][OH^-]^2[O_2] \qquad (I-1)$$

where

k_o = rate constant of homogeneous oxidation

$[Fe(II)]$ = concentration of ferrous iron in solution

$[OH^-]$ = concentration of hydroxyl ions in solution

$[O_2]$ = concentration of oxygen in solution

Present practice in design of iron removal is based mainly on our thermodynamic and kinetic knowledge. Figure 1 shows

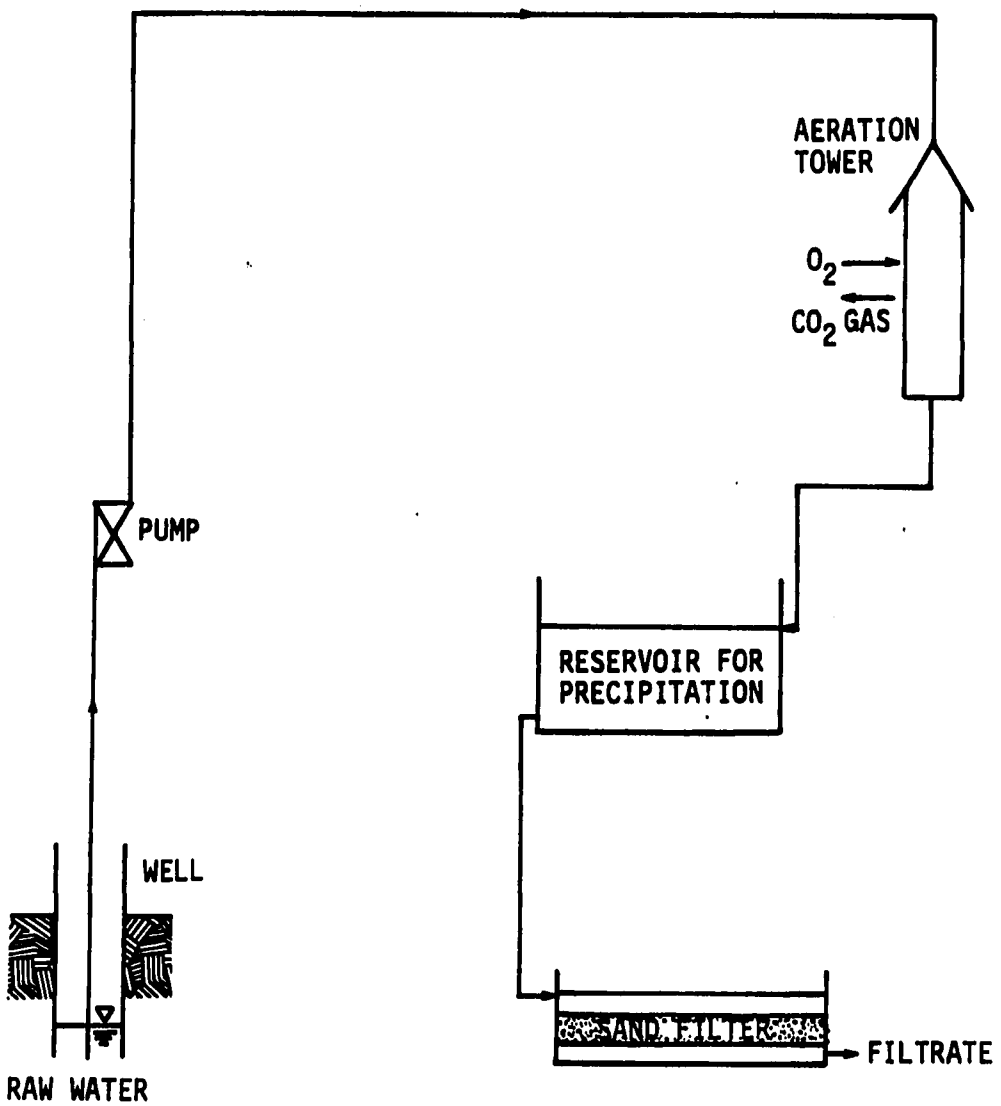

Figure 1. Present practice in municipal dissolved iron removal

the present practice of dissolved iron removal. Ground water is pumped up to an aeration tower where carbon dioxide gas is released from the water and oxygen dissolves into the water. The water leaving the aeration tower usually has sufficient dissolved oxygen to serve as an oxidizing agent for converting ferrous iron to ferric iron and a water pH high enough to provide rapid oxidation. The water then flows through a tank with 0.5 to 1 hour detention to provide enough time for the dissolved iron to precipitate. The water is then filtered by granular media filtration to remove the residual suspended iron particles.

Heterogeneous Oxidation Kinetics

While the main efforts in environmental engineering were directed at evaluation of homogeneous oxidation kinetics, several investigators suspected that a catalytic effect of ferric hydroxide on the oxidation of ferrous iron existed. Okura and Goto (1955) observed that the presence of ferric iron precipitate increased the oxidation rate of ferrous iron, whereas Stumm and Lee (1961) found no catalytic effect of ferric hydroxide precipitate up to concentrations of 10^{-4} M (5 mg/l as Fe). Takai (1973b) investigated the catalytic effect of iron oxides on oxidation of ferrous iron. He concluded that only lepidocrocite, which is one ferric iron precipitate, had a continuous catalytic effect.

Tamura et al. (1976b) also reported catalytic effects of ferric hydroxide at concentrations of 30 mg/l of ferric hydroxide. They assumed that the oxidation of ferrous iron in the presence of ferric hydroxide proceeded along two paths simultaneously. One was a homogeneous reaction taking place in the solution phase and the other was a heterogeneous reaction occurring on the surface of ferric hydroxide. They also presumed that the heterogeneous reaction was proportional to the amount of ferrous iron adsorbed on the surface of ferric hydroxide.

Based on their findings and assumptions, Tamura et al. (1976b) suggested a new kinetic equation which included the catalytic effect of ferric hydroxide:

$$\begin{aligned} -d[Fe(II)]/dt &= (-d[Fe(II)]/dt)_{homo} + \\ &\quad (-d[Fe(II)]/dt)_{hetero} \\ &= k_o[O_2][OH^-]^2[Fe(II)] + \\ &\quad k_s[Fe(II)_{ad}] \end{aligned} \qquad \text{(I-2)}$$

where

k_s = kinetic constant for heterogeneous oxidation.

The constant k_s turned out to be proportional to the concentration of dissolved oxygen and was expressed as $k_s=k_{s,o}[O_2]$. Tamura et al. also investigated the adsorption of ferrous iron on a ferric hydroxide surface. They found that the amount of ferrous iron adsorbed was proportional to the amount of ferric hydroxide and the

concentration of ferrous iron at equilibrium with the ferric hydroxide surface and inversely proportional to the concentration of hydrogen ions. The finding was formulated as follows:

$$[Fe(II)ad]/[Fe(II)]=K[Fe(III)]/[H^+] \quad (I-3)$$

where the authors (Tamura et al., 1976b) expressed the units in these terms:

[Fe(II)ad] = amount of ferrous iron adsorbed on the Fe(III) surface, mg/l.

K = equilibrium constant for the adsorption of Fe(II) on Fe(III) hydroxide, $10^{-9.6}$ mol/mg Fe(III).

[Fe(II)] = concentration of ferrous iron in the bulk liquid phase at equilibrium with the ferric hydroxide surface, mg/l.

[Fe(III)] = concentration of ferric hydroxide, mg/l.

$[H^+]$ = concentration of hydrogen ion, mol/l.

By replacing the terms $[Fe(II)_{ad}]$ and k_s in equation (I-2) with equation (I-3) and $k_{s,o}[O_2]$, the follow equation results:

$$-d[Fe(II)]/dt=k_o[O_2][OH^-]^2[Fe(II)] + k_{s,o}[O2]\{K[Fe(III)]/[H+]\}[Fe(II)] \quad (I-4)$$

where

k_o = real rate constant for homogeneous oxidation, 2.3×10^{14} $M^{-3}s^{-1}$ at 25 °C

$k_{s,o}$ = real rate constant for heterogeneous oxidation, 73 $M^{-1}s^{-1}$

At a constant pH and dissolved oxygen concentration, equation (I-4) was simplified:

$$-d[Fe(II)]/dt = (k + k'[Fe(III)])[Fe(II)]$$

where

k = rate constant for the homogeneous reaction and is equal to $k_o[O_2][OH^-]^2$

k' = rate constant for the heterogeneous reaction and is equal to $k_{s,o}[O_2]K/[H^+]$

After Tamura et al. (1976b), Sung and Morgan (1980) investigated autocatalytic oxidation of ferrous iron in solution and validated Tamura et al.'s heterogeneous kinetic equation. Davison and Seed (1983) also found that addition of ferric iron at concentrations of 10 mg/l or less had no effect on the rate of the reaction at pH 7. Addition of 50 mg/l of ferric iron, however, did produce a significantly higher rate by a factor of 2-5 at pH 7.13 through 7.18.

Based on these studies, it is believed that certain specific or several kinds of ferric compounds may have a catalytic effect on the oxidation of ferrous iron in the liquid phase. The reason Stumm and Lee (1961) did not find the catalytic effect of ferric iron could be that the 5 mg/l of ferric iron was too low to measure any catalytic effect.

Ferric Hydroxide and Lepidocrocite

The vague term "ferric hydroxide" has been widely used to describe the hydrated iron precipitate at the (III) oxidation state in water. There is a question, however,

whether or not ferric hydroxide is an existing compound. It has been accepted recently that ferric hydroxide is a general term for iron precipitates rather than the name of a precisely identified compound. There are varieties of ferric compounds registered in mineralogy depending on their associated bound minerals. From the view point of structure, however, they can be classified into several compounds such as ferrihydrate, ferric oxyhydroxides (FeOOH), and ferric oxides (Fe_2O_3). Each of them in turn exists at various degrees of crystalinity. Their names, formation, and interrelationship will be presented in the literature review chapter.

Lepidocrocite, which is gamma ferric oxyhydroxide (γ-FeOOH) among the four reported ferric oxyhydroxides (α-, β-, γ-, δ-FeOOH), has been cited in several reports which were concerned with iron oxidation. Lepidocrocite was claimed by Takai (1973b) to retain its catalytic effect in repeated tests. According to him, goethite (α-FeOOH) was exhausted soon and did not show a continuous catalytic effect. Sung and Morgan (1980) confirmed the heterogeneous kinetic equation and identified the product of iron oxidation formed in the laboratory as lepidocrocite. Robinson et al. (1981) implied that the precipitates of iron from well water were amorphous lepidocrocite due to the presence of silica in the water.

From these findings, the following hypothesis can be postulated: Even though lepidocrocite would not be the only iron precipitate encountered in water treatment, it is, at least, one of the major precipitates. Moreover, it has a continuous catalytic effect on oxidizing ferrous iron in water coming in contact with the precipitate.

Need for Research

The catalytic oxidation of ferrous iron has the potential for a great impact on the present practice of iron removal. By understanding more about the factors affecting catalytic oxidation, it would be possible to utilize already precipitated ferric iron to remove dissolved iron from water.

The equation from Tamura et al. (1976b) is the only kinetic equation involving the catalytic effect of ferric iron developed up to this time. In analyzing the heterogeneous kinetic term, it is noticed that the adsorption of ferrous iron on the ferric iron surface is the main factor in determining the rate of oxidation.

Tamura et al.'s investigation of the adsorption capacity of ferric iron for ferrous iron, however, had an unclear aspect. In his adsorption experiments, Tamura et al. produced ferric hydroxide in solution by hydrolyzing Fe(III) perchlorate at pH 7.0 for 30 minutes. It was not clear whether this Fe(III) perchlorate was a commercially

available reagent or a ferric iron stored after oxygenating ferrous iron in their laboratory prior to the adsorption experiment. If the Fe(III) perchlorate used by Tamura et al. was an oxidation product prepared in their laboratory, it might have been lepidocrocite, because Sung and Morgan (1980) conducted experiments in environments similar to Tamura et al.'s and identified the oxidation product as lepidocrocite. If the Fe(III) perchlorate used was a commercially available reagent, Tamura et al. determined that the adsorption capacity of the ferric perchlorate and used that result as if it applied to a different ferric compound formed by oxidation of ferrous iron in water. This is not an acceptable use of data. Although the adsorption term did not reflect correct adsorption capability, the heterogeneous kinetic term in the equation (I-4) could be valid within their experimental range due to another kinetic constant, $k_{s,o}$, which was determined by curve fitting to make the equation fit the experimental observations. That could be a reason why Sung and Morgan (1980) agreed to Tamura et al.'s heterogeneous kinetic equation when they examined the equation without investigating the actual adsorption capability of lepidocrocite.

In the kinetic equation, Tamura et al. related the adsorption capacity per unit weight of ferric iron while

adsorption capacity depends heavily on the surface area of adsorbent. Although it is not unusual to present the adsorption capacity of a material on a per unit weight basis in engineering practice, this is based on a basic agreement that the adsorbent uniformly has almost the same surface area per unit weight of the material. If this is not the case, the adsorption capacity of the material should be measured for the specific batch of adsorbent before use. Unfortunately, while lepidocrocite is the hypothesized catalyst in ferrous iron oxidation, reported surface area measurements of lepidocrocite has varied from 66 m^2/g (Kaneko and Inouye, 1979) to 171 m^2/g (Sung, 1981).

From all the facts discussed in this chapter, it is clear that heterogeneous oxidation has the potential to change the present practice used for removal of dissolved iron from water and that the most important factor in the heterogeneous oxidation is the adsorption capacity of the ferric iron for the ferrous iron in the water. Moreover, lepidocrocite is the most probable catalyst active in a heterogeneous oxidation process. However, the adsorption capability of lepidocrocite for ferrous iron has not been investigated intensively. Although Tamura et al.'s ferric iron could be lepidocrocite, there remains the definite possibility that lepidocrocite will have various adsorption capacities and these will be a factor of its surface area

or crystal size. An investigation to determine the adsorption capacities of lepidocrocites of different surface areas (crystal sizes) at various pH values must, therefore, be a very first step to enhance our knowledge of heterogeneous oxidation of ferrous iron in water.

CHAPTER II. PURPOSE AND OBJECTIVES

In environmental engineering, most of the research on dissolved iron removal has been directed at and limited to studies of iron oxidation kinetics. However, heterogeneous oxidation, where the oxidation product catalyzes the oxidation rate, justifies investigation of the characteristics of iron precipitates in water as well as kinetics.

This study was designed to investigate the adsorption capacity of lepidocrocite and to observe differences in lepidocrocites in terms of morphology, surface area, and relative crystal sizes. Lepidocrocite was chosen because it was suspected to be one of the major iron precipitates from water containing dissolved iron and was hypothesized to be the catalyst for the heterogeneous oxidation of ferrous iron in water.

One extra question on the role of lepidocrocite in heterogeneous oxidation was whether lepidocrocite acted as a seed material or as a catalyst. If lepidocrocite is a catalyst, it may be involved in the reaction process but will be dissociated from the product to remain without change itself. If it is a seed material for reaction, its crystallites may grow in size and/or the morphology may be changed. The answer to that question was also sought in this study.

The specific objectives of this study were:

1. To explore the possibility of removing dissolved iron from typical mid-western water by a heterogeneous oxidation mechanism.
2. To synthesize lepidocrocites with distinctive surface areas per unit weight.
3. To observe the morphology of lepidocrocites synthesized through different methods.
4. To investigate the differences in adsorption capacities of distinctive lepidocrocites.
5. To obtain an adsorption isotherm reflecting the effects of pH and concentration of ferrous iron at equilibrium.
6. To investigate the change in morphology of lepidocrocite after oxidation of ferrous iron in the presence of the lepidocrocite.

CHAPTER III. REVIEW OF LITERATURE

Formation of Ferric Oxides and Ferric Oxyhydroxides

Ferric oxides and ferric oxide hydrates in nature

In nature, ferric oxides exist in two forms (Dana, 1900): the rhombohedral α-Fe_2O_3 (hematite) and the cubic, ferromagnetic γ-Fe_2O_3 (magnetic hematite, or maghemite, or oxymagnite). Dana also noted several distinctive ferric oxide hydrates. They were goethite ($Fe_2O_3 \cdot H_2O$), turgite ($2Fe_2O_3 \cdot H_2O$), limonite($2Fe_2O_3 \cdot 3H_2O$), and xanthosiderite ($Fe_2O_3 \cdot 2H_2O$). However, X-ray diffraction work by Posnjak and Merwin (1919) showed that there is only one definite hydrate of ferric oxide, the monohydrate, $Fe_2O_3 \cdot H_2O$ or FeOOH(ferric oxyhydroxide, or ferric oxide hydroxide, or ferric oxide hydrate). Turgite was a microcrystalline hematite with adsorbed water. The limonite and xanthosiderite were goethite with adsorbed water and other impurities.

The first recognition of lepidocrocite as a distinctive mineral resulted from intensive X-ray work by Posnjak and Merwin (1919). Before Posnjak and Merwin, goethite and lepidocrocite were considered as the same monohydrate of ferric oxide. Four structurally different monohydrates were reported in all. They are orthorhombic α-FeOOH, tetragonal β-FeOOH, orthorhombic γ-FeOOH, and

hexagonal δ-FeOOH. Other iron oxides reported were FeO (wüstite) whose oxidation state is (II), and Fe_3O_4 (magnetite) which has a intermediate oxidation state between (II) and (III).

Formation of ferric oxides and ferric oxyhydroxides

The formation and transformation of the iron oxide/oxide hydrates system was first summarized by Bernal et al. (1959). They reported the existence of green rust II and formations of Wüstite (FeO) from siderite ($FeCO_3$) and ferrous hydroxide ($Fe(OH)_2$). The chart of formation and transformation is shown as Figure 2.

More recently, Misawa et al. (1974) presented a systematic formation diagram of iron oxide hydrates, which agreed with Bernal et al. but showed a bit more detailed pathway in formation of oxide hydrates. Misawa et al. also introduced concept of the green complex I and II which are formed by aerial oxidation of ferrous iron in neutral and slightly alkaline solution and, upon precipitation, turn to green rust I and II, respectively. The formation processes indicate that the end products are strongly affected by the oxidation rate, solution pH, and the structure and composition of the initial and intermediate species of iron. The diagram has been reproduced as Figure 3. Very rapid iron oxidation by addition of H_2O_2 to an alkaline solution in which Fe^{++} has been precipitated as $Fe(OH)_2$

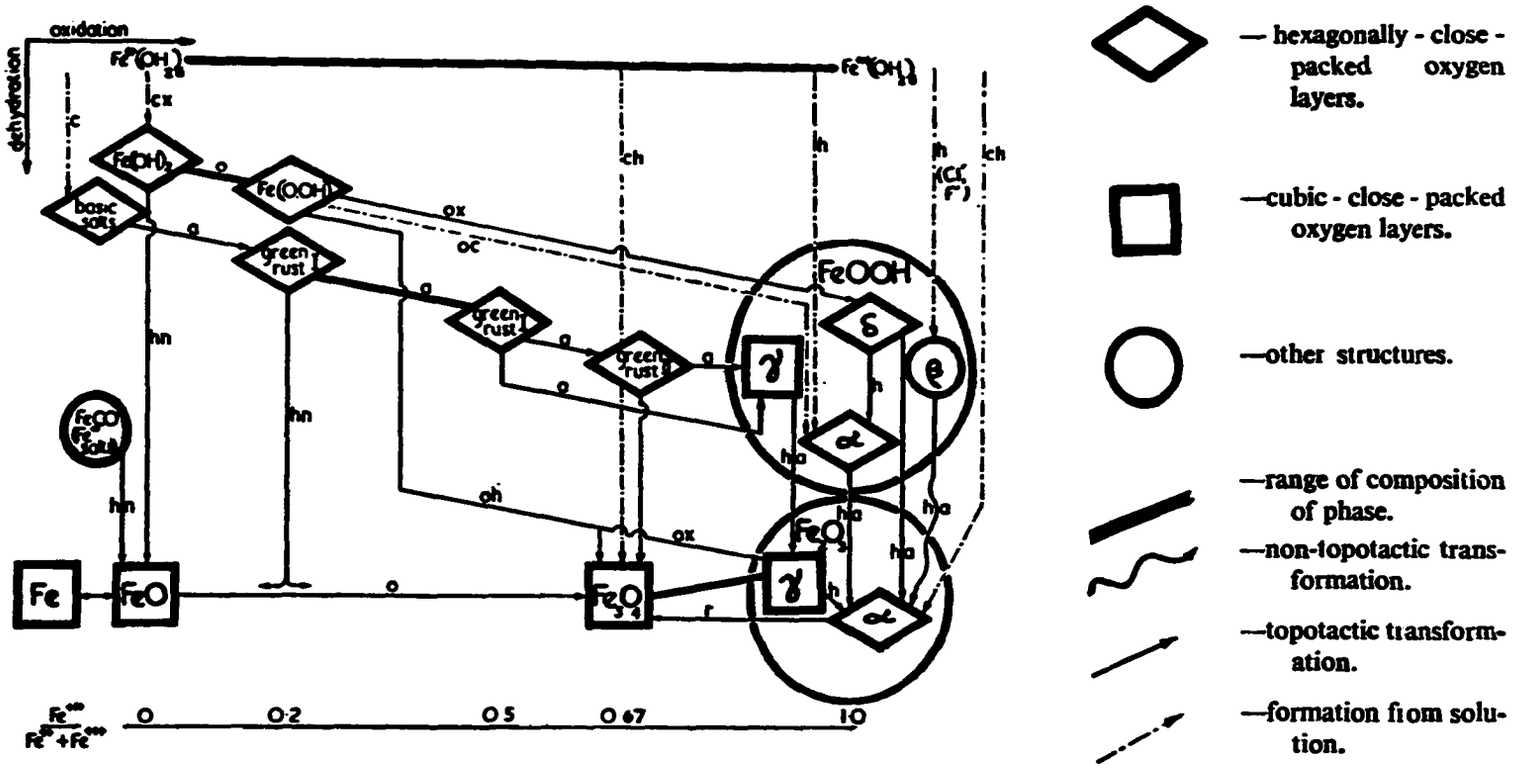

KEY: a= on exposure to air; c= in alkali; h= on heating; o= on oxidation; n= in nitrogen or in vacuo; r= on reduction; x= in excess

Figure 2. Formations and structural interrelations in iron oxide/oxide hydroxide system. After Bernal et al. (1959)

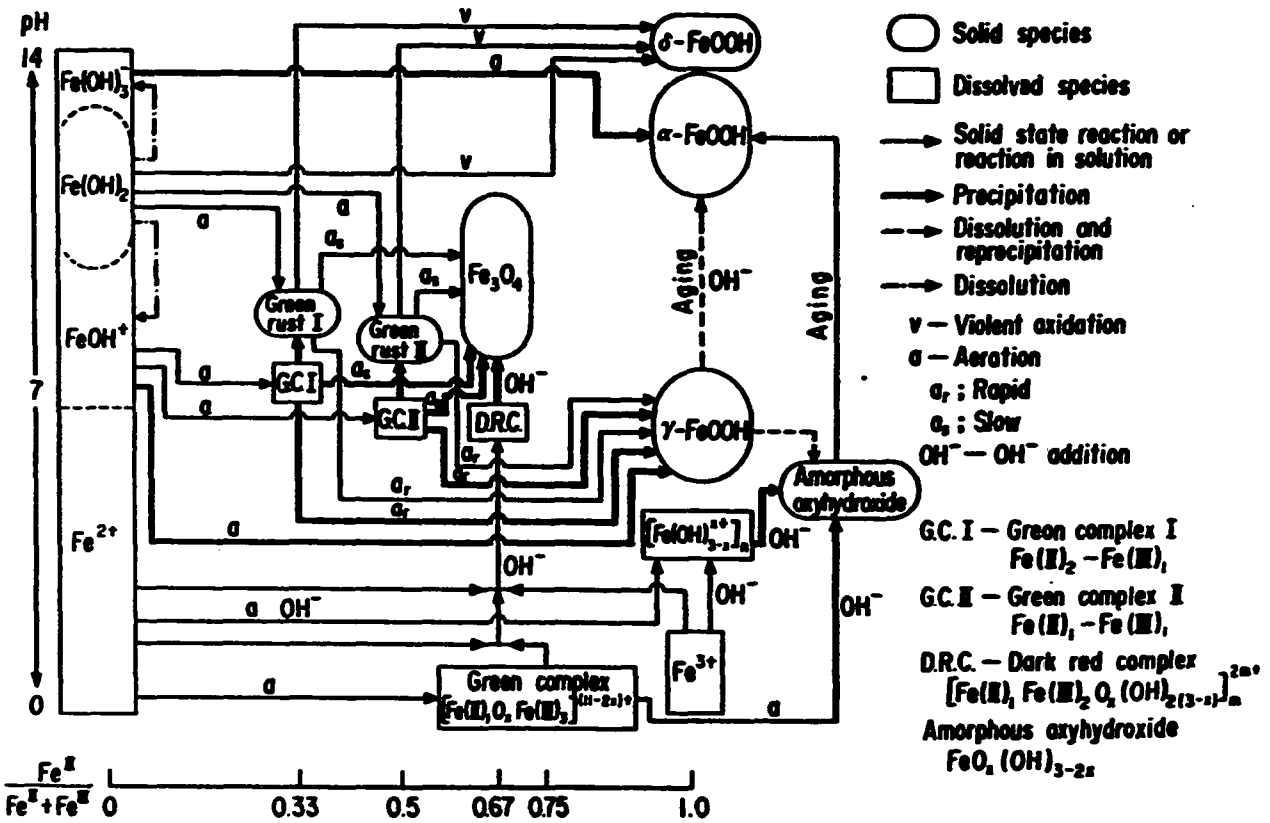

Figure 3. Schematic diagram of formation processes of intermediates, oxyhydroxides, and oxides of iron in aqueous solution at room temperature. Lines drawn parallel to the ordinate do not mean the necessity of pH change unless OH- addition is stated. After Misawa et al. (1974)

leads to the solid state transformation of $Fe(OH)_2$ to δ-FeOOH.

In strongly alkaline solutions, α-FeOOH is precipitated by aerial oxidation of $Fe(OH)_3^-$, which is dissolved from $Fe(OH)_2$.

In slightly alkaline solutions containing $Fe(OH)_2$ precipitates, intermediate green rust I and II are formed by solid state reaction during slow oxidation of $Fe(OH)_2$. Green rusts also precipitate from green complex I or II in neutral solutions and convert into Fe_3O_4 by slow oxidation and into γ-FeOOH by rapid oxidation. Coexisting anions in solutions, such as Cl^- and SO_4^{-2}, influence the formation of green complexes and rusts.

In slightly acidic solutions the formation of polynuclear species bound with oxo-bridges (-O-) reduces the positive charge of ferric polycation and results in precipitation of γ-FeOOH.

In acidic solutions, polynuclear species bound with hydrogen bonds and ol-bridges (-OH-) are formed by hydrolysis and polymerization during long period of oxidation and result in formation of the precipitate of amorphous ferric oxide hydrate which transforms to goethite by aging.

The effect of aging

Mackenzie and Meldau (1959) investigated the effect of aging on a freshly precipitated ferric iron gel. The gel had been prepared by adding ammonium hydroxide rapidly to a ferric chloride solution. Upon analysis, that gel turned out to be amorphous material and crystalline goethite. They observed that aging caused the primary particles to come together to form needles which, in early stages, consisted of primary particles cemented together in a row rather than true crystals. It was claimed that further aging at pH 10 resulted in formation of true acicular crystals. But how cemented primary particles become true crystals was not explained.

Formation of Lepidocrocite

Formation of lepidocrocite

Misawa et al. (1974) reported that the formation of lepidocrocite (γ-FeOOH) in aqueous solution was restricted to the cases of either the rapid aerial oxidation of ferrous ion or the Fe(II)-Fe(III) green intermediates in neutral and slightly acidic solutions. The three pathways claimed by Misawa et al. were the formation of γ-FeOOH by solid state transformation of green rusts by rapid aerial oxidation, precipitation of γ-FeOOH by rapid aerial oxidation of green complexes, and precipitation of γ-FeOOH by aerial oxidation of ferrous solution.

The observation of the formation of γ-FeOOH in slightly acidic solution by Misawa et al. agreed with Baudisch and Albrecht (1932) who were able to synthesize γ-FeOOH only in weakly acidic solution and Schwertmann and Thalmann (1976) who found that the best crystaline lepidocrocite was produced at pH 6.

Intermediate green rust

Green rust I was reported by Feitknecht and Keller (1950). Excessive ammonium hydroxide was added to a ferrous chloride solution buffered with ammonium chloride. Aerial oxidation of the mixture produced dark blue green rusts which had several different degrees of oxidation and proportions of chloride. The weight ratio of ferric iron to ferrous iron varied from 0.215 to 0.793.

Later, Bernal et al. (1959) reported on the formation of green rust II. The oxidation of a ferrous sulphate solution gave substantially the same result as that with the chloride solution. However, the oxidation of green rust I formed from a ferrous sulphate solution routed to another intermediate compound which showed a different structure instead of yielding lepidocrocite directly.

Bernal et al. (1959) realized that the green rust transforms topotactically by either dehydration and further oxidation to magnetite or by complete oxidation to lepidocrocite.

Effect of chloride on lepidocrocite formation

Taylor (1984) observed that the effect of chloride was significant in the crystallinity of lepidocrocite. As the initial [Cl]/[Fe] ratio was increased from 2, crystallinity increased in all axial directions, sharpening the width at half height of diffraction peaks. At [Cl]/[Fe] ratios greater than 8, the crystallinity did not increase further. Instead, it appeared to decrease in the a-axis direction. But the effect of [Cl] was modified when oxidation was not limited by the O_2 in solution.

Transformation of lepidocrocite to goethite

Lepidocrocite eventually transforms to the more stable goethite. The process has been studied by Schwertmann and Taylor (1972). The transformation was not topochemical but proceeded through the solution phase. The reaction starts with the dissolution of lepidocrocite under the influence of a high [OH^-] concentration.

$$FeOOH + OH^- + H_2O \text{ -----> } Fe(OH)_4^- \qquad \text{(III-1)}$$

This dissolution starts from crystal defects and highly exposed parts of the crystals. They postulated the reaction steps as:

1. penetration of OH^- into the outer layer of the crystal lattice.
2. diffusion of dissolved iron across the phase boundary.

3. formation of goethite nuclei from dissolved Fe(II).
4. Deposition of dissolved Fe on goethite nuclei and crystals.

The rate of transformation would be governed by the slowest step among them. Any of these processes might be rate determining under appropriate conditions. The conversion rate was also temperature dependent. In a 1 M KOH solution, the half conversion time took from 5 to 11 hours at 80 ^{o}C to 120 hours at 40 ^{o}C and to approximately 2000 hours at 20 ^{o}C. In the 0.12 M KOH solution, the a half conversion time took about 4 to 5 times more than that in a 1 M KOH solution.

Synthesis of Lepidocrocite

According to the Figure 2 and the Figure 3, lepidocrocite should be produced by rapid aerial oxidation of ferrous iron solution in weakly acidic regions. Actually, Schwertmann and Thalmann (1976), Sung and Morgan (1980), and Taylor (1984) were successful in producing lepidocrocite without using any complexing reagents. However, it is also true that the oxidation of more than 100 mg/l of concentrated ferrous iron solution usually ends up with an amorphous precipitate. More reliable methods for mass production of lepidocrocite were reported by several researchers.

Baudisch and Albrecht (1932) examined various methods

for synthesizing ferric oxide hydrates, especially gamma ferric oxide hydrate. They found that nitrogen containing, complex forming compounds are very helpful in synthesizing gamma ferric oxide hydrate, above all pyridine. One hundred cm^3 of the concentrated ferrous chloride solution were diluted with 100 cm^3 of water and 20 cm^3 of the purest pyridine was added. Addition of pyridine raised the pH of the mixture to about 6-6.4 and a green precipitate formed which, however, dissolved upon shaking. On passing air or oxygen through the mixture, the orange-red precipitate of gamma ferric oxide hydrate was formed. The pH remained practically constant after the oxidation. If an excess of pyridine was added to the solution, the solution solidified to a gray-green mass.

Another method was reported by Baudisch and Albrecht (1932) in which 20 cc. of 10 % sodium azide was poured into a mixture of 50 cc. of ferrous chloride solution (pH 5) and 50 cc. of water. The resulting red solution had a pH of 8.9. After oxidation with oxygen at water-bath temperature, the colorless solution had a pH of 2.4. The reddish-yellow precipitate was easily filtered, and washed, and then identified as gamma ferric oxide hydrate.

It has been noted that the formation of gamma ferric oxide hydrate was dependent on the hydrogen ion concentration. Gamma ferric oxide hydrate has only been

found in weakly acidic solutions (pH 6.5 to 2). Moreover, the nature of the anions in the salt solution appeared to be important for formation of gamma ferric oxide hydrate. It was impossible for Baudisch and Albrecht (1932) to obtain gamma ferric oxide hydrate from ferrous sulfate or ferrous fluoride solutions.

Contrarywise, Kaneko et al. (1975) have synthesized lepidocrocite from a ferrous sulfate solution. After 3.6 g of $FeSO_4 \cdot 7H_2O$ was dissolved in 600 ml of oxygen free water, the pH of the solution was adjusted to 4.3 -6.5 with 10 % NH_4OH. A lepidocrocite suspension was obtained by aerating with air for 3 hours. The suspension was aged for 5 days at 30 ^oC and pH 4.5. The crystals were filtered, washed with 2.5 liters of distilled water and dried at 60 ^oC for 9 hrs.

Kaneko and Inouye (1974) reported another way of obtaining lepidocrocite. Five hundred ml of 0.2 M $FeCl_2$ were mixed with 100 ml of 2 M hexamethylene tetramine, 13.5 ml of concentrated HCl, and 100 ml of 1 M sodium nitrite. Lepidocrocite was obtained by warming the mixture at 60 ^oC for 50 min. in a stream of nitrogen. The precipitates obtained were washed with water until no Cl^- was detected and dried at 60 ^oC for about 10 hours.

Structure of Lepidocrocite

Structure of lepidocrocite

Ewing (1935) studied the unit structure, space group symmetry, and detailed atomic arrangement of lepidocrocite (γ-FeOOH) using X-ray data. Ewing's analysis results could be described as:

1. The elements of the structure are iron centered oxygen octahedra. This octahedra layer forms by sharing edges and corners in such a way that the oxygen ions near the middle of the layers are common to four octahedra and correspond to O^{-2}, while the oxygen ions on the outer ridges of the layers are common to two octahedra and correspond to OH^{-}. The layers are parallel to the (010) plane and joined to each other by hydrogen bonds.
2. The dimensions of the orthorhombic unit cell are calculated as a_o=3.87, b_o=12.51, and c_o=3.06 angstroms. The a_o and c_o are contained in the plane of the layer and correspond to a body diagonal and an edge of an octahedron. The b_o axis is perpendicular to the layers. Its value of 12.51 angstroms is possibly explained if it represents two layer intervals. The most apparent way to satisfy this periodicity is to translate every other layer by c/2.

The prospective structure of lepidocrocite has been

reproduced as Figure 4.

Ewing postulated the location of the hydrogen ion at the center of the hydrogen bond. Christensen and Christensen (1978) reinvestigated the crystal structure of lepidocrocite using neutron powder diffraction methods, which revealed that the hydrogen ion which links the layers of lepidocrocite was not located at the center of the hydrogen bond. Figure 5 shows the locations of hydrogen ions in the structure of lepidocrocite. The distance between the two outer oxygen ions was 2.68 angstroms and divided by 0.93 and 1.75 angstroms by the hydrogen ion.

Orientation of axis and predominant plane of lepidocrocite

Oosterhout (1960) has used selected area electron diffraction to study the orientation of the needle axis of synthetic acicular crystals of goethite and lepidocrocite with respect to the unit cell. The needle axis of both goethite and lepidocrocite was the c axis (001).

Kaneko et al. (1975) postulated that the predominant plane of lepidocrocite (γ-FeOOH) is the (010) plane and has only one kind of hydroxyl ion.

Surface Area

Surface area by titration

Sears (1956) correlated the titration volumes of base with the surface areas of silica measured by the BET method

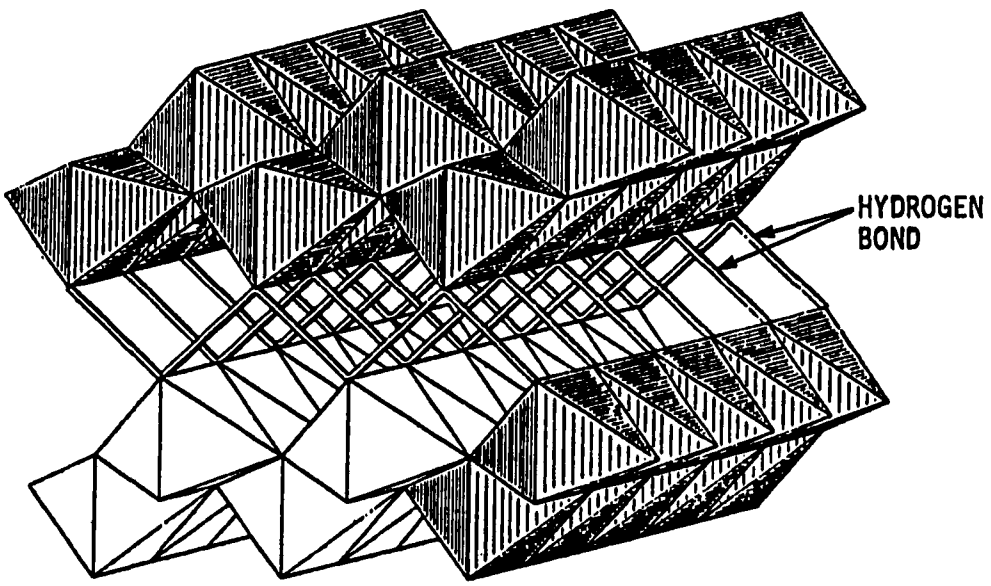

Figure 4. A portion of lepidocrocite layers. The iron-centered oxygen octahedra joined to form layers, and the layers are tied together with hydrogen bonds drawn as tubes. After Ewing (1935)

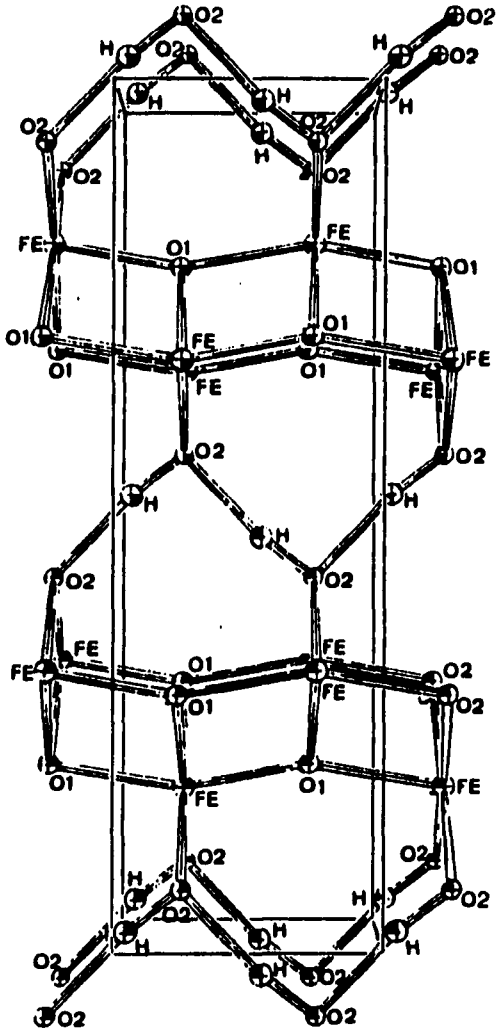

KEY: H = Hydrogen ion; Fe = Ferric iron;
01 = Oxygen ion common to four octahedra and correspond to O^{-2}
02 = Oxygen ion common to two octahedra and correspondto OH^{-}

Figure 5. Projection of the structure of lepidocrocite along the 100-direction. Hydrogen ions are not located at the center of the hydrogen bond. After Christensen and Christensen (1978)

and proposed a method for determining the surface area of various silica samples.

When Kozawa (1959) compared the ion exchange capacity of various manganese dioxides to the surface area of those samples measured by the BET method, he found a fairly good proportionality between them. In similar works, Kozawa (1961) proposed an alternative method for determining the surface area of silica where zinc adsorption and subsequent H^+ release was correlated to the surface area by the BET method. However, this method of measuring surface area is very specific to the system used to correlate the titration to the surface area. The number of hydrogen ions released per metal ion adsorbed depends on the pH of solution, adsorbates, pretreatment of adsorbent, and the coexisting salts (Kozawa, 1961, Gadde and Laitinen, 1974, James et al., 1975). This system specific nature of the method makes it difficult to use as a handy substitute for the BET method.

Area by particle size distribution

Sung (1981) calculated the surface area of lepidocrocite from its particle size distribution. The resulting cumulative specific area was 3.3 m^2/g, whereas the surface area determined by BET was 171 m^2/g. Based on this, he supposed that the lepidocrocite particles in suspension were strongly held aggregates or very porous, or

both.

Surface area of lepidocrocite by BET

Surface areas of lepidocrocites synthesized in many different manners have been measured by the BET method using N_2 gas at liquid nitrogen temperature. Kaneko and Inouye (1974) synthesized lepidocrocite and reported the surface area as 124 m^2/g whereas the lepidocrocite synthesized later using the same method had a surface area of 66 m^2/g (Kaneko and Inouye, 1979). Kaneko et al. (1975) used another method of lepidocrocite synthesis and found the surface area to be 100 m^2/g. Their method of lepidocrocite synthesis is described in the Synthesis of lepidocrocite section of this dissertation. Sung (1981) also measured the surface area of lepidocrocite oxidized by air from ferrous iron solution without adding any complexing or oxidizing agents and found the average surface area to be 171 m^2/g.

Surface charge density

Potentiometric titrations have been applied to studies of the surface charge of ferric oxide in aqueous suspensions. Kaneko et al. (1975) reported the site density of charge of lepidocrocite as 8.4 OH^- groups/nm^2 and Sung (1981) found it to be 9.2 OH^- groups/nm^2 in one titration and 8.1 OH^- groups/nm^2 in second titration.

Adsorption of Metal Ions on the Metal Oxide Surface

Adsorption of metal ions on the metal oxide hydrate surface has not been studied as intensively as adsorption of metal ions on the metal oxides surface. However, it is possible that both surfaces react similarly. Therefore, the adsorption of metal ions on metal oxide surface was reviewed.

Origin of charge at oxide surfaces

Many investigators (Zsigmondy and Spear, 1917, O'Connor and Buchanan, 1953, O'Connor et al., 1956, and Gaudin and Fuerstenau, 1955) have supposed that the mechanism of surface charge establishment may be a two step process: surface hydration followed by dissociation of the surface hydroxide. The hydration step may be understood as a tendency of the exposed surface atoms of completing their coordination shell. Exposed cations accomplish this by pulling an OH^- ion or water molecules and the oxygen ions by pulling a proton from the aqueous phase. The net result is that the surface now is covered by a hydroxyl layer with the cations buried below the surface. The surface whose coordination has been completed by hydration is then considered as an uncharged surface. The next, charge establishing process may be viewed as an adsorption of protons resulting in a positively charged surface or

dissociation of H^+ from the surface hydroxides leaving a negatively charged surface. Adsorption of protons at the oxide surface has been observed by Onoda and De Bruyn (1966). Adsorption of OH^- on the uncharged surface which is an imaginable way of being a negatively charged surface is not likely to occur because the additional OH^- would increase the coordination number of Fe(III) to seven. The preference between proton adsorption and dissociation of surface hydroxide is highly dependent on the pH environment.

Three models of metal ion adsorption

There could exist variety of models which would explain the uptake of hydrolyzable metal ions at solid/aqueous solution interface. Recently, three of the most conceivable models were figured out by MacNaughton and James (1974). These include the ion exchange reaction, the adsorption and hydrolysis at the surface reaction, and hydrolysis followed by an adsorption reaction. However, it also has been pointed out that the two latter models are thermodynamically undistinguishable. Furthermore, the ion exchange and the adsorption with hydrolysis models are indistinguishable unless there is some additional evidence which concerns the type of bonding at the surface other than the metal ion concentration in solution phase, pH, or the adsorption density. These similarities let James et

al. (1975) draw the conclusion that even though the models have somewhat different physical representations, their quantitative forms are quite similar. Figure 6 is the schematic diagrams of three adsorption models.

Ion exchange model The "ion exchange model" often considers the reaction of the free metal ions with surface hydroxyl groups to form a coordinate metal-oxygen bond with release of protons and/or H_2O. The simplest model assumed for ion exchange is;

$$nSH + {}_{aq}M^{m+} \quad <---------> \quad S_nM^{m-n+} + nH^+ \qquad \text{(III-2)}$$

where

n,m = stoichiometric constant
(n is not necessarily equal to m)

SH = protonated solid surface

${}_{aq}M^{m+}$ = metal ion in solution phase

S_nM^{m-n+} = solid surface with adsorbed metal ion

The number of protons released per M^{m+} may vary with pH, i.e., the stoichiometry of the reaction may change and hence the average number of protons released will be a function of pH.

Surface hydrolysis model This model reflects an adsorption of metal ions followed by a surface hydrolysis scheme.

$$S + {}_{aq}M^{m+} \quad <---------> \quad SM^{m+} \qquad \text{(III-3)}$$

$$SM^{m+} + nH_2O \quad <--------> \quad SM(OH)_n{}^{m-n+} + nH^+ \qquad \text{(III-4)}$$

where

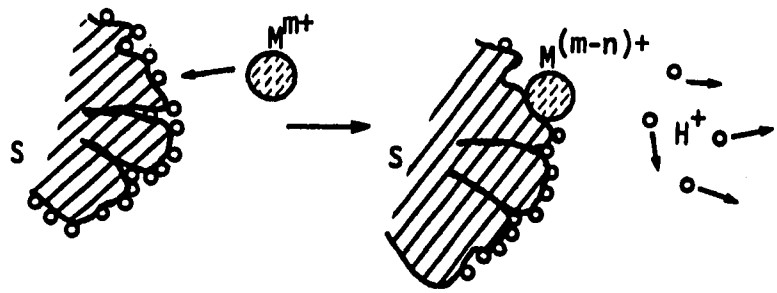

(a) Ion Exchange Model

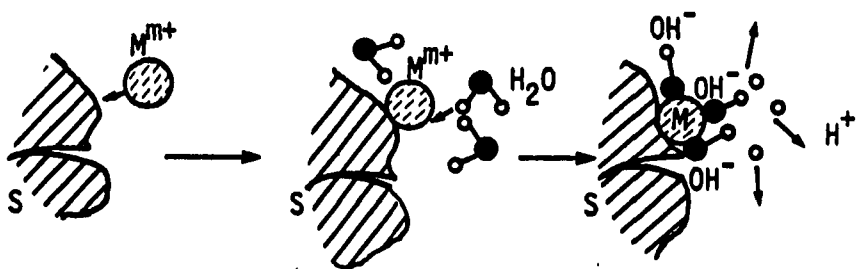

(b) Surface Hydrolysis

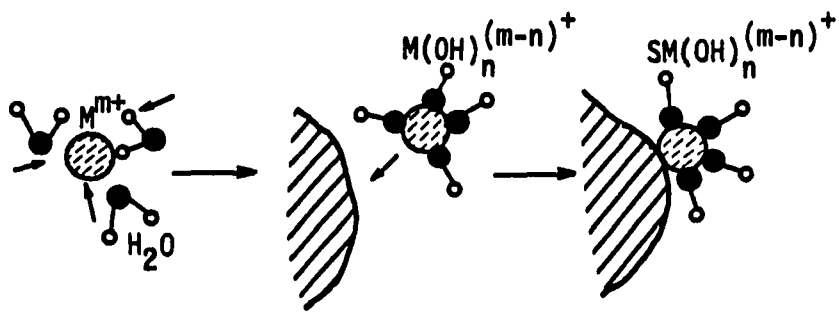

(c) Hydrolyzed Metal Ion Adsorption Model

Figure 6. Schematic diagrams of three adsorption models

SM^{m+} = solid surface with adsorbed metal ions

$SM(OH)_n^{m-n+}$ = surface with adsorbed hydrolyzed metal ion

It is implied that the coordinated H_2O molecules may lose protons to form hydroxo complexes.

Hydrolyzed metal ion adsorption model James and Healy (1972) presented an adsorption model of hydrolyzed metal ions where the preferential adsorption of hydrolyzed species from a suite of complexes could be due to a combination of coulombic, solvation, and chemical energy changes as adsorbates approach the interface. The thermodynamic side of this model will be presented briefly in the next section. The physical meaning of the model could be formulated as;

$$_{aq}M^{m+} + nH_2O \text{ <------> } M(OH)_n^{m-n+} + nH^+ \qquad \text{(III-5)}$$

$$S + M(OH)_n^{m-n+} \text{ <-------> } SM(OH)_n^{m-n+} \qquad \text{(III-6)}$$

where

$M(OH)_n^{m-n+}$ = hydrolyzed metal ion in solution

Thermodynamic aspect of metal ion adsorption

A thermodynamic model for the adsorption of hydrolyzable metal ions at the oxide-water interface has been presented by James and Healy (1972). According to the model, the adsorption of metal ions is the result of the free energy changes favorable to adsorption, i.e.,

coulombic and chemical energy, and the unfavorable solvation energy change.

The physical representation of the model is that the solvation energy presents an energy barrier to close approach of highly charged ions to the interface of a low dielectric constant solid such as silica. As the ionic charge is lowered by hydrolysis or ligand complex formation, the ion-solvent interaction is decreased abruptly because of the quadratic dependence of solvation energy change on the charge of the ion. The decrease in solvation energy consequently lowers the energy barrier. Ions may then approach closer to the interface which results in greater coulombic energies, which is favorable to adsorption.

James and Healy (1972) also noted that if the oxide is a semiconducting oxide whose dielectric constant is similar to that of the solvent, solvation energy changes are minimal and do not prevent adsorption of unhydrolyzed ions. The dielectric constant of a specific oxide should be determined experimentally. However, it is possible that due to the formation of gel-like amorphous layers at the surface, the dielectric in this region may differ from the value measured for single crystals or dry powders.

An additional fact found in their investigation was that the adsorbed species, whatever they may be, were

separated from the surface by at least one layer of water molecules so that direct chemical bonding was precluded. Consequently, the metal ions were not required to lose their primary hydration sheaths. James and Healy were not the only persons who observed the retention of primary hydration sheaths. Cornet and Burwell (1968) investigated the physical and chemical states of a series of chromium compounds deposited on wide pore silica gel by Electron Paramagnetic Resonance (EPR). They found that aqueous chromium compounds existed in the same environment in the pores of silica gels as in bulk solution. During the exploration of the electronic spectra of nickel(II), cobalt(II), and copper(II) ions adsorbed on Dowex 50WX8 resin from dilute solution, Nortia and Laitinen (1968) observed that the spectra of adsorbed ions were similar to those of respective hydrated ions.

Adsorption on lepidocrocite

Kaneko and Inouye (1979) studied the adsorption of water on ferric oxyhydroxide. They also reported (1976) the chemisorption of oxygen on the lepidocrocite surface. Electrical conductivity measurement results were interpreted as a defect property of the surface. Possibly a reasonable model would include the adsorption of aqueous oxygen on the surface prior to surface oxidation. Preliminary studies by Kaneko and Inouye showed that

adsorption of oxygen, if it occurs in solution, would involve very small amounts well below our measurement capabilities.

Using an electrostatic model, Sung (1981) predicted that adsorption of positively charged ions such as Fe(II) would only be promoted by a negatively charged surface. The values of zero point of charge for ferric oxyhydroxides are generally reported to be around pH 7. Consequently, Fe(II) oxidation is dominated by the homogeneous oxidation for pH values less than 7.

Homogeneous Oxidation

The rate law of homogeneous oxidation

Just (1908) proposed that the kinetics controlling the oxidation of ferrous iron by dissolved oxygen in neutral solution would be in the form of;

$$-d[Fe(II)]/dt = k[Fe(II)][OH^-]^2[O_2] \qquad \text{(III-7)}$$

where

k = rate constant

$[Fe(II)]$ = concentration of ferrous iron in solution

$[OH^-]$ = concentration of hydroxyl ion in solution

$[O_2]$ = concentration of oxygen in solution

More recently, Stumm and Lee (1961) and Schenck and Weber (1968) confirmed the validity of the equation. The oxidation kinetics of ferrous iron have been investigated by many researchers under various conditions. Those

kinetic constants were well summarized by Sung and Morgan (1980) and Davison and Seed (1983).

In case of Fe(II) oxidation, the rate constant, k, was shown to be dependent on ionic strength, temperature, and anion concentration in the solution.

Effect of anion

Cher and Davidson (1955) and Stumm and Lee (1961) hypothesized that any anion having complexing affinity for ferric iron accelerates the oxidation. Tamura et al. (1976a) reported that the rate constant, k, decreased in order in the presence of ClO_4^-, NO_3^-, Cl^-, $H_3SiO_4^-$, Br^-, I^-, and SO_4^{-2}. But, anions such as F^- and $H_2PO_4^-$ were found to accelerate the reaction remarkably. Tamura et al. (1976a) explained that phenomenon as a function of the reactivity of the ferrous-anion complex formed. In short, if the complex is less reactive than $FeOH^-$, the rate constant, k, is expected to be smaller than that in the absence of the complex. Or, if the reactivity of the complex is comparable or superior to that of $FeOH^-$, the rate of oxidation would be proportional to $[OH^-][X^-]$ instead of $[OH^-]^2$ where $[X^-]$ stands for the anion concentration in the solution. Liang and Kester (1977) showed the presence of Cl^- or SO_4^{-2} can effectively reduce the oxidation rate. Sung (1981) also confirmed the order effect of ClO_4^-, Cl^-, and SO_4^{-2}. Later, Sung and Forbes

(1984) investigated the effect of chloride on the oxidation rate constant. They formulated the ratio of the rate constant of chloride solution to that of perchlorate ion as;

$$k_{Cl}/k_{ClO4} = 0.99\text{-}1.0x[Cl^-] \qquad \text{(III-8)}$$

where

k_{Cl} = kinetic constant of iron oxidation in the presence of chloride ion, $M^{-3}s^{-1}$

k_{ClO4} = kinetic constant of iron oxidation in the presence of perchlorate ion, $M^{-3}s^{-1}$

$[Cl^-]$ = concentration of chloride ion, M

The k_{ClO4} stands for the kinetic constant which is least affected by complexing anions. Thus, the equation (III-8) shows the effect of the chloride ion concentration on the kinetic constant. The higher the chloride ion concentration, the smaller the kinetic constant.

Effect of organic contaminants

Organic impurities may accelerate or retard oxidation reactions. Stumm and Singer (1966) found that a variety of organic substances, especially those that contain hydroxylic or carboxylic groups, or both (e.g., phenols, polyphenols, gallic acid, humic acid, etc.), can reduce ferric iron to ferrous iron reasonably fast in synthetic solutions. Their hypothesized reaction cycle is;

$$Fe(II) + 1/4O_2 + Org. = Fe(III)\text{-}Org.\ Complex \qquad \text{(III-9)}$$

$$Fe(III)\text{-}\ Org.\ Complex = Fe(II) + Oxidized\ Org. \qquad \text{(III-10)}$$

$$Fe(II) + 1/4O_2 + Org. = Fe(III)\text{-}Org.\ Complex \quad (III\text{-}11)$$

In such cases, the ferrous-ferric system acts as an electron transfer media for the oxidation of organic materials.

Effect of ionic strength

Ghosh (1974) showed that the rate constant, k, increased with ionic strength. His measurements were made in a bicarbonate solution and the ionic strength was between 0.3 and 41 mM. This trend has not yet been confirmed by other researchers. On the contrary, Sung and Morgan (1980) have reported that the oxidation rate constant, k, decreased as the ionic strength, I, increased within the ionic strength range from 0.009 M to 0.11 M. The relationship developed is;

$$\log k = 13.76 - 2.06(I)^{1/2} \quad (III\text{-}12)$$

Using this relation, Sung and Morgan (1980) were able to explain various values of the rate constant, k, reported by other researchers. Later, Sung and Forbes (1984) extended the range of the ionic strength up to 0.7 M and found that the rate constant, k, increases as the ionic strength increases after an ionic strength of 0.25 M is reached. Thus, the previous model has been modified to;

$$\log k = 13.76 - 2.83(I)^{1/2} + 2.31(I) \quad (III\text{-}13)$$

Dependence of rate constant on pH measurement

The consequence of probable error in pH measurement on the rate constant k has been analyzed by Davison and Seed (1983). The deviation of ±0.2 pH unit causes the rate constant to differ by up to a factor of 6 and ±0.1 pH unit by up to 2.5 and the likely precision error of ±0.05 pH unit can produce a range of almost a factor of 1.5.

Effect of buffer intensity

Jobin and Ghosh (1972) investigated the rate of oxidation of ferrous iron in highly buffered bicarbonate solutions and presented the rate law as:

$$d[Fe(II)]/dt = -k[Fe(II)][OH^-]^2[Po_2][\beta]^{1/2} \qquad \text{(III-14)}$$

where

$[Po_2]$ = partial pressure of oxygen in atm.

$[\beta]$ = buffer intensity in eq./pH

k = rate constant, 13×10^{14} $M^{-2}min^{-1}atm^{-1}$ at 25 °C

But, it was also emphasized that the effect of buffer intensity became significant only at values in excess of 4.0×10^{-3} eq./pH. To the author, it is not impossible, but unusual to encounter a water with that high a buffer intensity in nature. To have that high a buffer intensity, a water at 15 °C and pH 7 should have approximately 417 mg/l of total alkalinity as $CaCO_3$. The required alkalinity to have a buffer intensity of 4.0×10^{-3} eq./pH drops to

about 120 mg/l as $CaCO_3$ for water at pH 6 and 15 ^oC. This requires approximately 0.0063 mole of dissolved CO_2 and, in turn, demands about 0.15 atm of CO_2 partial pressure. Even the raw water of Ames, IA., which is known as a well-buffered mid western water, fails to have that high a buffer intensity. Calculation is shown in Appendix A.

Sung and Morgan (1980) were uncertain about the role of bicarbonate alkalinity in oxidation kinetics. They presumed that any effect would be due mainly to its contribution to the solution ionic strength.

Effect of temperature

It has been reported by Stumm and Lee (1961) that the oxidation rate increased about 10 fold for a 15 ^oC temperature increase at a given pH. However, Sung and Morgan (1980) concluded that the true temperature effect would be relatively slight if the change in both O_2 solubility and ionization constant of water due to temperature were counted.

Mechanism of Homogeneous Iron Oxidation

Weiss (1935) proposed the radical oxidation mechanism which rationalized the first order dependence of the rate both on dissolved oxygen and on the ferrous ion.

$$Fe^{++} + O_2 \text{ --------> } Fe^{+++} + O_2^- \quad \text{(rate determining)} \qquad \text{(III-15)}$$

$$O_2^- + H^+ \text{ <--------> } HO_2 \qquad \text{(III-16)}$$

$$Fe^{++} + HO_2 \text{ -------> } Fe^{+++} + HO_2^- \quad \text{(III-17)}$$

$$HO_2^- + H^+ \text{ --------> } H_2O_2 \quad \text{(III-18)}$$

$$Fe^{++} + H_2O_2 \text{ ------> } Fe^{+++} + OH^- + OH \quad \text{(III-19)}$$

$$Fe^{++} + OH \text{ --------> } Fe^{+++} + OH^- \quad \text{(III-20)}$$

However, Weiss' model failed to explain the second order dependence of the rate on the hydroxyl ion concentration. That led Abel (1955) to suggest a different model which was able to support the general rate law.

$$O_2 + OH^- \text{ <--------> } O_2OH^- \quad \text{(III-21)}$$

$$O_2OH^- + OH^- \text{ <-----> } O_3^{--} + H_2O \quad \text{(III-22)}$$

$$Fe^{++} + O_3^{--} \text{ ------> } Fe^{+++} + 3O^- \quad \text{(III-23)}$$
(rate determining)

$$3O^- + 3H^+ \text{ <--------> } 3OH \quad \text{(III-24)}$$

$$3Fe^{++} + 3OH \text{ ------> } 3Fe^{+++} + 3OH^- \quad \text{(III-25)}$$

The key assumption in Abel's mechanism is the existence of the O_3^{--} ion in the solution in equilibrium with the O_2 and OH- ion. He considered that the O_3^{--} ion is much more reactive toward ferrous ion than is the ordinary O_2 molecules. These assumptions were analyzed by Goto et al. (1970). They ended up with the conclusion that the equilibrium concentration of the O_3^{--} ion would be equal to that of the ordinary O_2 molecules at a pH of about 13. This, in turn, meant to them that the total concentration of oxygen, $[O_2] + [O_2OH^-] + [O_3^{--}]$, should change remarkably around pH 13 because of the existence of

the O_3^{--} ion. But the experimental results by Linke (1965) showed that there is no appreciable change in the solubility of oxygen over a wide range of pH's from strongly acidic to strongly alkaline. As a result of this apparent mechanism conflict, Goto et al. (1970) proposed a new mechanism.

$$Fe^{++} + OH^- \longleftrightarrow FeOH^+ \qquad \text{(III-26)}$$

$$O_2 + OH^- \longleftrightarrow O_2OH^- \qquad \text{(III-27)}$$

$$FeOH^+ + O_2OH^- \longrightarrow Fe(OH)_2^+ + O_2^- \qquad \text{(III-28)}$$
(rate determining)

$$O_2^- + H^+ \longleftrightarrow HO_2 \qquad \text{(III-29)}$$

Even though Goto et al. haven't completed the reaction cycle after the production of HO_2, it would not be unreasonable to assume that the HO_2 follows the reaction cycle of Weiss' model thereafter.

Although Goto et al. apparently solved the conflict in the oxygen solubility, their model resulted in other questions. The value of the overall rate constant, k_o, in the general rate law would be reduced to half of that at pH 9.5. Furthermore, around pH 11.5, the oxidation rate should be proportional to the first order of the hydroxyl ion concentration instead of the second order. This phenomenon, however, has not yet been studied. The analysis will be shown in Appendix B.

The author cannot agree with Goto et al.'s analysis where they claimed that the existence of an equal amount of

O_3^{-2} ion in equilibrium with the O_2 molecules has to change the total concentration of oxygen. As the reaction equations indicate, O_3^{-2} ions have been transformed from the ordinary O_2 molecules in the solution. It seems to this author that the appearance of the O_3^{-2} ion accompanies the disappearance of the O_2 molecule which results in an unchanged total oxygen concentration even with the existence of an equal amount of O_3^{--} ions in equilibrium with the ordinary O_2 molecules.

CHAPTER IV. EXPERIMENTS, RESULTS, AND ANALYSIS

Scope of Experiments

The many experiments conducted in this study were intended to provide a better understanding of the characteristics of lepidocrocite, the role of lepidocrocite in heterogeneous oxidation, the adsorption capacity of lepidocrocite for ferrous iron, and the correlation of lepidocrocite surface area to its adsorption capacity. The experiments involved four different areas of study:

1. Testing the applicability of heterogeneous oxidation in dissolved iron removal practice.
2. Synthesis of lepidocrocites and subsequent examination of their physical characteristics, such as their morphology and surface area.
3. Investigation of the adsorption capacities of three distinctive lepidocrocites followed by a model construction.
4. Observing morphology and structure of precipitates after oxidation of ferrous iron in the presence of lepidocrocite.

Equipment

The major equipment utilized during the research are listed below:

pH meter; Beckman [illegible] meter [illegible]

D. O. meter; Ye[illegible] Spr[illegible] Mo[illegible]

Spectrophotometer; Beck[illegible]

Freeze dryer; [illegible]

Masterflex pump; [illegible]

Centrifuge; Iv[illegible] Sorv[illegible] (2[illegible] r[illegible]

Oven; Fisher [illegible]

Shatter box; [illegible] Ind[illegible]

X-ray diffrac[illegible]

X-ray fluor[illegible]

Scanning ele[illegible]

Energy disp[illegible]

Surface ar[illegible]

Particle s[illegible]

Fe[illegible]

Objectives and [illegible]

This par[illegible] the catalytic oxid[illegible] waters conta[illegible] fer[illegible]

pH meter; Beckman Co. ALTEX model 4500 digital pH meter reference junction.

D. O. meter; Yellow Springs Instrument Co. Model 54 & 58

Spectrophotometer; Beckman Co. Model B

Freeze dryer; VIRTIS 10-020

Masterflex pump; Cole-Parmer Instrument Co.

Centrifuge; Ivan Sorvall Inc. Servall (20,000 rpm max.)

Oven; Fisher Isotemp 100 series Model 126G

Shatter box; SPEX Industries,

X-ray diffractometer; SIEMENS D500 equipped with copper KÁ line, diffracted beam monochromator, and pulse height analyzer

X-ray fluorescence spectrometer; SIEMENS SRS 200

Scanning electron microscope; Japan Electron Optical Laboratories. Model JEOL 840A

Energy dispersive spectrometer; Tracor Northern TN-2000

Surface area analyzer; Micromeritics Co. AccuSorb 2100E

Particle size analyzer; HIAC Model 320

Feasibility for Engineering Practice

Objectives and scope of the experiment

This part of the study was designed to examine whether catalytic oxidation could be practical for midwestern waters containing ferrous iron. It required the

combination of several hypotheses and assumptions.

Assume that, as reported, lepidocrocite has a catalytic effect on ferrous iron removal and that it is possible to precipitate lepidocrocite from iron-bearing midwestern water. By providing a suitable environment, the ferrous iron in water would be precipitated as lepidocrocite, which, in turn, would adsorb ferrous iron in water. The adsorbed ferrous iron would then be oxidized to the same substance, lepidocrocite. Thus, this cycle of catalytic removal could go on and on.

The purpose of this experiment was to provide an environment for lepidocrocite precipitation and to observe whether or not the catalytic removal of ferrous iron occurred. However, this experiment was limited to the qualitative observation because of many unknown factors including correlation between surface area and adsorption capacity, reliability of the heterogeneous rate equation with raw ground water, and the effects of anions and organic matter on heterogeneous oxidation. A sand filter was utilized to retain the oxidation product which might be lepidocrocite.

Experimental procedures

Water was obtained at the water treatment plant of Iowa State University, Ames, IA., whose water source was ground water. Before each experiment, 5 gallons of raw

water were collected from a tap between the well and the aeration tower. The 5 gallon container had been filled with carbon dioxide gas and capped prior to the collection of raw water. In this way, the carbon dioxide gas dissolved into the raw water to some extent during collection; this procedure allowed the ferrous iron to remain in solution while the raw water was transported to the laboratory. It took about 10 minutes to transport the samples from the water treatment plant to the laboratory.

Misawa et al. (1974) reported that rapid oxidation of ferrous iron by air in weakly acidic solution results in the precipitation of lepidocrocite. Schwertmann and Thalmann (1976) reported that a water pH range from 5 to 7 was suitable for precipitation of lepidocrocites. Based on their report, the pH of the raw water was adjusted to 6 in the laboratory with carbon dioxide gas.

Figure 7 shows the experimental layout. The water was recycled through a sand filter until all the ferrous iron in the water was oxidized and deposited in the filter. After recirculation was completed, which usually took about 24 hours, the recycled water was discarded and a fresh batch of raw water was picked up at the water treatment plant and passed through the filter. Before starting recirculation, the concentrations of dissolved iron in the influent and effluent were checked by atomic absorption

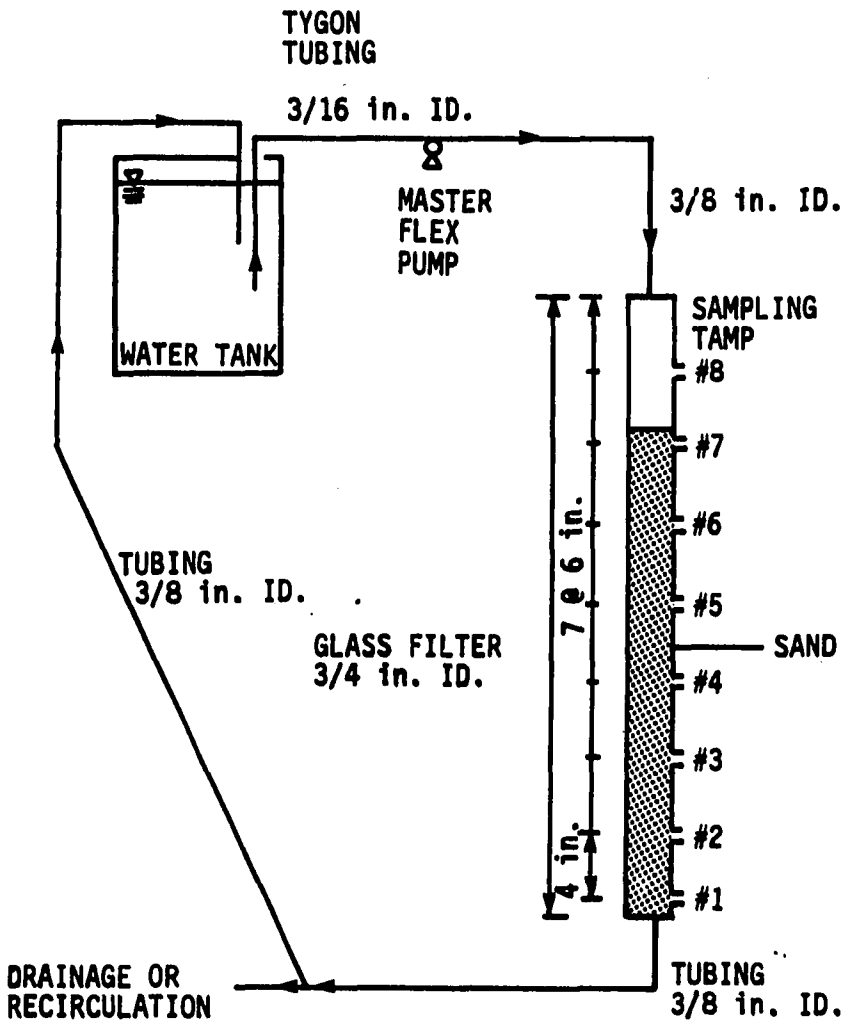

MEDIA: SAND #25-30

CHEMICALS USED: CO_2 GAS

FLOW RATE: 3.14 gpm/ft^2

Figure 7. Experimental setup for feasibility test

spectrometry to monitor the performance of the filter in ferrous iron reduction.

The filter media was silica sand collected between U.S. standard sieve No.25 and No.30. The diameter of the filter column was 0.75 inch, and the sand depth was 38 inches. The rate of recycle was fixed at 36 ml/min which corresponded to a filtration rate of 3.1 gal/ft^2/min. The dissolved oxygen concentration was about 3.5 mg/l after pH adjustment using carbon dioxide gas. Even though carbon dioxide gas was not bubbled in after initial treatment, the pH of the water stayed relatively constant to the end of recycling.

Determination of the dissolved iron concentration

The concentration of dissolved iron in the influent and effluent was determined using an atomic absorption spectrometer. Ten milliliter of sample was taken from a sampling tap and transferred to a volumetric flask where 0.4 ml of 0.002 N perchloric acid was already present to prevent aerial oxidation of dissolved iron in the sample. The acidified sample was vacuum filtered through a 0.1 μm membrane filter to remove already precipitated ferric iron particles. Then, the concentration of dissolved iron was determined using an atomic absorption spectrometer at a wavelength of 249 nm. The spectrometer was calibrated using standard solutions prepared in accordance with

Standard Method (1985). The mean concentration of iron present was represented by the mean of three separate measurements.

Results and analysis of iron removal performance

As recycling progressed, the filter effluent contained less and less dissolved iron. The iron precipitate was deposited mostly within the upper 12 to 15 inches of the sand. After approximately 230 mg of iron accumulated in the filter, ferrous iron was not detected in the effluent even though the concentration of ferrous iron in influent was 3.80 mg/l. The pH of the influent was 6.1; the concentration of dissolved oxygen was 3.6 mg/l; and the temperature was 10 ^{o}C. The filter was operated continuously for 8 hours without recirculation (on a once-through basis) at a flow rate of 3.1 gpm/ft^2. Figure 8 shows the concentration of dissolved iron in the influent and in the effluent. Then, the filtration was stopped for 12 hours to prepare new raw influent water for the next run.

Fresh ground water from the physical plant was brought to the laboratory, adjusted for pH, then passed through the iron-deposited filter at a flow rate of 3.1 gpm/ft^2. The influent concentration of dissolved iron was 5.12 mg/l at the beginning of the run and dropped to 4.04 mg/l at the end. Dissolved iron was not detected in the effluent. The

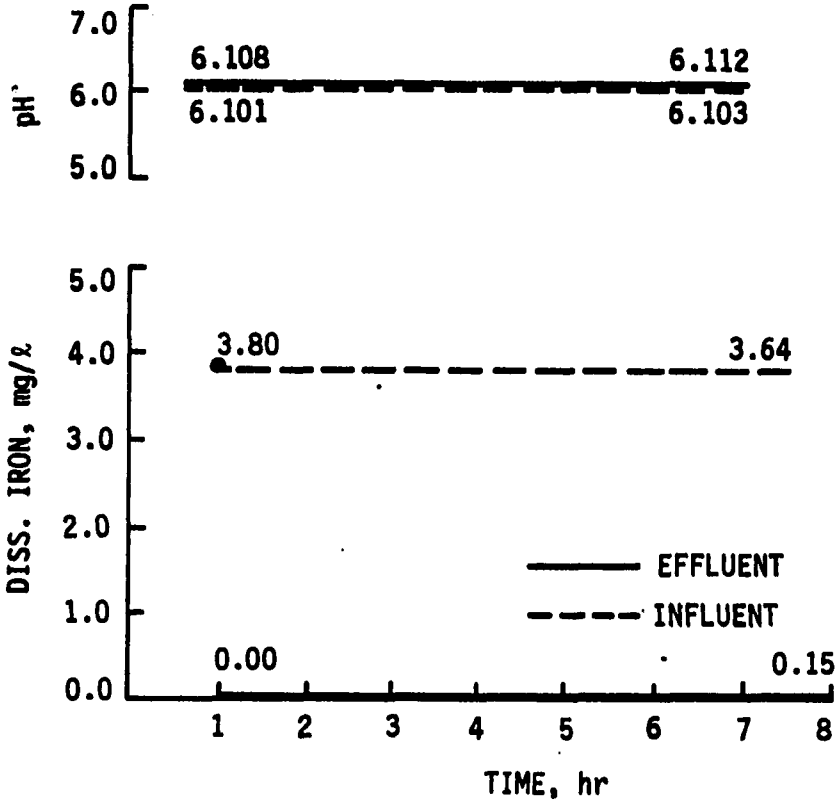

Figure 8. The concentrations of dissolved iron in the influent and in the effluent of the filter containing iron deposit

filtration went on for 7 hours without interruption. The filtration was stopped after strong acidic water of pH 3 was accidentally admitted into the filter. The filter was backwashed to investigate the possibility of reproduction of the test results.

Reproduction of the iron filter

The filter in Figure 7 was backwashed with distilled water. A batch of 4 gallons of raw ground water from the University water treatment plant was recycled through the filter. The flow rate was fixed at 3.1 gpm/ft^2, and the pH was adjusted to 6 using carbon dioxide gas. Recycled water was discarded after all the dissolved iron was precipitated and retained in the filter. Four batches of 4 gallons of raw water were able to restore the ability of the filter for removal of dissolved iron. Approximately 300 mg of dissolved iron was deposited in the filter.

Continuous operation of the filter

The next step was to determine whether the filter was able to remove dissolved iron continuously. The first run consisted of 4.5 hours of continuous filtration of raw water containing ferrous iron at a flow rate of 3.1 gpm/ft^2. The concentration of dissolved iron in the influent was 4.18 mg/l at the beginning and 2.85 mg/l at the end of the run. This variation was due to

precipitation of dissolved iron in the water tank. The concentration of dissolved oxygen was 3.6 mg/l and the pH was about 6. These values stayed stable during the run. Dissolved iron was not detected in the effluent by atomic absorption spectrometry. Figure 9 shows the level of dissolved iron in the filter as a function of depth of filter media.

The second batch was started one hour after the first run was completed. The flow rate was 3.1 gpm/ft^2 and the pH was adjusted using carbon dioxide gas to 6; the concentration of dissolved oxygen was 3.8 mg/l after pH adjustment. The filter was operated for 9 hours continuously. The concentration of dissolved iron at the end of the run was 4.23 mg/l in the influent and 0 in the effluent.

The third batch was prepared four hours after the second batch was finished and run for 9 hours without interruption. The flow rate was 3.1 gpm/ft^2, the pH was 6, and the concentration of dissolved oxygen was 3.6 mg/l after pH adjustment. The concentration of dissolved iron varied from 3.02 mg/l to 2.64 mg/l in the influent and was 0 in the effluent.

The fourth batch was started 30 minutes after completion of the third batch and run continuously for 9 hours. The conditions of the run were quite similar to

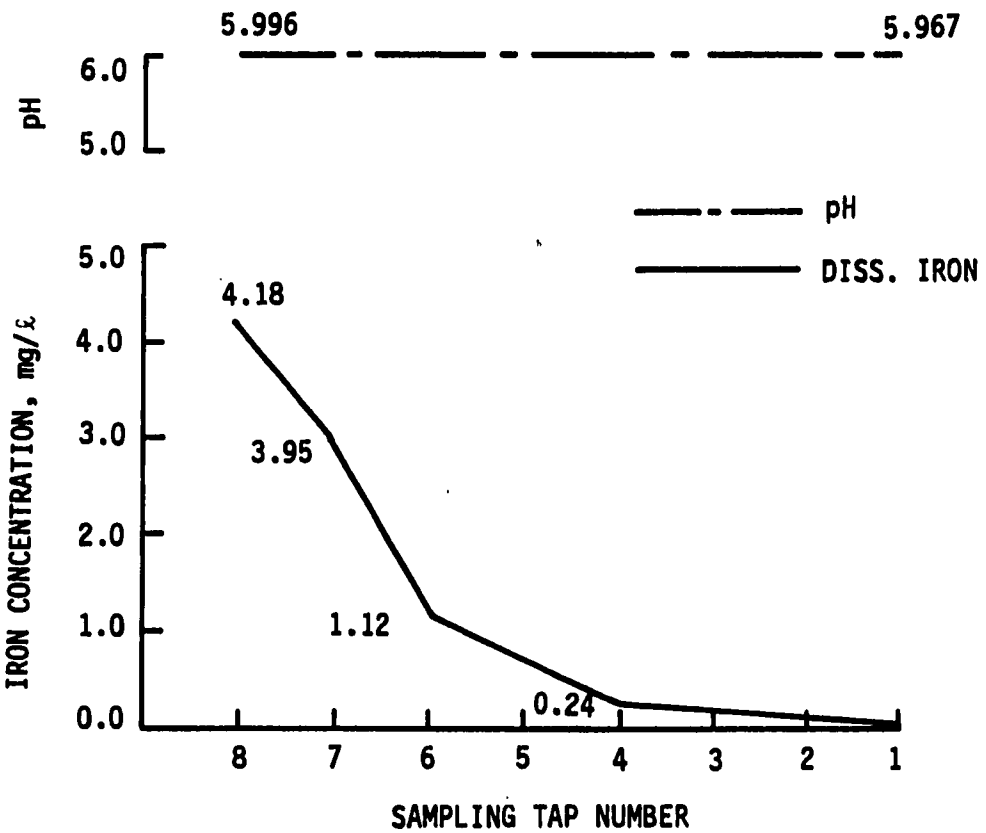

Figure 9. Typical change in dissolved iron concentration as a function of filter depth

those in the previous three runs. The filter was still successful in completely removing dissolved iron from an influent value of 3.27 mg/l. The influent dissolved iron concentration dropped to 2.28 mg/l at the end of the run.

The fifth batch was prepared 7 days after the fourth run. During those 7 days, the water level was kept above the surface of the sand so that air didn't get in the filter. This was a continuous filtration operation for 8 hours. The dissolved iron concentration in the influent varied from 4.89 mg/l at the beginning to 3.47 mg/l at the end of of the 8 hours operation because of precipitation of iron in the tank. Flow rate, pH, and concentration of dissolved oxygen were the same as in previous runs. As expected, the filter removed dissolved iron perfectly and the effluent didn't contain any iron at all.

Screening for microorganisms

A treatment was needed to separate any effect on iron precipitation by microorganisms from that of catalysis by the iron precipitates. Because the iron filter deposits were produced by recycling ground water for several days, it was possible that microorganisms, especially iron bacteria, in the raw water might grow in the filter, and contribute to removal of dissolved iron from the influent. However, the treatment required to remove the effect of microorganisms must not affect or alter the precipitation

environments of dissolved iron and the characteristics of the precipitates in the filter.

The method used in this experiment involved the physical filtration of raw water through an 0.45 μm membrane filter in conjunction with sterilization of the filters. Two identical filters were prepared and placed side by side. Each filter had the same arrangements as the one shown in Figure 7 except the packing depth of sand was 20 inches instead of 38 inches. The sand depth was reduced because dissolved iron was removed within the first 6 inches of the filter in most cases in the previous experiments. One sand media filter was autoclaved under 18 lbs of pressure and 275 ^{o}F for one hour. The glass filter tubings and all the connectors were sterilized prior to the set up. In each run, a 5-gallon batch of raw water was treated with carbon dioxide gas for pH adjustment and divided into two equal volumes. One was filtered through a 0.45 μm membrane filter. The filtrate was collected into a sterilized container and capped. It was examined for pH and dissolved iron concentration. In spite of the filtration process, the pH and the dissolved iron concentration were not changed appreciably.

The two waters were recycled through the filters. Dissolved oxygen concentrations were 3.7 mg/l and 4.5 mg/l for the unfiltered and the filtered raw water,

respectively. The pH of the influent was about 6 for both waters. Aliquots of recycling water from both filters were examined for dissolved iron concentration during the recirculation period. The dissolved iron concentrations in both filter systems decreased with time and finally disappeared about 18 hours after starting recirculation. That batch of water was discarded and a new batch was prepared for the next recirculation trial.

Both filters removed dissolved iron more and more as recycling proceeded. However, the filter recycling unfiltered water built an iron removing capability faster than the other filter and started to remove dissolved iron from the influent after approximately 200 mg of iron was deposited. One day later, the filter recycling filtered water removed all dissolved iron from the influent, too. About 240 mg of iron had been deposited at that time.

Lepidocrocite-deposited filter

A filter containing precipitated iron was made by recycling a lepidocrocite suspension. The diameter of the filter was 0.375 in. and sand depth was 20 in. The sand utilized had passed a U.S. Standard No.25 sieve but was retained on a No.30 sieve. The flow rate was 4.13 gpm/ft^2. The suspension was prepared by soaking 100 mg of lepidocrocite in 2 liters of redistilled water. The lepidocrocite suspension was recycled through the filter so

that lepidocrocite could be deposited in the filter media. However, there was difficulty in quantifying the amount of lepidocrocite in the filter because some particles had settled to the bottom of the suspension bottle and some had deposited on the tubings between the suspension bottle and the filter. Furthermore, some of the deposited lepidocrocite was washed out during the experiment.

Experiment with the filter containing lepidocrocite

An iron-containing water was synthesized using carbon dioxide gas and electrolytic grade iron powder. Synthesized water instead of natural well water was used to remove the effects of unknown factors including silica, anions, microorganisms, and other minerals. About 1 gram of iron powder was put in 100 ml of redistilled water and carbon dioxide gas was bubbled in for 2 hours. The supernatant was filtered through an 0.1 μm membrane filter, and 50 ml of the filtrate was mixed with 5 liters of deionized water. Although the concentration of dissolved iron differed in each preparation, it usually fell between 1.5 to 2.0 mg/l. This water was used as a raw iron-containing water. The 1,10-phenanthroline method (Standard Methods, 1985) was used to measure the dissolved iron concentration in this experiment.

The lepidocrocite deposit in the filter was successful in removing ferrous iron continuously from the influent.

Typical results from the filter are shown in Figure 10. The concentration of dissolved iron in the effluent indicated that the lepidocrocite would have a continuous capability of removing dissolved iron. If lepidocrocite does not have a continuous effect, the concentration of dissolved iron in the effluent should be zero until the capacity of lepidocrocite was exhausted, and then the effluent concentration would increase gradually to the influent concentration. The experimental data, however, showed a stable concentration of dissolved iron in the effluent, which meant that the available sites on the lepidocrocite for ferrous iron was recovered at a steady rate by oxidizing the adsorbed ferrous iron. Judging from this experiment, it would be possible to reduce dissolved iron to the desired effluent iron concentration provided sufficient lepidocrocite were present in the filter media system.

Synthesis of Lepidocrocite

Objective and scope of the synthesis

The objective of the synthesis was to produce the lepidocrocites which could be used in adsorption and oxidation experiments. It was also planned to explore the differences between the lepidocrocites in terms of morphology, surface area, etc. when different methods were

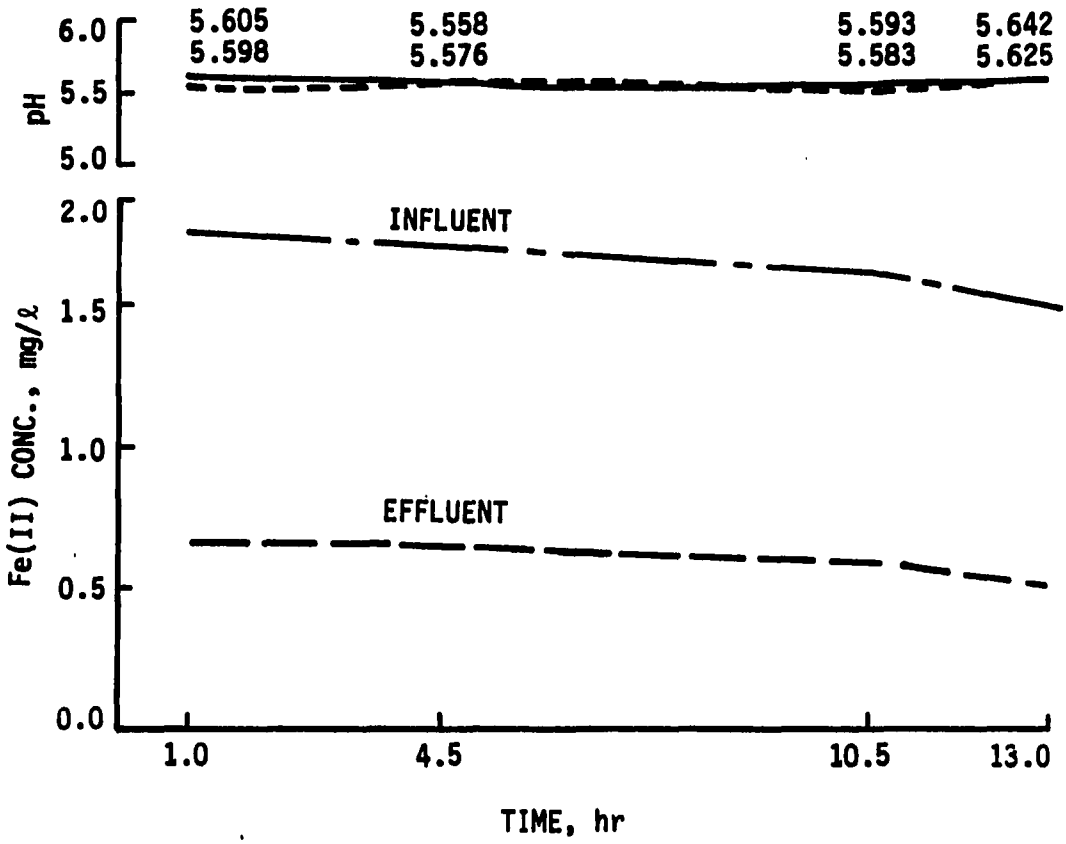

Figure 10. Dissolved iron removal by the filter containing a lepidocrocite deposit.

used to synthesize the lepidocrocites.

The products were identified by their X-ray diffraction patterns. The surface areas were investigated using BET adsorption isotherms and the morphologies by Scanning Electron Microscopy (SEM). The possible deposition of impurities on the products was examined using Energy Dispersive Spectrometry (EDS) and X-ray fluorescence spectrometry.

Synthesis of lepidocrocites

Two lepidocrocites were synthesized in the laboratory using different methods and a third was obtained from the 3M Co. in Minneapolis, MN.

One method was described by Baudisch and Albrecht (1932). They reported the successful synthesis of lepidocrocite by adding pyridine, which has also been utilized by Sung and Morgan (1980). In this experiment, 0.2 M $FeCl_2$ was dissolved in 1 liter of deoxygenated redistilled water and filtered a through 0.45 μm membrane filter. Fifty milliliters of pyridine were added and air was bubbled through the reactor for 2 hours. The greenish black complexes which formed upon the addition of pyridine were oxidized to yellow brown precipitates after 2 hours of oxidation. The precipitates were centrifuged at 15,000 rpm. After discarding the supernatant, the precipitates were washed with distilled water repeatedly until no

chloride was detected. It took about 25 centrifuging and washing cycles. The washed precipitates were divided into two portions. One portion was placed in a drying oven for 12 hours at 60 ^{o}C. No weight change was detected during the last 3 hours. The other part was dried using the freeze drier for 5 days.

Another method of synthesis was described by Kaneko and Inouye (1974). Ferrous chloride was dissolved in deoxygenated redistilled water to make 500 ml of 0.2 M solution. This solution was vacuum filtered through 0.45 μm membrane filters. The filtrate was mixed with 100 ml of 2 M hexamethylene tetramine, 13.5 ml of concentrated HCl, and 100 ml of sodium nitrite. Nitrogen gas was bubbled into the mixture while it was warmed in a water bath at 60 ^{o}C for 50 minutes. The resulting brown precipitate was split in two portions. One portion was dried in drying oven at 60 ^{o}C for 12 hours. The other part was freeze dried.

For convenience, a third sample of lepidocrocite obtained from the 3M Co. is referred to as lepidocrocite-3M. Similarly, the ferric compound synthesized using the techniques of Baudisch and Albrecht (1932) is referred to as lepidocrocite-B&A and that using the techniques of Kaneko and Inouye (1974) is referred to as lepidocrocite-K. They were identified as lepidocrocite by X-ray diffraction

patterns, as described in the next section.

Identification of the product by X-ray diffraction

Even though the synthesis was performed for the production of lepidocrocite, it was also possible that amorphous and/or other ferric oxides were produced along with the lepidocrocite. Thus, X-ray diffractometry was used to identify the synthesized precipitates. The scanned 2θ range was from 2 to 70 degree and the X-ray was beamed for 2 seconds at every 0.05 degree. Figures 11, 12, and 13 are the resulting plots of X-ray patterns and Tables 1, 2, and 3 are the identified peaks of the synthesized lepidocrocites. The X-ray powder data of lepidocrocite by the American Society of Testing Material (ASTM) are listed in Table 4. The matching of the patterns for identification was limited to the patterns among the ferric compounds because the three synthesized compounds were the oxidation products of ferrous iron. As shown, the X-ray diffraction data of the three synthesized compounds agreed very well with those of lepidocrocite in terms of the d-spacing and relative intensities of the peaks. There were no peaks at the d-spacings other than those of lepidocrocite. Moreover, the backgrounds were quite flat, which means that the synthesized compounds were well crystallized rather than amorphous. Thus, it is concluded that the three materials are crystalline lepidocrocites and

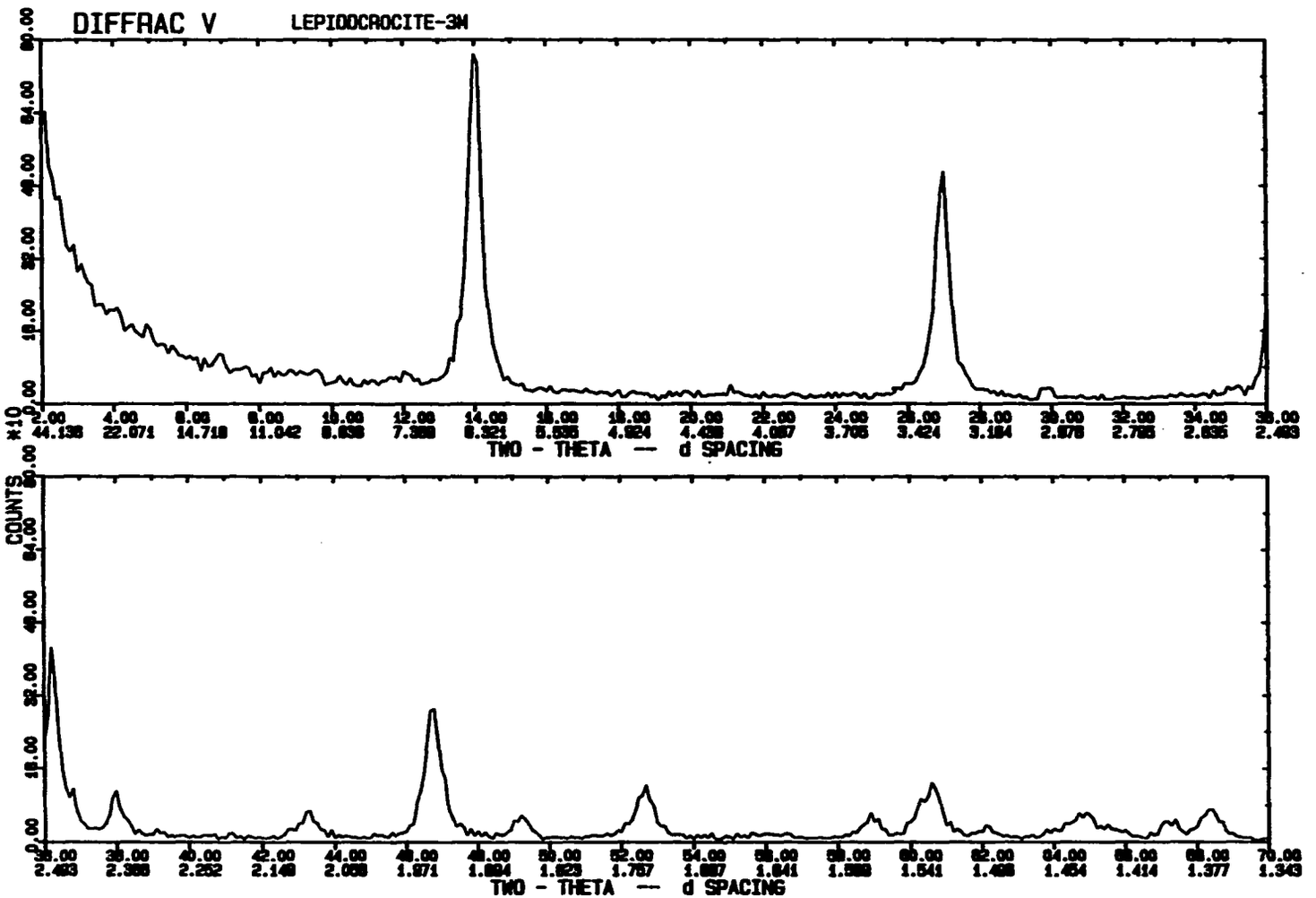

Figure 11. The X-ray diffraction pattern of lepidocrocite-3M. Copper tube with diffracted beam monochromator and pulse height analyzer was used. Copper K_α line was generated at 50 KV, 25 mA.

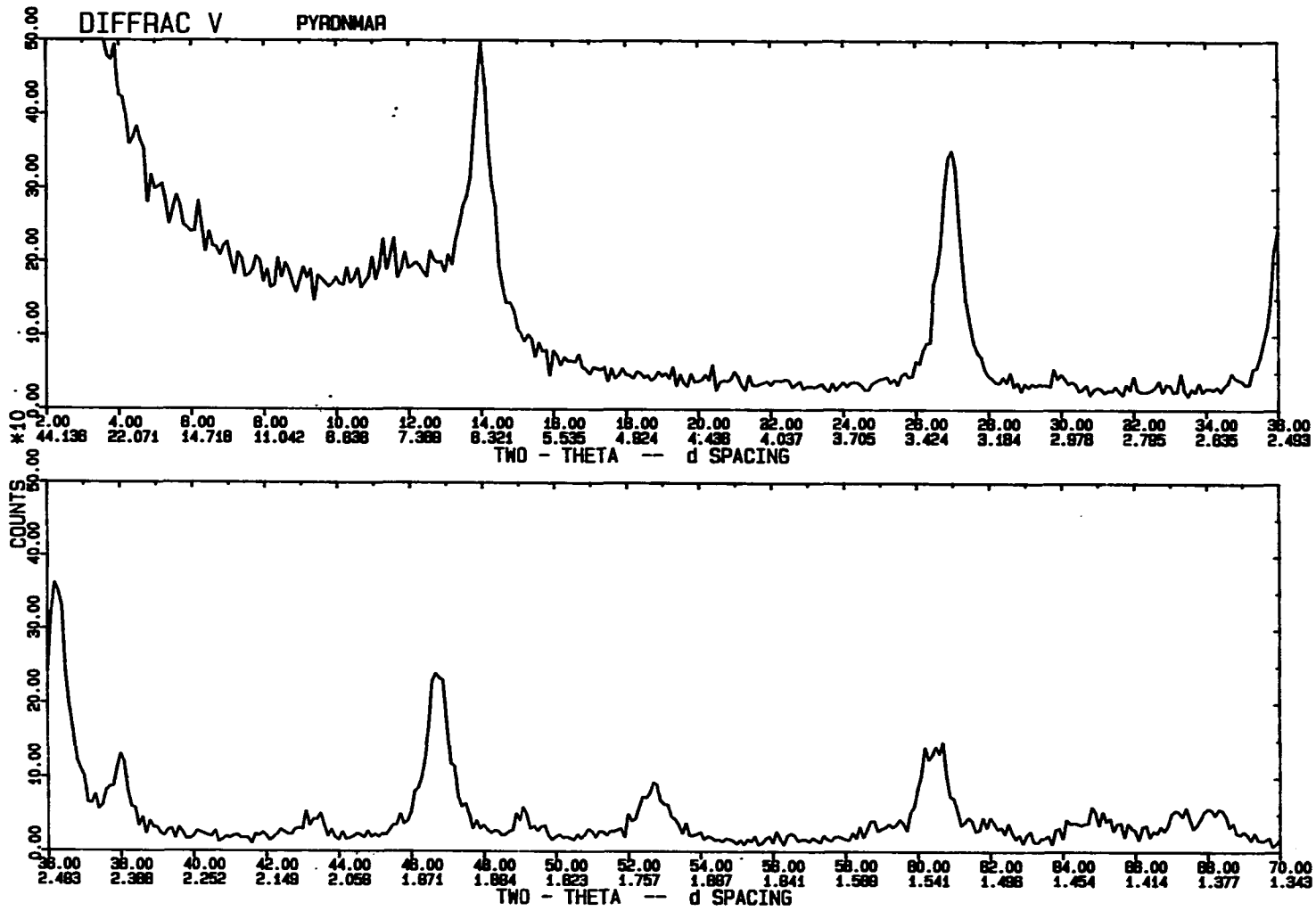

Figure 12. The X-ray diffraction pattern of lepidocrocite-B&A. Copper tube with diffracted beam monochromator and pulse height analyzer was used. Copper K_α line was generated at 50 KV, 25 mA.

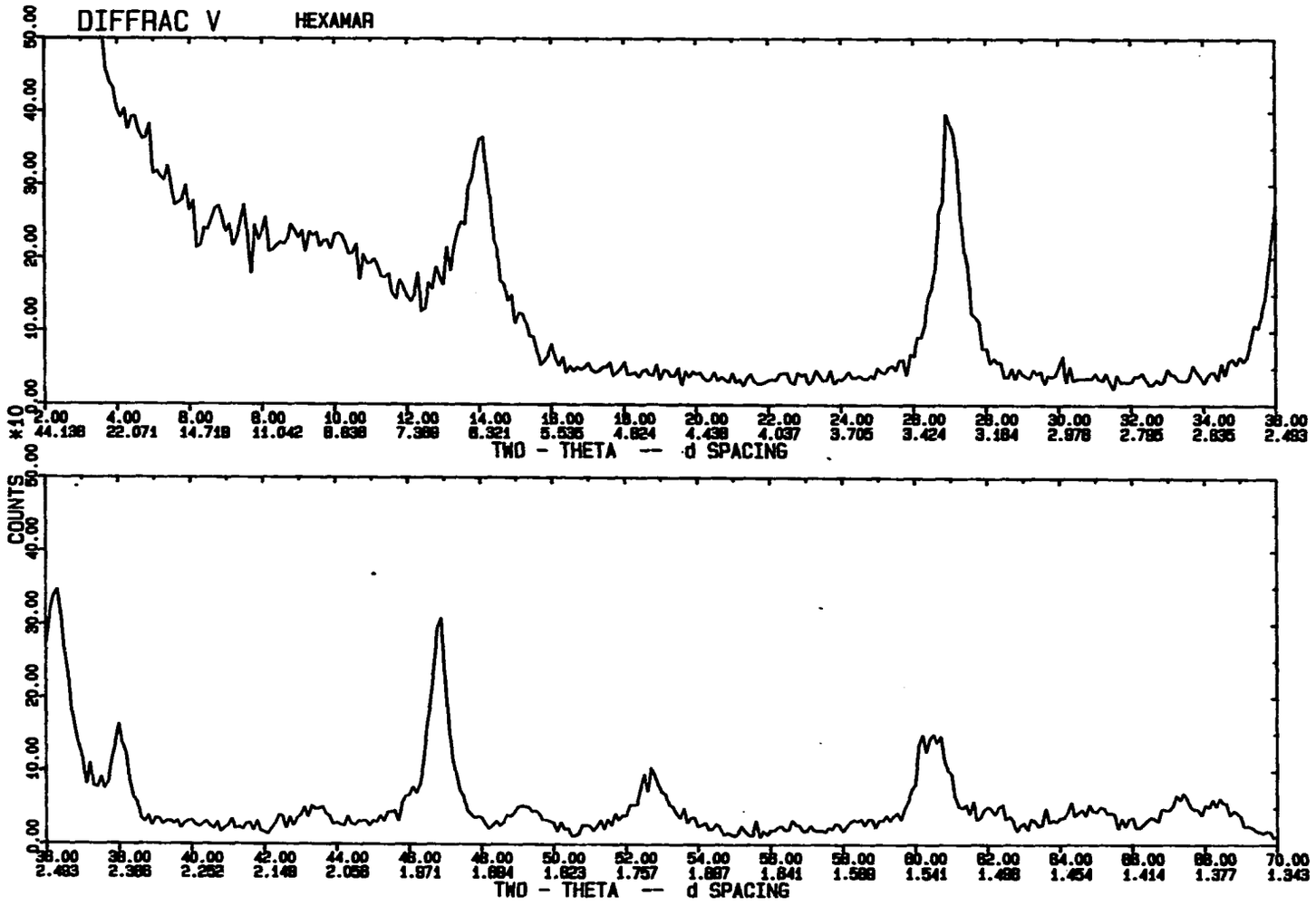

Figure 13. The X-ray diffraction pattern of lepidocrocite-K. Copper tube with diffracted beam monochromator and pulse height analyzer was used. Copper K_α line was generated at 50 KV, 25 mA.

Table 1. Peaks of the X-ray diffraction pattern of lepidocrocite-3M

No.	2θ	d-spacing	Integ.I(%)	FWHM
1	6.938	12.7293	2.3	0.264
2	14.069	6.2896	100.0	0.543
3	27.014	3.2978	69.3	0.572
4	29.932	2.9826	2.6	0.351
5	36.260	2.4753	54.4	0.523
6	38.001	2.3658	9.7	0.408
7	43.306	2.0875	7.9	0.541
8	46.809	1.9391	43.8	0.605
9	49.238	1.8490	5.7	0.498
10	52.710	1.7351	14.6	0.550
11	58.930	1.5659	5.8	0.451
12	60.679	1.5249	21.1	0.829
13	62.156	1.4921	2.5	0.425
14	64.084	1.4518	2.2	0.374
15	64.936	1.4348	9.2	0.682
16	65.475	1.4243	2.9	0.434
17	67.211	1.3917	5.0	0.613
18	68.380	1.3707	9.8	0.677

1. The peaks were detected by the IDENT software provided with SIEMENS X-ray diffractometer.

2. Maximum background slope over one degree=0.30. The smallest peak relative to the strongest=1.0. 3 points were averaged.

3. The peaks detected may be only background noise. Significance of a peak should be determined by matching it with the plot.

Table 2. Peaks of the X-ray diffraction pattern of lepidocrocite-B&A

No.	2θ	d-spacing	Integ.I(%)	FWHM
1	14.070	6.2890	100.0	0.756
2	27.034	3.2954	94.6	0.772
3	32.696	2.7366	2.1	0.238
4	33.292	2.6889	3.1	0.267
5	36.281	2.4739	92.6	0.702
6	38.034	2.3638	16.1	0.498
7	43.375	2.0843	9.4	0.644
8	45.822	1.9785	1.3	0.221
9	46.782	1.9402	60.9	0.812
10	49.148	1.8522	4.8	0.385
11	52.731	1.7344	23.0	0.861
12	60.242	1.5349	14.1	0.368
13	60.548	1.5279	25.3	0.613
14	64.005	1.4534	5.3	0.455
15	67.179	1.3923	7.3	0.443

1. The peaks were detected by the IDENT software provided with SIEMENS X-ray diffractometer.

2. Maximum background slope over one degree=0.30. The smallest peak relative to the strongest=1.0. 3 points were averaged.

3. The peaks detected may be only background noise. Significance of a peak should be determined by matching it with the plot.

Table 3. Peaks of the X-ray diffraction pattern of the lepidocrocite-K

No.	2θ	d-spacing	Integ.I(%)	FWHM
1	7.495	11.7850	6.5	0.221
2	8.101	10.9041	7.5	0.368
3	14.073	6.2877	96.7	1.063
4	19.605	4.5242	2.1	0.172
*	27.050	3.2935	100.0	1.038
5	30.067	2.9695	2.4	0.224
6	36.290	2.4733	100.0	0.858
7	38.036	2.3637	17.6	0.442
8	42.428	2.2186	2.0	0.226
9	46.902	1.9355	75.8	0.716
10	49.237	1.8490	10.5	0.736
11	52.550	1.7400	12.5	0.455
12	52.764	1.7334	13.1	0.384
13	60.278	1.5341	14.8	0.363
14	60.528	1.5283	28.9	0.663
15	62.368	1.4876	3.4	0.245
16	63.617	1.4613	1.4	0.138
17	64.312	1.4472	2.0	0.252
18	64.998	1.4336	5.3	0.571
19	67.250	1.3910	5.2	0.437

1. The peaks were detected by the IDENT software provided with SIEMENS X-ray diffractometer.

2. Maximum background slope over one degree=0.30. The smallest peak relative to the strongest=1.0. 3 points were averaged.

3. The peaks detected may be only background noise. Significance of a peak should be determined by matching it with the plot.

4. The peak at the d-spacing of 3.2935 was detected by 5 points average. Averaging 3 points of raw data didn't detect the peak.

Table 4. X-ray diffraction pattern of lepidocrocite in ASTM X-RD Powder File

No.	(hkl)	d-spacing	Integ.I(%)
1	020	6.26	100
2	120	3.29	90
3	011	2.79	10
4	031	2.47	80
5	111	2.36	20
6	131,060	2.09	20
7	051,200	1.937	70
8	220	1.848	20
9	151	1.732	40
10	080	1.566	20
11	002	1.535	20
12	231	1.524	40
13	022	1.496	10
14	180	1.449	10
15	171	1.433	20
16	260	1.418	10
17	122	1.389	10
18	251	1.367	30
19	091,320	1.261	10
20	280	1.213	10
21	022,191	1.196	20
22	110	1.189	20

that no other ferric compounds existed in detectable amounts.

Impurities on the surface

Although the synthesis products were throughly washed with distilled water, it was still possible that some impurities remained on the surface or incorporated in the crystal structure. Energy Dispersive Spectrometry (EDS) and X-ray fluorescence were utilized to investigate for possible deposit of impurities. Both equipments detect elements of the sample compound. The X-ray fluorescence has the advantage of better resolution than the EDS. Even though the detection limit depends on the preparation of the sample, the samples in this investigation are believed to have a resolution limit of about 100 ppm. On the other hand, EDS could be a useful tool if impurities existed under the detection limit of X-ray fluorescence. Because it could identify the elements on a scanned area, if the investigator was lucky enough to focus the electron microscope on the impurities which might have a somewhat different morphology than the main compound, the elements of the impurities could be identified regardless of the concentration present. The limitation, however, still exists that X-ray fluorescence cannot detect elements placed before fluoride in the periodic chart and the EDS can not detect those before sodium.

When the chemicals used in the synthesis of lepidocrocites were considered, the primary potential elements involved were iron, carbon, nitrogen, hydrogen, chloride, sodium, and oxygen. Among them, carbon, nitrogen, and hydrogen cannot be detected by EDS or X-ray fluorescence. Iron and oxygen are the elements in lepidocrocite. Therefore, sodium, chloride, and silica were searched as typical elements representing potential impurities. The results of the X-ray fluorescence showed no trace of impurities in any of the lepidocrocites. The spectra from EDS also indicated the clean surfaces of the lepidocrocites. The typical EDS spectra of the lepidocrocites are presented in Figures 14, 15, and 16.

Morphologies of the three lepidocrocites

The morphologies of the three lepidocrocites were observed by Scanning Electron Microscopy (SEM) at 1,000, 10,000, and 30,000 magnification levels. The microphotographs at 30,000 magnification are presented in Figures 17, 18, and 19.

It was clear that the three lepidocrocites had very different shapes. This could be due to the different rate of oxidation during their formation. The lepidocrocite formed by Kaneko and Inouye (1974) method probably crystallized more rapidly than any other compound. The lepidocrocite from the 3M Co. must have been formed slowly

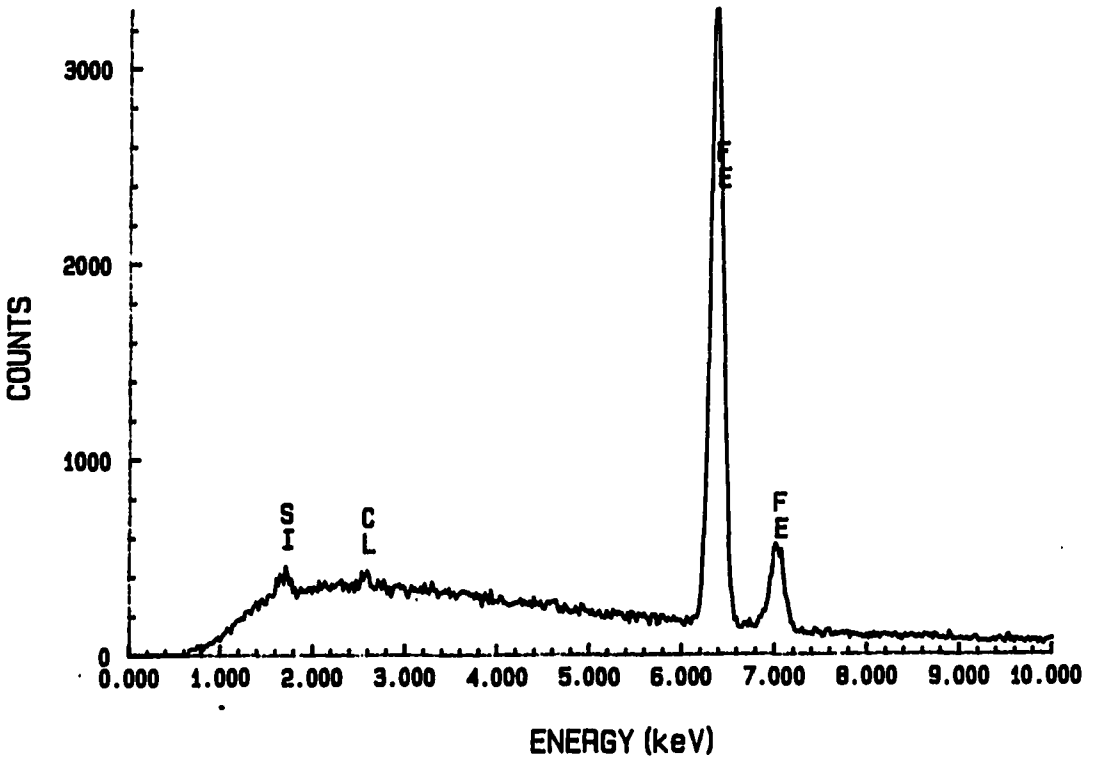

Figure 14. Typical EDS spectrum obtained from lepidocrocite-3M. No trace of impurities was observed. EDS was scanning at 1,000 magnification level and the spectrum was gained for 100 seconds

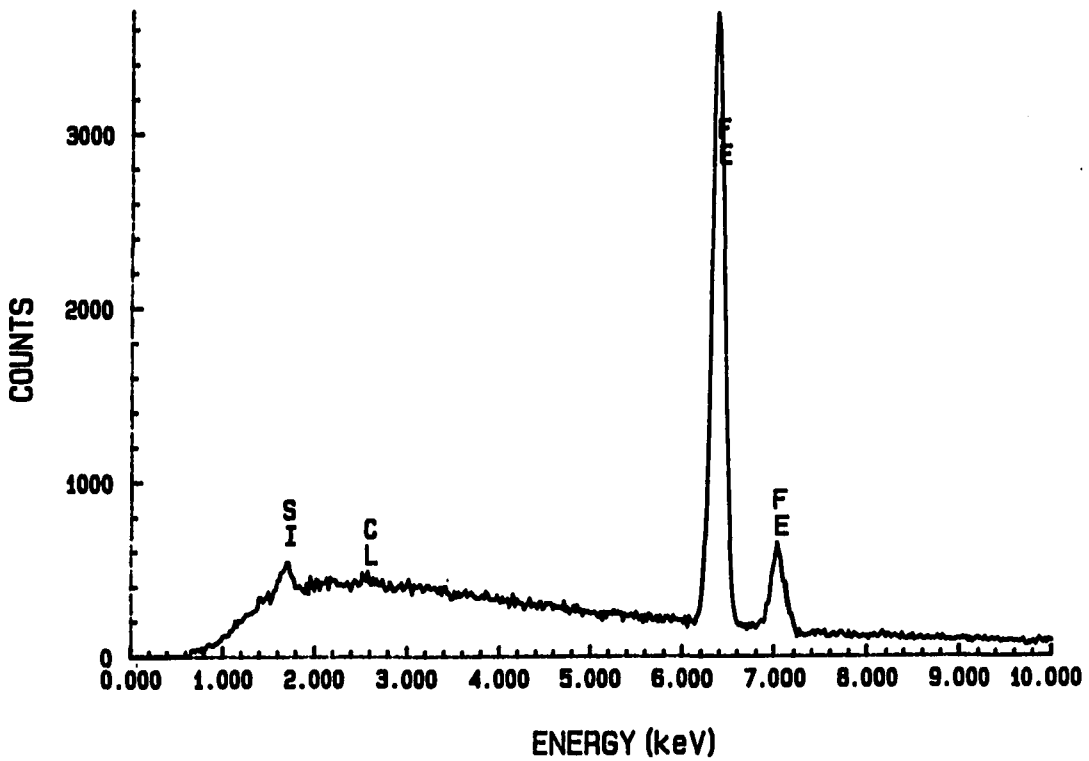

Figure 15. Typical EDS spectrum obtained from lepidocrocite-B&A. No trace of impurities was observed. EDS was scanning at 1,000 magnification level and the spectrum was gained for 100 seconds

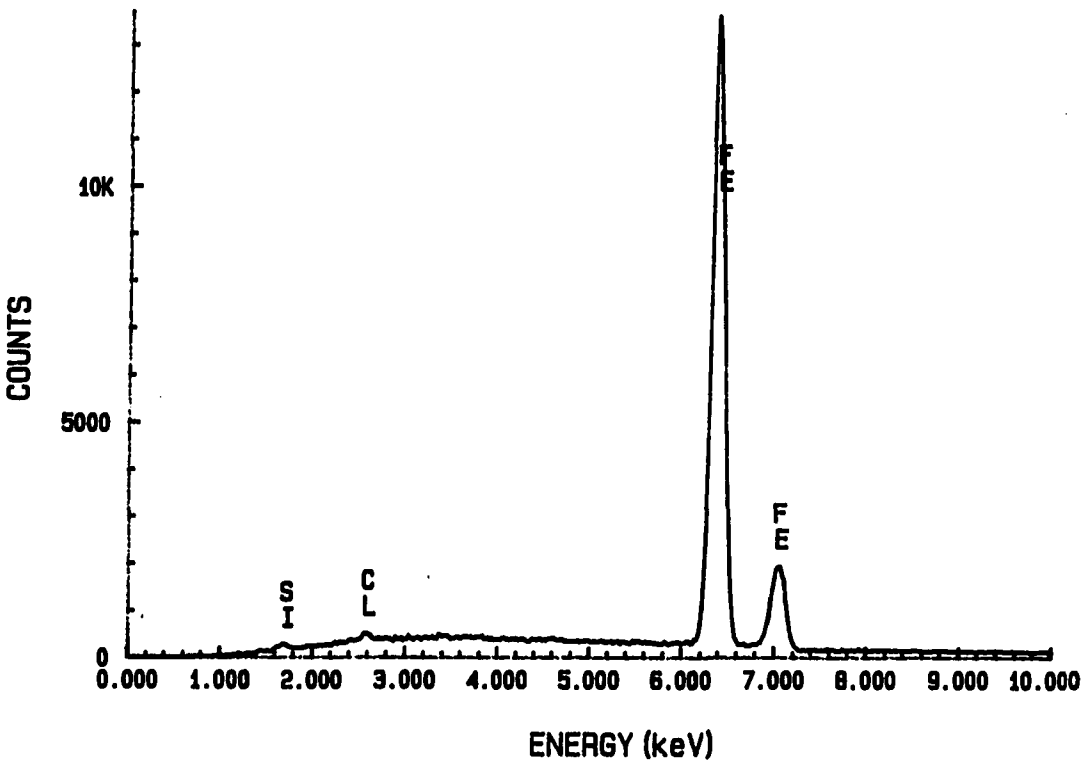

Figure 16. Typical EDS spectrum obtained from lepidocrocite-K. No trace of impurities was observed. EDS was scanning at 1,000 magnification level and the spectrum was gained for 100 seconds.

(a) At X10,000 Magnification Level

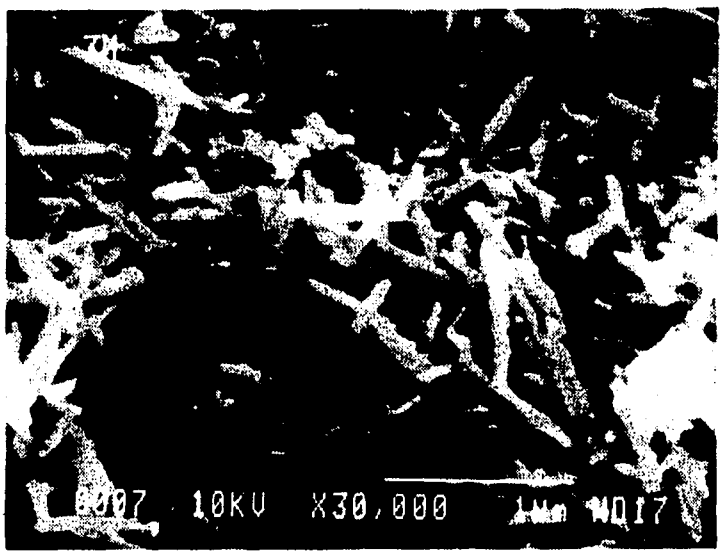

(b) At X30,000 Magnification Level

Figure 17. Microphotograph of lepidocrocite-3M

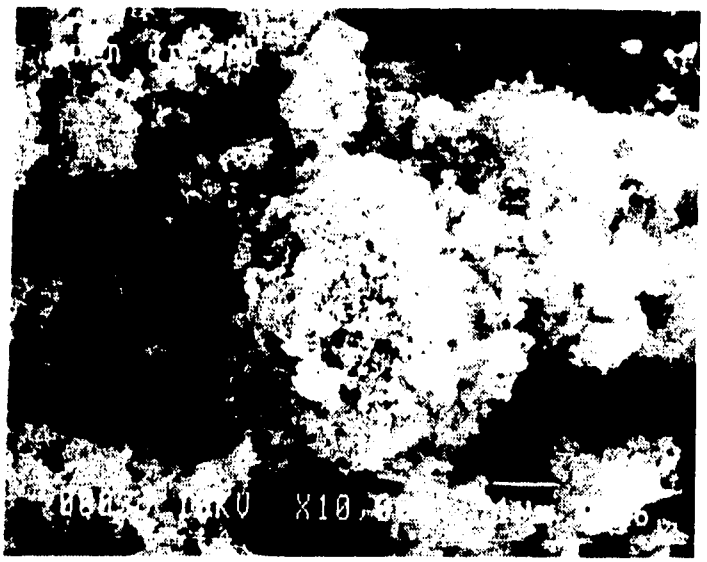

(a) At X10,000 Magnification Level

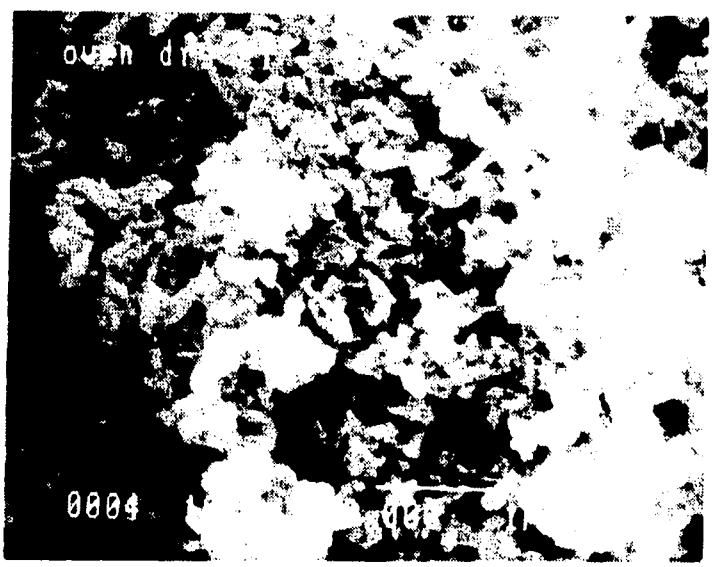

(b) At X30,000 Magnification Level

Figure 18. Microphotograph of lepidocrocite-B&A.

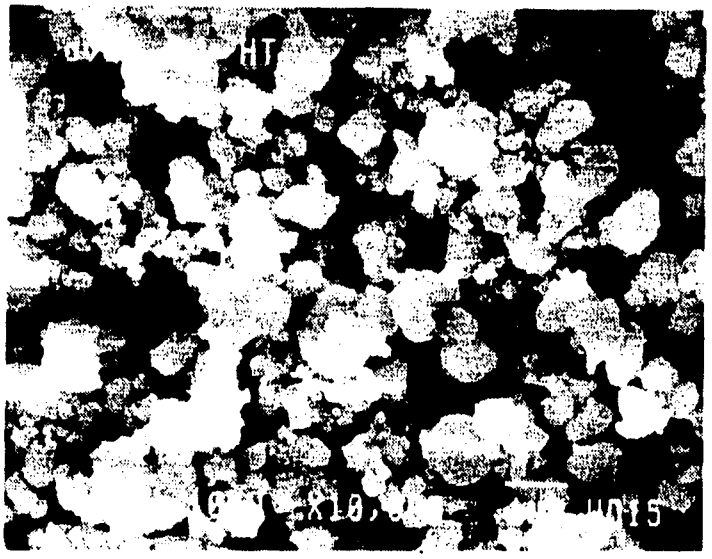

(a) At X10,000 Magnification Level

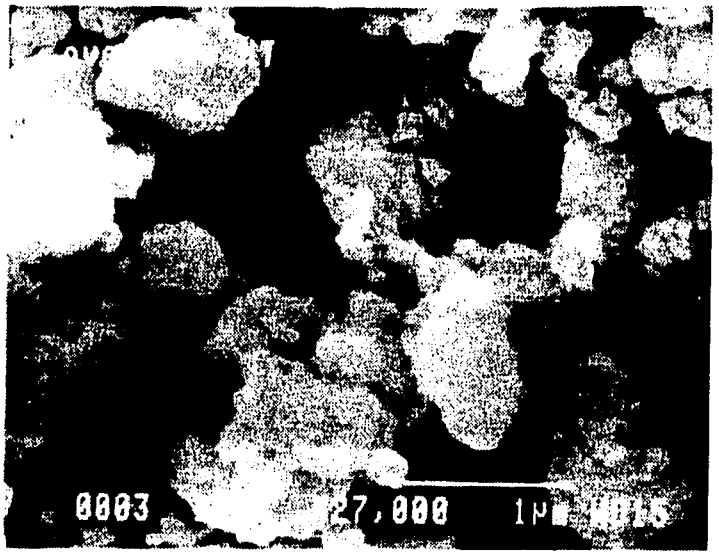

(b) At X30,000 Magnification Level

Figure 19. Microphotograph of lepidocrocite-K

over a long period of time. Naturally, it could be speculated that the crystal size of the compound from 3M Co. would be the largest of the three lepidocrocites. The pictures of the three lepidocrocites revealed that lepidocrocite can have morphology of agglomerated flocs as well as acicular crystals. Therefore, this study proved that microphotograph of lepidocrocite can show not only the sheet structure but various morphologies.

Average sizes of the crystals

The Scherrer equation has been accepted widely for use in calculating the average crystal size normal to the diffraction plane:

$$L = K \lambda/\beta \cos\theta \qquad \text{(IV-1)}$$

where

L = mean dimension normal to the diffracting plane (angstrom)

K = constant

λ = wavelength of the X-ray (angstrom)

β = diffraction line broadening at half maximum intensity (radian)

θ = diffracting angle with respect to the plane (degree)

The constant K, which depends on several factors including crystal shape, ranged from 0.7 to 1.7 by various investigators. However, it is not feasible to set a constant for a substance because the shape may vary within

the same sample as well as between samples, Klug and Alexander (1954) suggested setting the K equal to unity, which lead to an effective crystallite dimension derived by Stokes and Wilson (1942). The physical meaning of the effective crystallite dimension is the volume average of the crystallite dimension normal to the diffracting plane. The β could be obtained from the measured full width at half maximum intensity after the correction for the $K\alpha_2$ line and the equipment line broadening.

The applicability of the Scherrer equation to lepidocrocite has not yet been verified. The main uncertainty has been addressed to the constant, K. However, it was possible to determine the relative sizes of lepidocrocites by setting the K value equal to the unity for all three lepidocrocites. The mean crystal sizes normal to the (020) plane were calculated using the data in Table 1, 2, and 3 and the calculations are shown in Appendix C. The (020) plane was chosen because it was parallel to the (010) plane which Kaneko et al. (1975) postulated as the predominant plane. The wavelength was 1.54050 angstroms for the copper $K\alpha_1$ line and the θ was available by dividing the 2θ value of the (020) plane by 2, which were 7.035 degrees. The values of the full width at half maximum (FWHM) on the tables were corrected values for the Kα2 line and expressed in degrees. Thus, β was

obtained by subtracting the equipment broadening from the FWHM and converting it to radians. In turn, the line broadening by the equipment was attained from the X-ray diffraction pattern of the mica. Since mica usually forms a very large crystal, it is accepted that the line broadening of mica is negligible. Therefore, the FWHM value of the mica around the designated peak could be the line broadening caused by the equipment. The FWHM of mica at the 2θ of 8.8 degree was 0.194 degree. The calculated average crystal sizes were 254.8 angstrom for the lepidocrocites-3M, 158.2 angstrom for the lepidocrocite-B&A, and 102.3 angstrom for lepidocrocite-K.

As discussed, these crystal sizes might not be the precise values of the crystal sizes. However, the relative sizes of the three lepidocrocites are correct.

Surface areas of the lepidocrocites

The surface areas of three lepidocrocites were measured by the BET adsorption isotherm method using nitrogen gas at the liquid nitrogen temperature. The average surface area was 48.98 m^2/g (with standard deviation of 3.27 m^2/g) for lepidocrocite-3M, 118.45m^2/g (with standard deviation of 5.26 m^2/g) for lepidocrocite-B&A, and 150.28 m^2/g (with standard deviation of 0.78 m^2/g) for lepidocrocite-K. This wide variation in the surface area of the lepidocrocites agrees with the results of

others which range from 66 m^2/g to 171 m^2/g (Kaneko and Inouye, 1974, Kaneko et al., 1975, Kaneko and Inouyc, 1979, Sung, 1981).

The ratio of the surface area of the three lepidocrocites based on BET isotherms also agreed with that calculated from X-ray diffraction data. As calculated in the previous section, the ratio of crystal sizes, $L_K:L_{B\&A}:L_{3M}$, was approximately 1:1.55:2.50, where the subscript K, B&A, and 3M represented the lepidocrocite-K, lepidocrocite-B&A, and lepidocrocite-3M, respectively. Assuming that the crystal shapes of the three lepidocrocites are similar, the ratio of surface areas of the individual crystallites, which is a square function of ratio of sizes, $a_K:a_{B\&A}:a_{3M}$, was 1:2.40:6.25 and that of individual volume, which is a cube function of ratio of sizes, $v_K:v_{B\&A}:v_{3M}$, would be 1:3.7:15.4. Because the three had the same chemical composition, it would also be rational to presume that the three lepidocrocites had the same specific weight and thus, the same specific volume per unit mass even though they could have different void ratios. This implies that the number of the crystallites per unit mass should be inversely proportional to the individual volumes. Therefore, the ratio of number per unit mass, $N_K:N_{B\&A}:N_{3M}$, was 1:0.27:0.065. Finally, the ratio of area per unit mass, $A_K:A_{B\&A}:A_{3M}$, which is the

ratio of the product of number and individual area, became 1:0.65:0.41 whereas the ratio of area by the BET method was 1:0.79:0.33. When all the uncertainties involved were taken into account, there is relatively good agreement between the relative surface areas found from the BET data and those predicted from X-ray diffraction data.

Adsorption Experiments

Objective and scope of the experiments

These experiments were intended to investigate the adsorption capacities of the various lepidocrocites for ferrous iron. The adsorption data are presented using Freundlich isotherms. The effects of pH and the equilibrium concentration of ferrous iron on the adsorption capacity were analyzed by multiple regression of the data.

Materials and equipments

Doubly distilled water was used to prepare all reagents and for the adsorption experiments. All chemicals were A.C.S. analyzed reagent grade if not specified. The concentration of dissolved oxygen in the system was measured by D. O. meter before injection of the stock ferrous iron solution and the solution pH was monitored continuously throughout the experiment. The standard buffers for pH meter calibration were Fisher Scientific certified solutions which were traceable to the NBS

standards. The claimed error range was ±0.01 pH unit at 25 ^{o}C. Argon and carbon dioxide gases in conjunction of 1 N sodium bicarbonate ($NaHCO_3$) were utilized to buffer the system and to control the pH. The gases prepared by Cook's Inc. in Algona, Iowa were 99.996 % pure and were used without further purification. Spectrophotometry with a 5 cm cell was used for the colorimetric determination of the ferrous iron concentration. An atomic absorption spectrophotometer model 305B from Perkin-Elmer was also used from time to time to confirm that the results of the colorimetric determinations were not giving the totally wrong records because of an incorrect calibration or certain unnoticed malfunctions. Membrane filters of 0.45 μm pore size in conjunction with a vacuum pump were utilized to separate the solution phase from the suspension.

The layout of the system

Figure 20 shows the reactor setup for adsorption experiment. The reactor was a glass bowl with a lid. The capacity of the reactor was 2 liters and the lid had four openings. The center opening was for the glass stirring rod which was attached to a small mixer to keep the solid from settling to the bottom of the reactor. Two openings were used for the reference and glass junction electrodes of the pH meter. The fourth was for the glass gas-

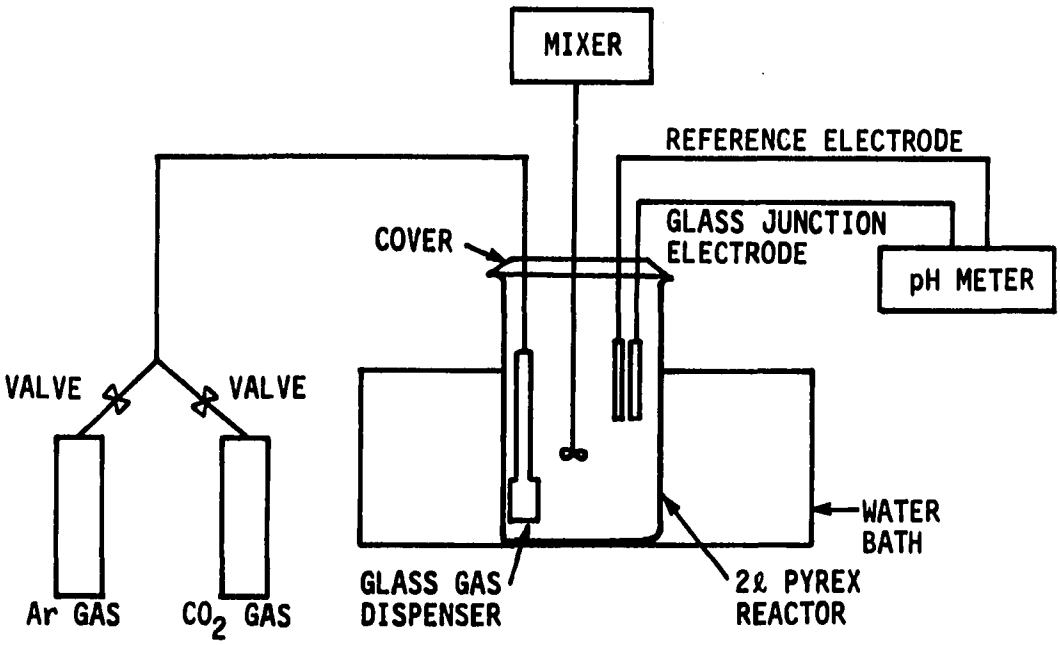

(a) Reactor Arrangement

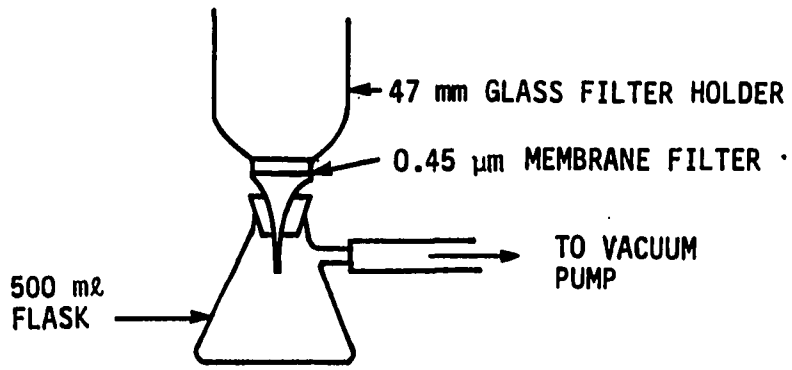

(b) Solid-liquid Separation

Figure 20. Setup for the adsorption experiments

dispenser through which the argon and carbon dioxide gases were bubbled into the system.

The buffer intensity of the system

The buffer intensity of the system was provided by 5 ml of 1 N sodium bicarbonate per liter of suspension. The flow rates of carbon dioxide and argon gases were adjusted to get the desired pH value. Carbon dioxide gas lowers the pH of the suspension as it is dissolved in the aqueous phase. On the other hand, argon gas raises the pH by stripping out the dissolved carbon dioxide gas. Stable pH values were obtained by adjusting the flow rates of the two gases.

Colorimetric determination of ferrous iron

The modified 1,10-phenanthroline method (Tamura et al., 1974) with one additional pre-treatment was used to determine the concentration of ferrous iron in the liquid phase. An aliquot from the adsorption reactor was vacuum filtered through a 0.45 μm membrane filter before it was acidified. This separation process was necessary not only because the acidifying of the suspension may cause desorption of the ferrous iron already adsorbed on the solid surfaces but also because the solids in suspension were settling causing errors in measurement. Although Tamura et al. pointed out that their modification was valid

up to 7 ppm of Fe(II) in 2500 ppm of Fe(III), this method didn't present any trouble at all up to 15 mg/l of ferrous iron after separation of the solids by the membrane filter.

The stepwise procedures including the separation process were as follows:

1. The vacuum filter holder was mounted to the flask and the flask was connected to the vacuum pump. Ten ml of redistilled water was filtered prior to filtering the sample to rinse the glass filter holder and the membrane filter. The filtrate was discarded.
2. One milliliter of 6 N H_2SO_4 was injected into the flask, so that the sample could be acidified at the moment it was filtered. Then, an aliquot of 10 ml from the reactor was filtered.
3. The acidified filtrate was transferred to a volumetric flask and 2 ml of 2 mol/l ammonium fluoride, 2 ml of 1 % 1,10-phenanthroline and 5 ml of ammonium acetate buffer were added. The filtrate was stirred vigorously after addition of each reagent.
4. The mixture was diluted 5, 10, or 20 times with redistilled water so that the resulting transmittance fell between 20 and 80 % when a 5 cm cell was used. It turned out that a dilution factor of 5 was good for iron concentrations less than 3 mg/l, 10 for concentrations from 3 to 7 mg/l, and 20 for

concentrations over 7 mg/l.

5. The iron concentration was determined after 15 minutes at a wavelength of 510 nm using 5 cm cells. The spectrophotometer was zeroed using the blank solutions which were prepared at the beginning of the adsorption experiment.

Preparation of stock iron solution

The 400 mg of electrolyte grade iron powder was placed in 200 ml of redistilled water to which 4 ml of 70 % concentrated perchloric acid was added. This was warmed on a hot plate until all the iron powder was dissolved. The solution was then filtered through 0.45 μm membrane filters and the ferrous iron concentration of the filtrate was measured using the modified 1,10-phenanthroline method. Redistilled water was added to the filtrate to make the ferrous iron concentration equal to 0.5 mg/ml.

Procedures of the adsorption experiment

The flow chart showing the stepwise order of conducting experimental procedures is shown in Figure 21. The procedures were:

1. All the glassware was soaked in 6N sulfuric acid for 24 hrs. The glassware was washed with laboratory detergent and rinsed with distilled water at least 4 times.

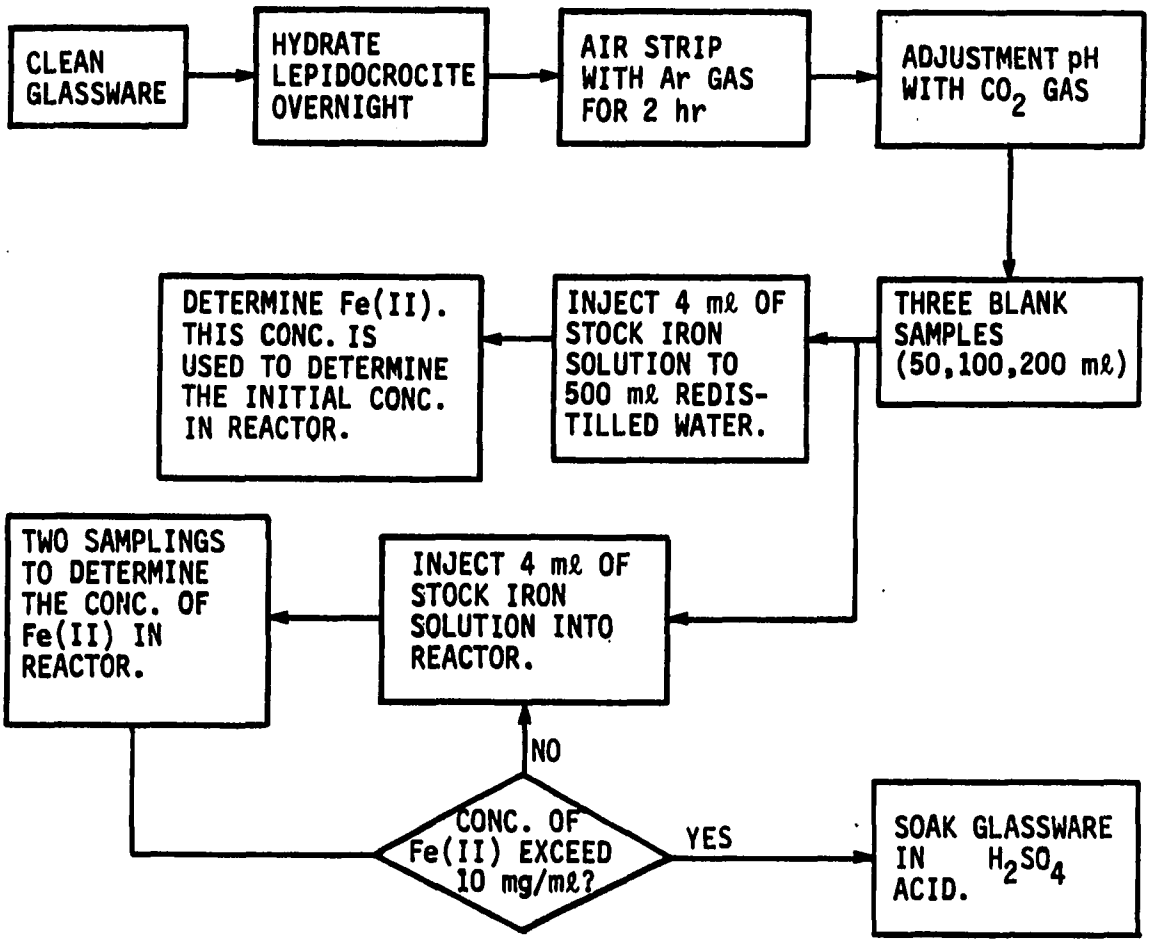

Figure 21. Flow chart for the adsorption experiments

2. One liter of redistilled water was transferred to the reactor and 200 mg of dry lepidocrocite (γ-FeOOH) was introduced in the reactor. The suspension was placed in a water bath and the solids were hydrated for at least 20 hours. The temperature of the water in the reactor was stable at 23 ^{o}C after 20 hours in the water bath.
3. After 20 hours of soaking, 5 ml of 1 N sodium bicarbonate ($NaHCO_3$) were added to buffer the system. The mixer with stirring rod was turned on to prevent the lepidocrocite solids from depositing on the bottom. Argon gas was bubbled into the suspension through the glass gas dispenser to strip out the dissolved oxygen. This oxygen stripping proceeded for at least 2 hours.
4. Carbon dioxide gas was bubbled into the suspension and the flow rate was adjusted to achieve the desired pH value.
5. A 10 ml aliquot of the reactor suspension was transferred to the vacuum filter by volumetric pipet and filtered through a 0.45 μm membrane filter. The filtrate was transferred to a 50-ml volumetric flask and the reagents were added according to the modified 1,10-phenanthroline method (Tamura et al., 1974). This treated aliquot was diluted to 50 ml and utilized

as one of the blanks in colorimetric determination of the ferrous iron concentration.

6. Step 5 was repeated two more times. Every detail was the same except that the filtrates were transferred to 100-ml and 200-ml volumetric flasks. They also were used as blanks. Thus, three blanks at different dilution levels were prepared before the injection of stock iron solution.
7. Four ml of stock iron solution, whose concentration was about 0.5 mg Fe^{++}/ml, was injected into the reactor suspension. The pH of the system dropped because the stock iron solution was a strong acidic solution. The flow rate of argon gas was adjusted to raise the pH to the desired value.
8. Four ml of stock iron solution was injected into the separated 500 ml of redistilled water acidified by 1 ml of 6 N sulfuric acid. The ferrous iron concentration of this solution was measured to determine the injected iron concentration.
9. Ten ml of reactor suspension was transferred to the vacuum filter and filtered through a 0.45 μm membrane filter 30 minutes after pH equilibrium was obtained. The filtrate was acidified by 1 ml of 6 N sulfuric acid which had already been injected into the receiving flask prior to the filtration of the 10 ml

sample. The acidified filtrate was transferred to a 50-ml volumetric flask. Reagents of the modified 1,10-phenanthroline method were added to develop color and the mixture was diluted to 50 ml.

10. The filter holder and the flask were rinsed with acidified distilled water (0.001 N H_2SO_4) and the membrane filter was replaced. Another 10 ml of suspension was filtered, treated to develop color, and diluted to 50 ml. Thus, two samples were prepared at that specific concentration.
11. Step 8, 9, and 10 were repeated four more times so that samples at five different concentrations could be obtained. At the higher concentrations, the filtrates were diluted to 100 or 200 ml so that the transmittance through the 5 cm cell could fall between 20 % and 80 %.
12. Each sample was stored for fifteen minutes to develop color fully before it was analyzed for ferrous iron concentration using the spectrophotometer. The wavelength of the light beam was 510 nm and the 5 cm spectrophotometer cell was used. Before reading sample transmittance, the spectrophotometer was standardized using the blank solutions which were prepared in steps 5 and 6.
13. After the experiment was done, all glassware was

soaped, washed, and then soaked in 6 N sulfuric acid.

Adsorption of ferrous iron by membrane filter

Adsorption of ferrous iron by membrane filters was noticed during the adsorption experiments. For the calibration purpose, standard solutions at concentrations of 0.3, 0.4, 0.6 and 0.7 mg ferrous iron /liter of solution were prepared following Standard Methods (1985). The transmittances of the standard solutions were measured for each concentration and used to prepare a calibration curve. The transmittance of the sample from the reactor was read on the calibration curve to determine the concentration of ferrous iron in the reactor.

However, the transmittances of the standard solutions without filtering through a 0.45 μm membrane filter were approximately 96.5 % of those after filtering, which meant that the filtration process reduced transmittances by about 3.5 %. Among all suspected causes, the adsorption of ferrous iron by the membrane filters was the most logical. The aerial oxidation of ferrous iron during or after filtration was not likely because the filtration took only several seconds and the receiving flask contained 1 ml of 6 N sulfuric acid before filtration started, enough to keep the iron in the ferrous form.

The calibration curve in the adsorption experiments was prepared using the standard solutions without

filtration through a 0.45 μm membrane filter. Therefore to correct for this problem, the transmittances of the samples from the reactor were multiplied by 0.965 before being projected to the calibration curve.

Adsorption isotherms

Adsorption isotherms are a very convenient way of presenting the variation of adsorption with respect to the concentration of adsorbate in the bulk solution at constant temperature. Langmuir (1918) derived the first isotherm model by assuming single layer adsorption, constant energy of adsorption, and no transmigration of adsorbate on the surface. However, adsorption may occur on more than a single layer. By assuming continuous condensation of adsorbates over the monolayer, Brunauer et al. (1938) developed a multi-layer adsorption model which has been known as BET model. The BET model is reduced to the Langmuir equation when the adsorption is limited to the first layer of adsorbate.

The Langmuir and BET models were deduced from either kinetic considerations or from the thermodynamics of adsorption. Another isotherm has been derived empirically by Freundlich (1926) and recently rationalized on theoretical grounds (Adamson, 1967). While the Langmuir equation (Langmuir, 1918) assumes uniform energy of adsorption throughout the surface and the BET equation

rests on a basic assumption of uniform condensation energy beyond the first layer, the Freundlich equation is a special case where the surface energy varies as a function of surface coverage due to variations in the heat of adsorption. The Freundlich isotherm agrees quite well with the Langmuir equation and experimental data over moderate ranges of concentration. The advantages of the Freundlich equation over the BET model could be that its parameters are easier to use in experiments or in design practices and it implies variation of adsorption energy as a function of surface coverage.

The general form of Freundlich equation is as follow:

$$q_e = K\, C^{1/n} \qquad \text{(IV-2)}$$

where

q_e = amount of solute adsorbed per unit weight of adsorbent at the equilibrium concentration of C (mg/g or mole/g)

C = concentration of solute in bulk solution at equilibrium (mg/g or mole/g)

K = constant related to the adsorptive capacity

n = constant related to the adsorption intensity

This transforms in logarithmic form to;

$$\log q_e = \log K + (1/n) \log C \qquad \text{(IV-3)}$$

Therefore, the plot of log q_e vs. log C would give a straight line whose slope is 1/n and intercept is log K at C=1.

Adsorption model

The results of the adsorption experiments conducted in this study have been presented as Freundlich isotherms and analyzed using multiple regression techniques. However, some modification of the Freundlich equation was necessary to represent the effects of adsorbent surface area and solution pH.

The term q_e in the Freundlich equation stands for the amount of solute adsorbed per unit weight of adsorbent at the equilibrium concentration, C. If the adsorbent in question is so unique as to have about the same surface area per unit used at all times, the term q_e may be a convenient form for use in design or in practice. The lepidocrocites used in this research, however, had quite different surface areas per unit weight depending on how they were prepared. Since adsorption phenomena depend heavily on the available surface sites, the term q_e was not adequate to interpret the resulting data of these adsorption experiments. Therefore, the term q_a was used to represent the amount of solute adsorbed per unit surface area of the adsorbent.

The Freundlich equation does not contain any term reflecting any pH effect on adsorption. It implies that the constants obtained from any experiment are valid only at the pH of the experiment. However, the present study

was designed to obtain the constants which could be used in adsorption experiments conducted at various pH values; therefore, a term for accounting for pH effects has been included in the modified model. The model is;

$$q_a = (K_1 C^{1/n})/[H^+]^{Ko} \qquad \text{(IV-4)}$$

where

q_a = amount of solute adsorbed on a unit surface area of the adsorbent, mg/m^2 (in arithmetic form, $((C_o-C)/(m A))$

C_o = injected concentration of ferrous iron, mg/l

C = concentration of ferrous iron in bulk liquid phase at equilibrium, mg/l

m = weight of adsorbent per liter of suspension, g/l

A = surface area per unit weight of adsorbent, m^2/g

K_1, K_o, n = constants

In the above model, the term q_a corresponds to q_e/A. Furthermore, at a fixed pH, the term of $[H^+]^{Ko}$ should be a constant. Thus, the above model is a Freundlich equation whose constant K is replaced by $A K_1/[H^+]^{Ko}$.

In logarithmic form, it becomes;

$$\log q_a = \log K_1 + (1/n) \log C - K_o \log [H^+]$$

$$= \log K_1 + (1/n) \log C + K_o \text{ pH} \qquad \text{(IV-5)}$$

The values of $\log K_1$, $(1/n)$, and K_o can be obtained by multiple regression without difficulty. The corresponding regression model is:

$$Y = B_o + B_1X_1 + B_2X_2 \qquad \text{(IV-6)}$$

The dependent variable, Y, was log q_a and X_1 and X_2 were log C and pH, respectively. Bo, B1, and B2 correspond to log K_1, (1/n), and K_o. The multiple regression can be made either by a stepwise method or by forcing both variables to enter the regression.

Plots of adsorption isotherms and multiple regression

As mentioned in the previous section on objectives and scopes, the adsorption capacities of the three lepidocrocites for ferrous iron have been investigated. The concentration of ferrous iron varied from approximately 2 to 10 mg/l and the solution pH from 6 to 6.75, which would cover most well water situations. The Freundlich isotherms of log q_a vs. log C have been presented in Figures 22, 23, and 24.

Multiple regression of the adsorption data were calculated using SPSS/PC$^+$, a computer program distributed by SPSS Inc. The log q_a was set as dependent variable and both pH and log C were forced to enter as independent variables. Major parameters obtained were coefficients of the model, 95 % confidence intervals on each coefficient, and the coefficient of determination. They are tabulated in Table 5.

The models for the three lepidocrocites developed are as follows:

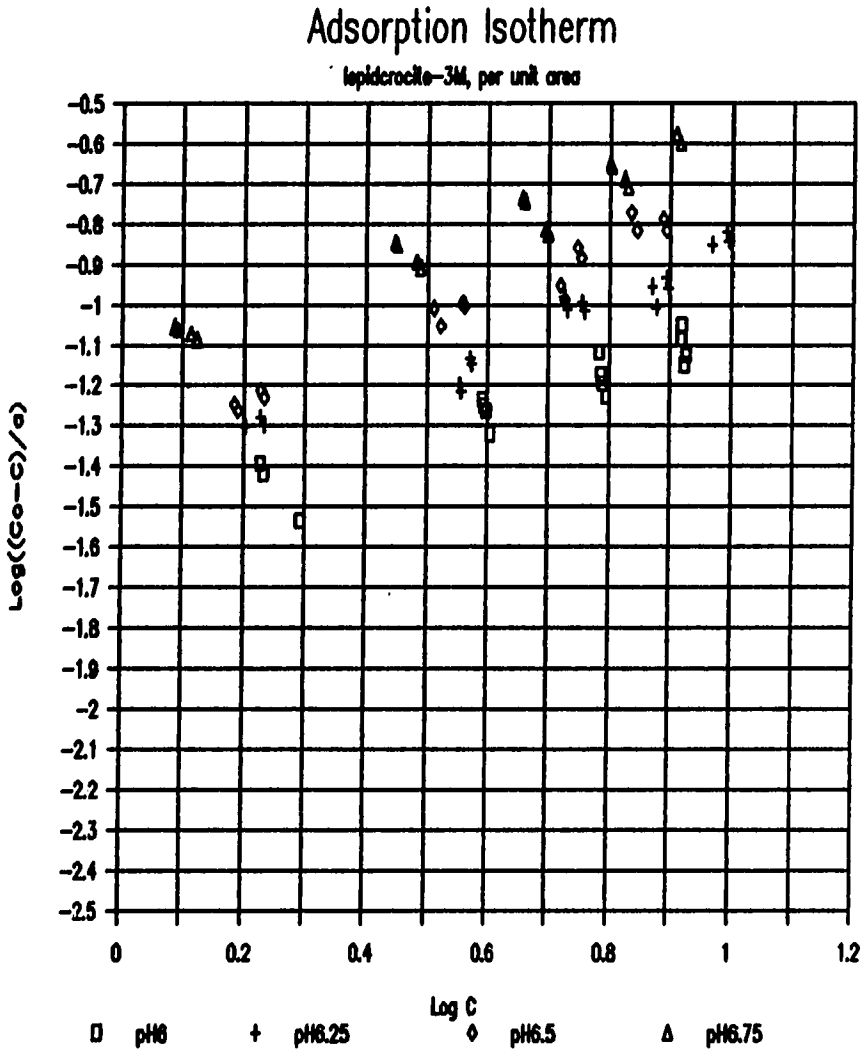

Figure 22. Adsorption isotherm for lepidocrocite-3M based on unit surface area (1 m^2). (log q_a vs. log C)

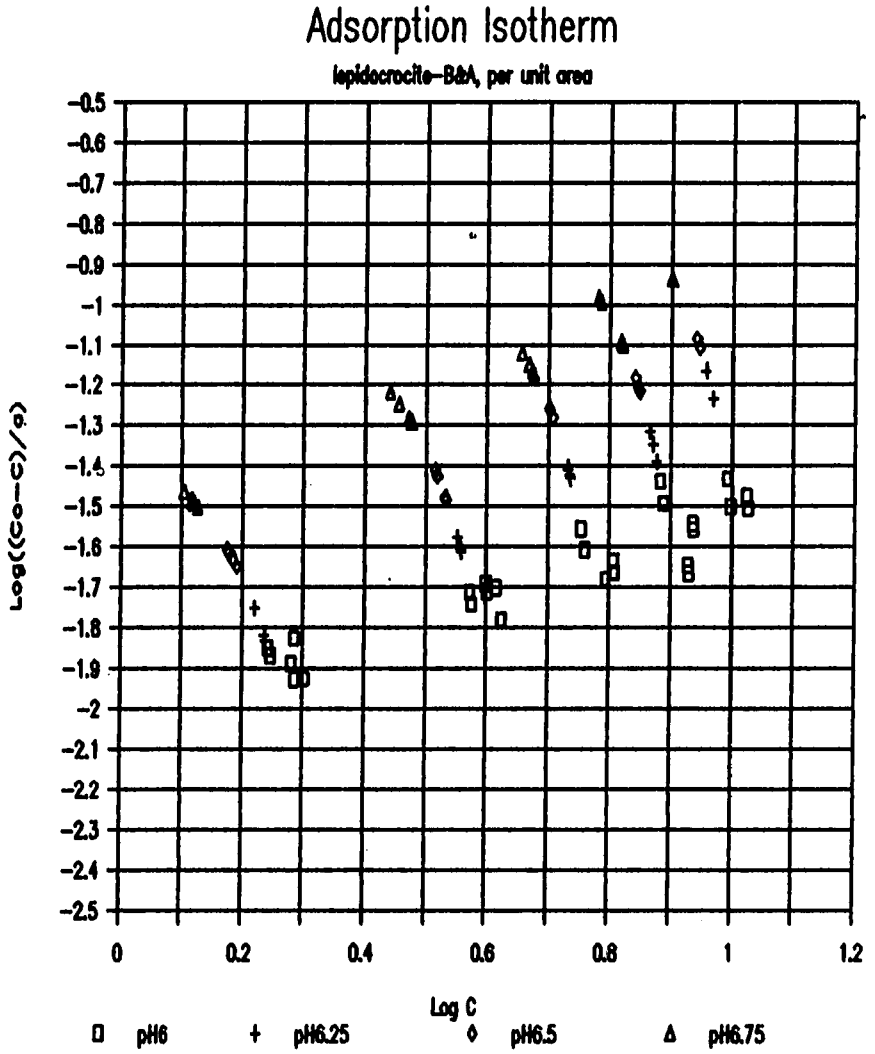

Figure 23. Adsorption isotherm for lepidocrocite-B&A based on unit surface area (1 m^2). (log q_a vs. log C)

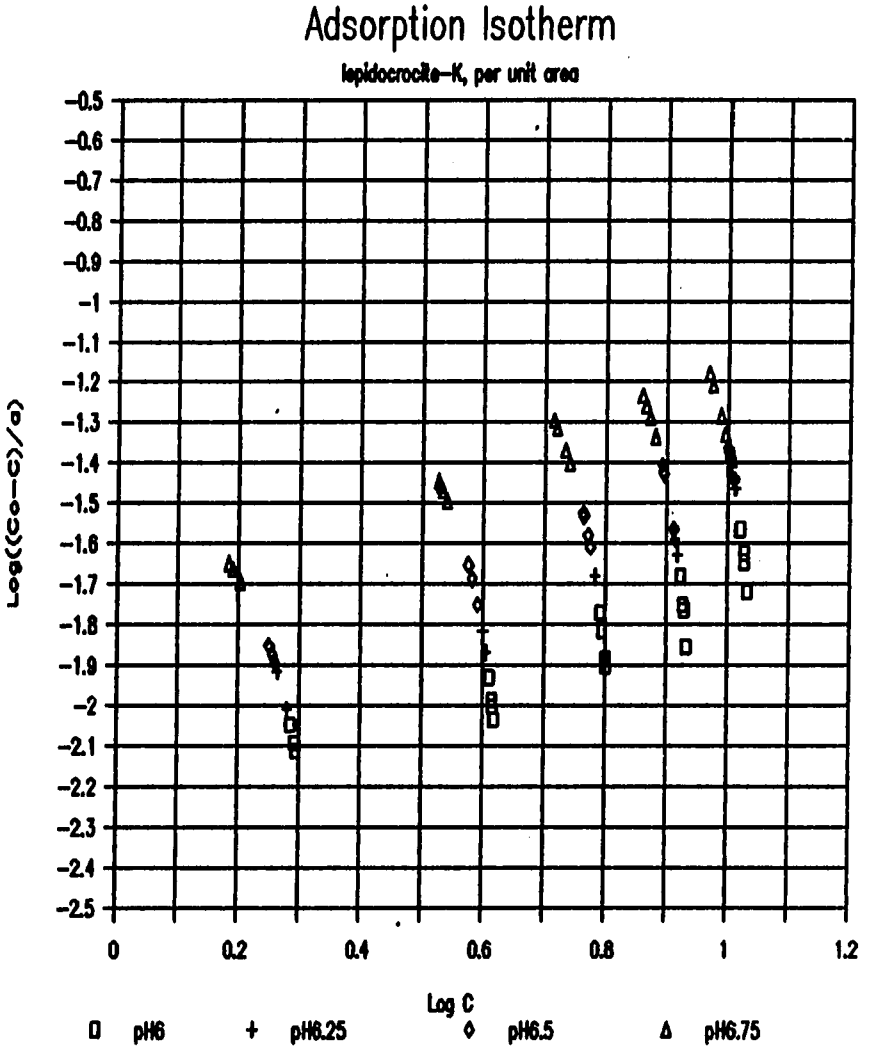

Figure 24. Adsorption isotherm for lepidocrocite-K based on unit surface area (1 m^2). (log q_a vs. log C)

Table 5. Parameters resulting from multiple regression of adsorption data

Parameters	Lepidocrocite -3M	-B&A	-K
No. of data pts.	69	82	80
R^2	0.956	0.955	0.935
Standard error	0.046	0.054	0.062
Variable			
1/n	0.576	0.632	0.608
K_o	0.615	0.738	0.648
$\log K_1$	-5.306	-6.529	-6.195
95% C.I. on			
1/n	0.534-0.617	0.586-0.677	0.556-0.660
K_o	0.575-0.656	0.696-0.780	0.598-0.697
$\log K_1$	-5.570--5.041	-6.802--6.257	-6.518--5.872

$$\log q_a \text{ (lepidocrocite-3M)} = -5.306 + 0.576 \log C + 0.615 \text{ pH} \qquad \text{(IV-7)}$$

$$\log q_a \text{ (lepidocrocite-B\&A)} = -6.529 + 0.632 \log C + 0.738 \text{ pH} \qquad \text{(IV-8)}$$

$$\log q_a \text{ (lepidocrocite-K)} = -6.195 + 0.608 \log C + 0.648 \text{ pH} \qquad \text{(IV-9)}$$

The units of variables in the above equations are the same as those in equation (IV-4).

Analysis of the results of regression

From plots of the data, it was not difficult to conclude that the three lepidocrocites had different adsorption capacities for ferrous iron per unit surface area. The amounts of adsorbed ferrous iron on the unit surface areas of lepidocrocites were calculated from the regression model of each lepidocrocite and tabulated in Table 6. Instead of having the same or even close adsorption capacities, the amount of adsorption by lepidocrocite-K was about one fifth of that by lepidocrocite-3M. Lepidocrocite-B&A showed approximately one third the capacity of lepidocrocite-3M for ferrous iron adsorption.

The plots raised at least two questions to be discussed. Why were the adsorption capacities for ferrous iron per unit surface area unequal for the three lepidocrocites. Why did the lepidocrocite which had the

Table 6. Comparison of the adsorption capacity of three lepidocrocites by regression model

pH	[Fe(II)] (mg/l)	Adsorbed Fe(II) (mg/m2) lep.-3M	lep.-B&A	lep.-K
6.00	2.00	0.036	0.012	0.008
6.00	4.00	0.054	0.019	0.011
6.00	6.00	0.068	0.025	0.015
6.00	8.00	0.080	0.029	0.017
6.00	10.00	0.091	0.034	0.020
6.25	2.00	0.051	0.019	0.011
6.25	4.00	0.077	0.029	0.017
6.25	6.00	0.097	0.038	0.021
6.25	8.00	0.114	0.045	0.025
6.25	10.00	0.130	0.052	0.029
6.50	2.00	0.073	0.029	0.016
6.50	4.00	0.109	0.045	0.024
6.50	6.00	0.138	0.058	0.031
6.50	8.00	0.163	0.069	0.037
6.50	10.00	0.185	0.079	0.042
6.75	2.00	0.104	0.044	0.023
6.75	4.00	0.156	0.068	0.035
6.75	6.00	0.197	0.088	0.045
6.75	8.00	0.232	0.106	0.053
6.75	10.00	0.264	0.121	0.061

smallest surface area have the largest adsorption capacity per unit surface area and vice versa?

As the Freundlich equation implies, the available adsorption sites on the crystal surface might be distributed in a logarithmic manner. The surface areas were 48.98 m^2/g, 118.45 m^2/g, and 150.28 m^2/g for lepidocrocite-3M, lepidocrocite-B&A, and lepidocrocite-K, respectively. Therefore, the logarithmic ratio of the surface area per unit weight was 1:1.227:1.288. The ratio of the adsorbed ferrous iron per unit weight of lepidocrocite should perhaps have been approximately the same, 1:1.227:1.288, if the BET surface area properly represented the surface area for ferrous iron adsorption. Thus, by dividing the ratio by each surface area, the ratio of adsorbed ferrous iron per unit surface area should be (1/48.98) : (1.227/118.45) : (1.288/150.28) which was 1:0.51:0.42 for the lepidocrocite-3M, the lepidocrocite-B&A, and the lepidocrocite-K, respectively. However, the ratio from the experiments did not correlate well with the calculated ratio, which was approximately 1:0.30:0.22.

This fact indicated that all the surface available for adsorption of nitrogen gas molecules was not available for ferrous iron adsorption. In other words, accessibilities of adsorption sites to different adsorbates were distinctive.

Possibly, the ferrous iron adsorbed and accumulated at the pore entrance resulting in clogging the pore, which, in turn, prohibits further access to the adsorption site inside the pore. The size of the adsorbate could be another main reason for controlling site accessibility. The effective diameter of the hydrated ferrous iron in water was calculated by Kielland (1937) and reported as 6 angstrom. The reported Van der Waal's radius of nitrogen is only 1.5 angstroms (CRC Handbook of Chemistry and Physics, 1985-1986) whereas 16.2 sq. angstroms is generally accepted as the cross sectional area of the nitrogen molecules (McClellan and Harnsberger, 1967). From both approaches, the diameter of the nitrogen molecule must be between 3 and 4.02 angstroms. When the difference in size between the nitrogen and iron is taken into account, it was natural that certain adsorbent surface area between narrow pores is not even approachable by the ferrous iron whereas they were accessible to the nitrogen molecules. Therefore, the surface areas measured using nitrogen gas can not properly represent the surface areas for the ferrous iron adsorption. The adsorption capacity of the lepidocrocites may depend more on their pore size distribution.

If adsorbent pore size distribution is a determining factor for adsorption capacity, it can be deduced that every lepidocrocite may have a discrete capacity for

ferrous iron adsorption because no two lepidocrocites likely will have the same pore distributions. Thus, it was not strange that the three lepidocrocites had different adsorption capacities for ferrous iron.

From the view point of the discussed hypothesis of the effects of pore size distribution on adsorption capacity, the fact that the lepidocrocite-K had the smallest capacity among them was understandable because it had the smallest crystal size and thus, not necessarily but probably, had more narrow pore distributions. Therefore, the ratio of the available surface for ferrous iron to total BET surface calculated using nitrogen gas was smaller than that of the lepidocrocite-3M, which resulted in lower adsorption capacity per unit surface area.

Besides the physical characteristics of lepidocrocites, differences in chemical potentials between each of the lepidocrocites in suspension might be a possible factor explaining their different behavior in ferrous iron adsorption. However, that is unlikely because they had the same chemical compositions and same structural arrangements.

The adsorption model per unit weight

As discussed, no two lepidocrocites necessarily have the same capacities for ferrous iron adsorption because of variation in their surface area per unit weight and

characteristic distributions of the pore size. In fact, the adsorption capacities of the three lepidocrocites varied by as much as five times. Therefore, it was less favorable from the scientific view point to determine the quantitative adsorption model without further understanding pore size distribution and other related surface characteristics. From the view point of an engineer, however, it might be interesting to examine the adsorption capacities of the three lepidocrocites on the basis of their unit weight.

The data from adsorption experiments were organized to show the amount of adsorbed ferrous iron per unit weight of each lepidocrocite and are presented in Figures 25, 26, and 27. The data were then reorganized to compare the capacities of the three lepidocrocites at each pH value. The reorganized data are shown in Figures 28, 29, 30, and 31.

As expected, the capacities were not proportional to either the arithmetic ratio or the logarithmic ratio of their surface areas. In fact, lepidocrocite-K which had the largest surface area showed the smallest adsorption capacity of all. However, the three lepidocrocites had very close ferrous iron adsorption capacities per unit weight. The three lepidocrocites had very distinctive morphologies and a wide range in their surface areas,

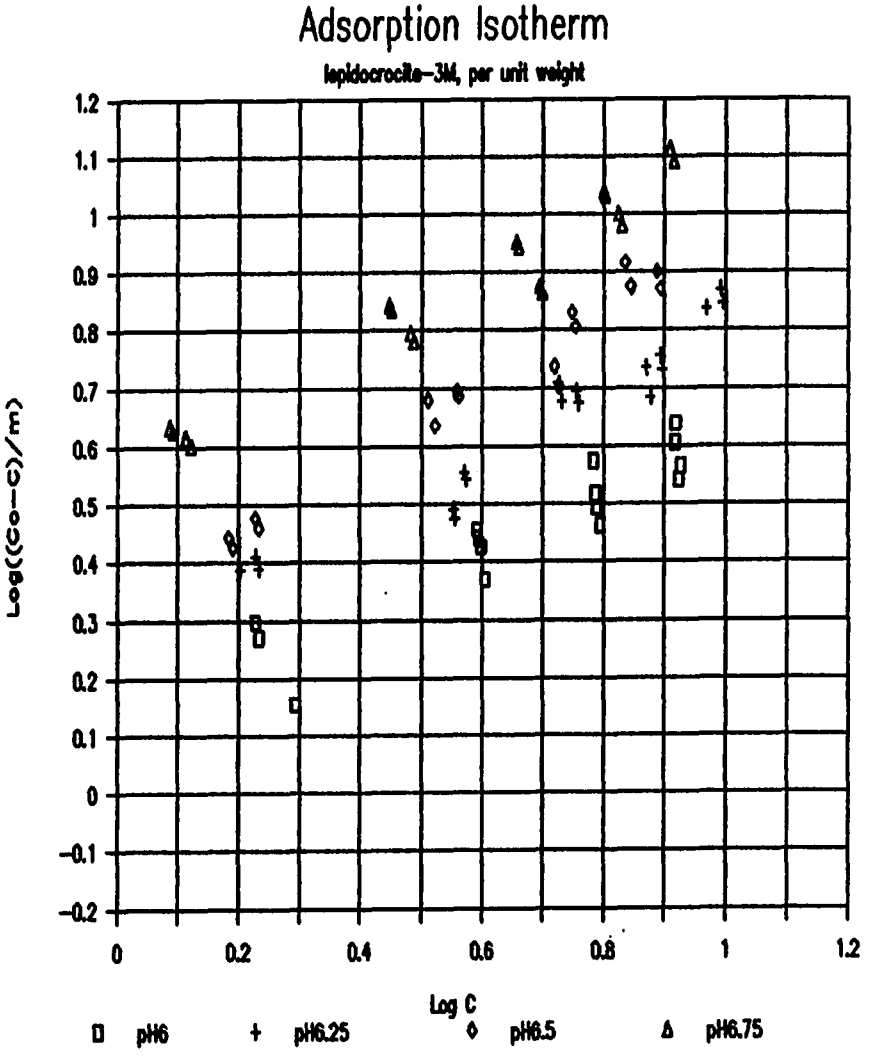

Figure 25. Adsorption isotherm for lepidocrocite-3M based on unit weight (1 g). (log q_e vs. log C)

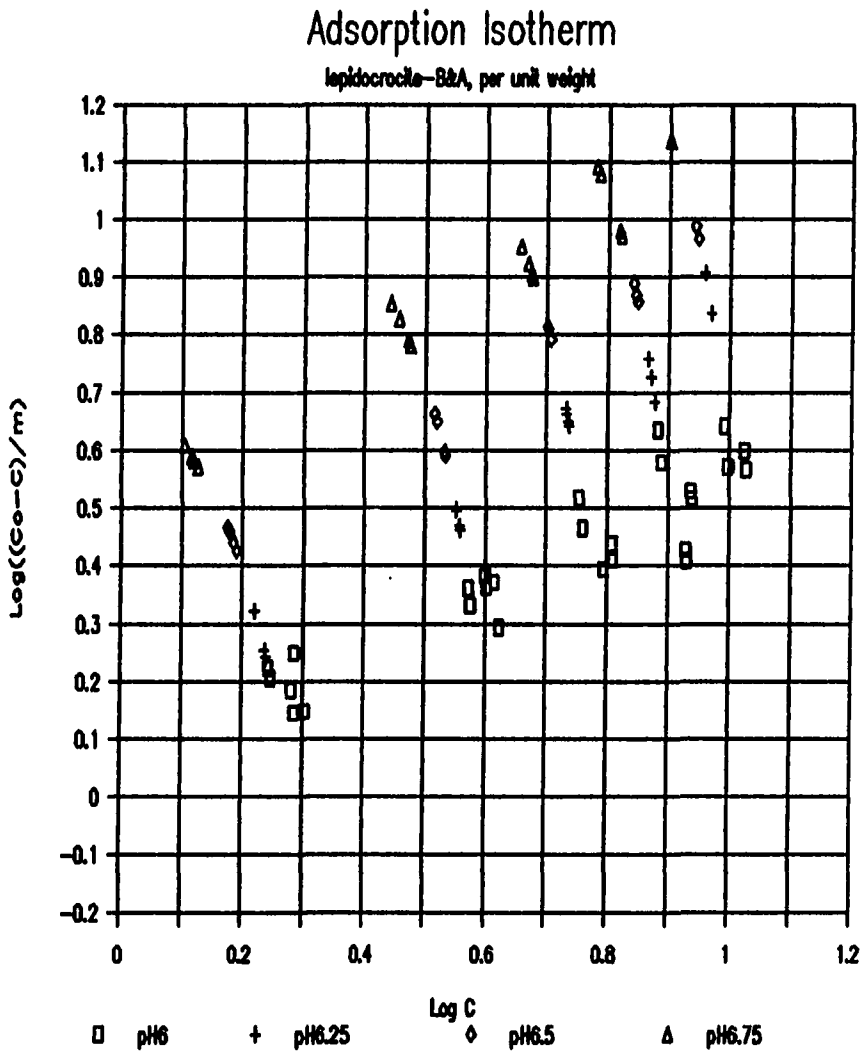

Figure 26. Adsorption isotherm for lepidocrocite-B&A based on unit weight (1 g). (log q_e vs. log C)

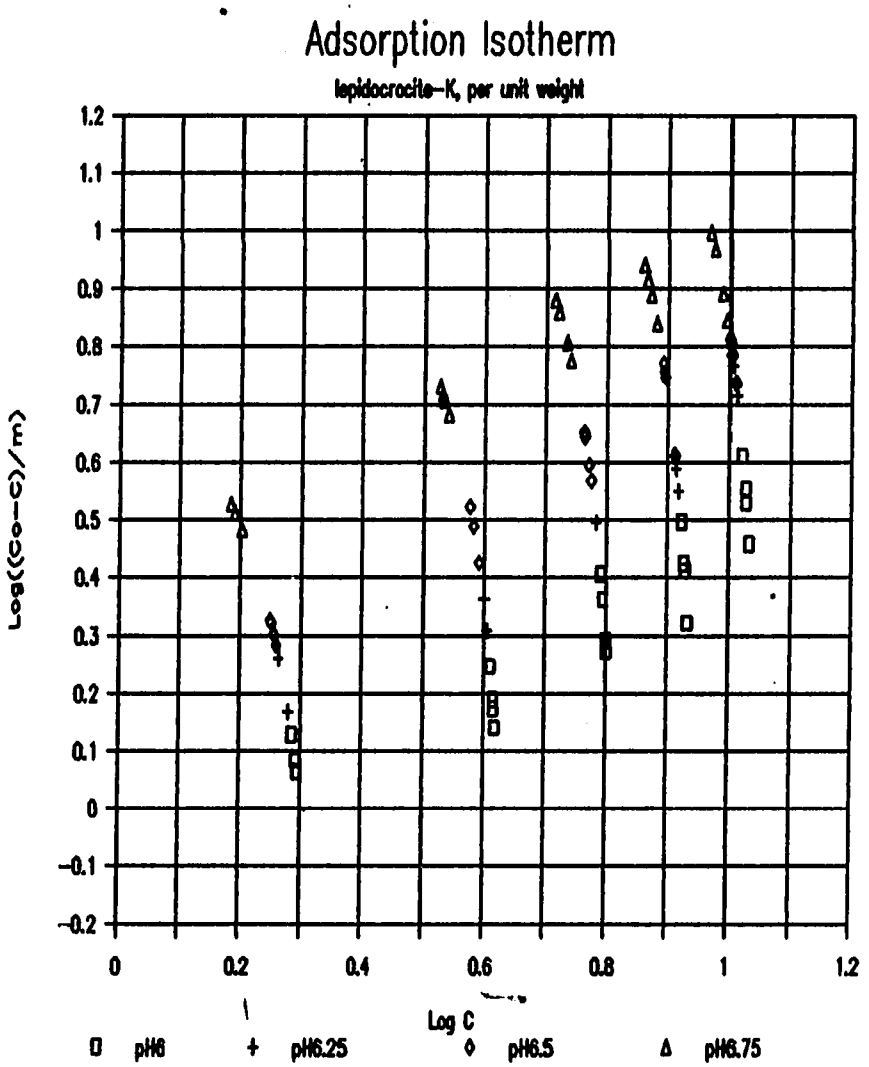

Figure 27. Adsorption isotherm for lepidocrocite-K based on unit weight (1 g). (log q_e vs. log C)

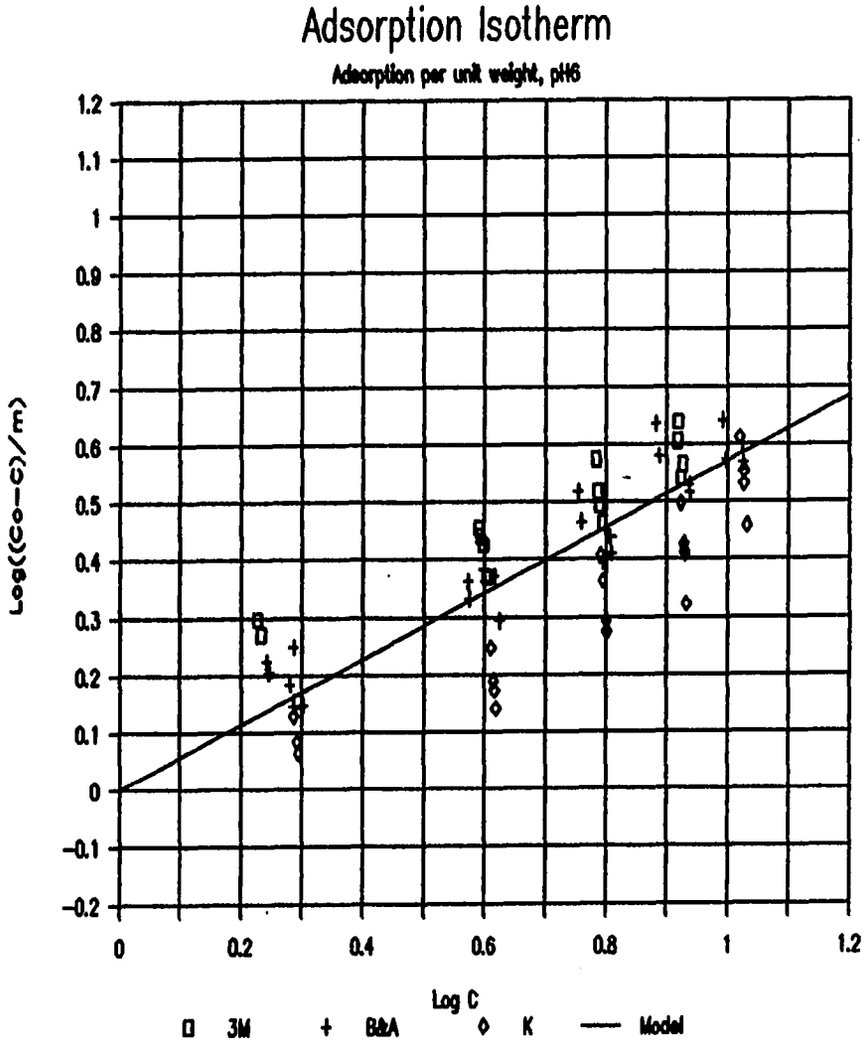

Figure 28. Adsorption isotherm for the three lepidocrocites at pH 6. The line in the plot represents predicted values by the regression model based on unit weight. (log q_e vs. log C)

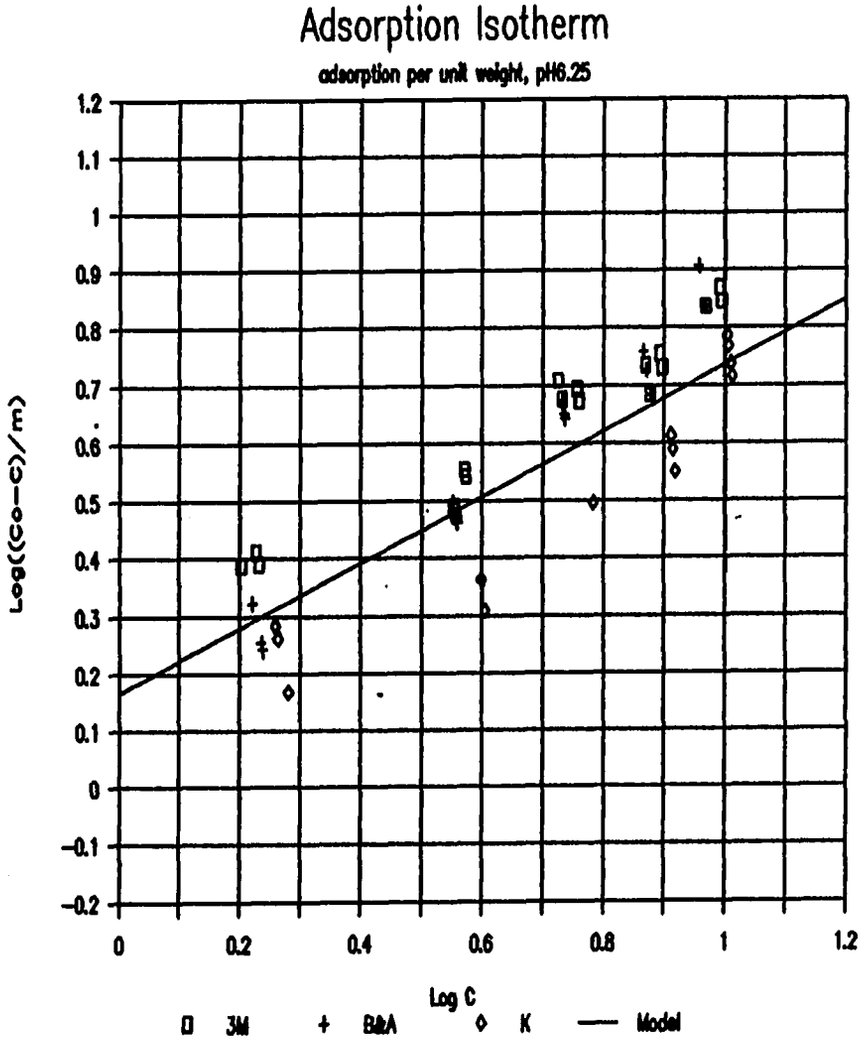

Figure 29. Adsorption isotherm for the three lepidocrocites at pH 6.25. The line in the plot represents predicted values by the regression model based on unit weight. (log q_e vs. log C)

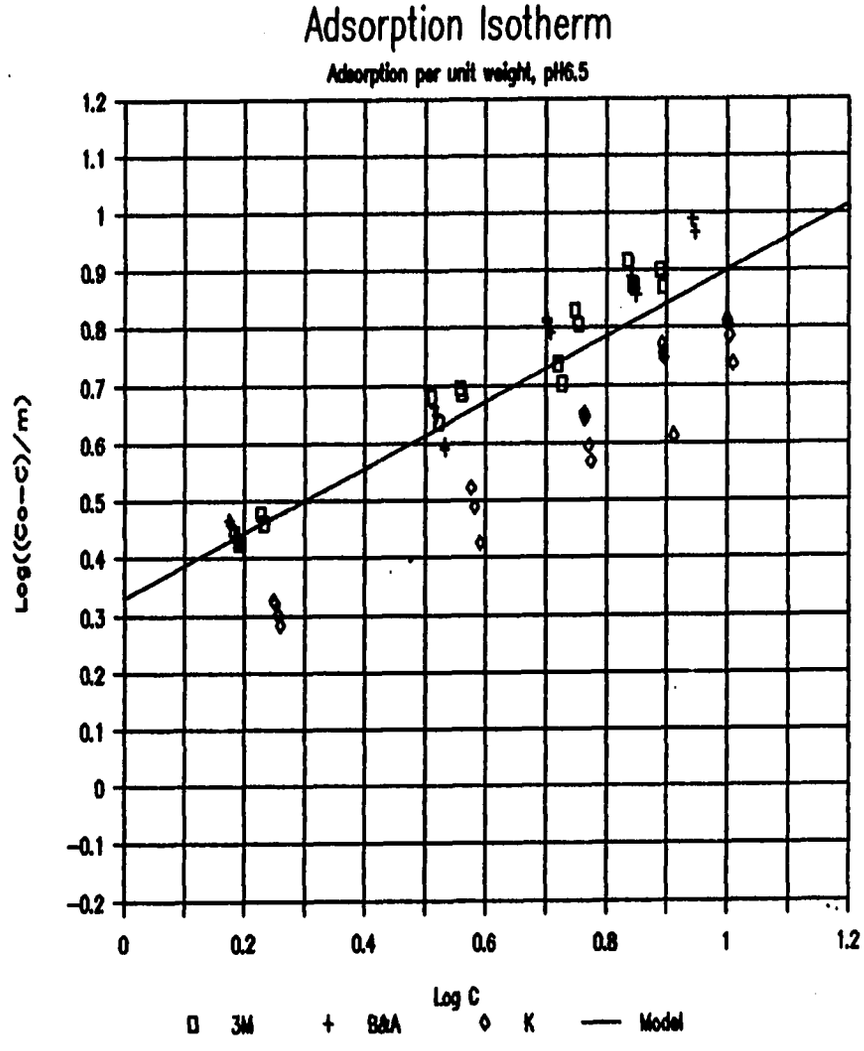

Figure 30. Adsorption isotherm for the three lepidocrocites at pH 6.5. The line in the plot represents predicted values by the regression model based on unit weight. (log q_e vs. log C)

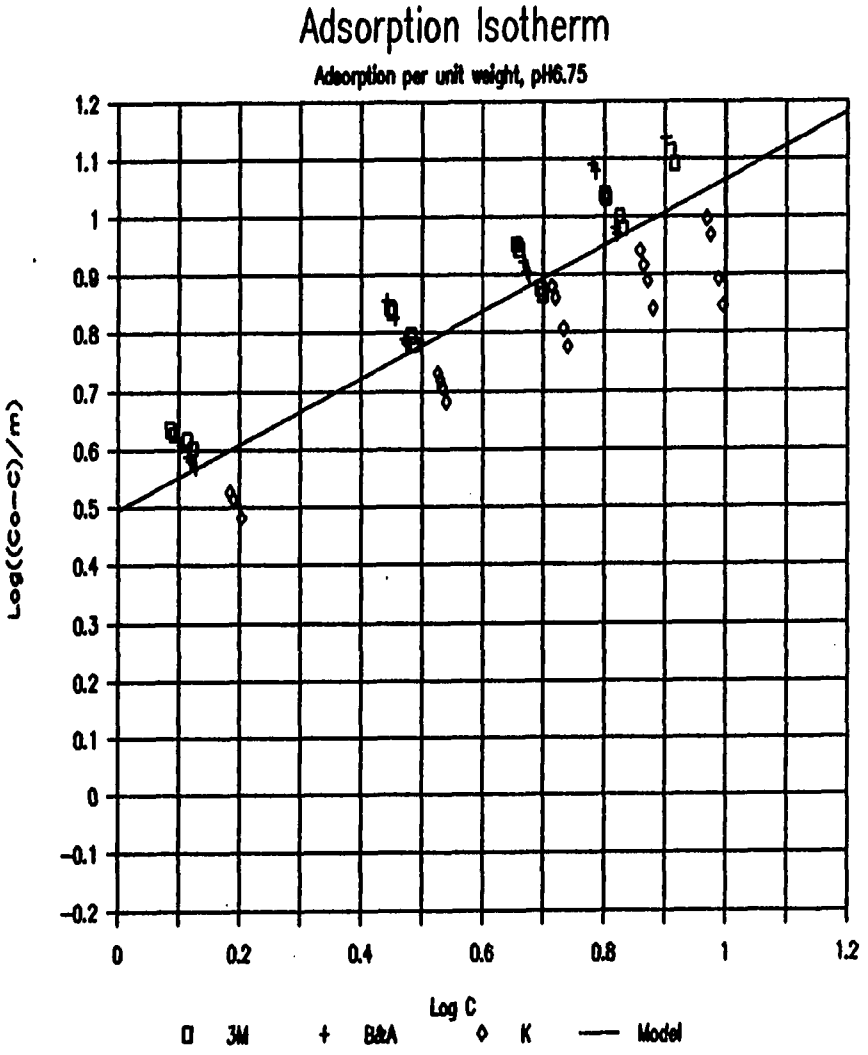

Figure 31. Adsorption isotherm for the three lepidocrocites at pH 6.75. The line in the plot represents predicted values by the regression model based on unit weight. (log q_e vs. log C)

which, in turn, might result in quite different pore size distribution. Since the three have close adsorption capacities, it is possible that the ferrous iron adsorption capacities per unit weight of most lepidocrocites may vary within a tolerably narrow range. On this hypothesis of "narrow range variation", the model can have an engineering value.

The Freundlich isotherm was used to develop a new model, as follows:

$$\log q_e = \log K_2 + (1/n) \log C + K_o \, pH \qquad \text{(IV-10)}$$

where

q_e = amount of solute adsorbed per unit weight of adsorbent at the equilibrium concentration C in bulk suspension, mg/g (= $(C_o-C)/m$ in arithmetic expression)

C_o = initial concentration of adsorbate, mg/l

C = concentration of adsorbate in bulk suspension at equilibrium, mg/l

m = weight of adsorbent per liter suspension, g/l

K_2, K_o, n = constants

All data for the three lepidocrocites were treated by multiple regression to obtain the values of the constants in the model. The quantitative model which resulted is:

$$\log q_e = -3.96 + 0.57 \log C + 0.66 \, pH \qquad \text{(IV-11)}$$

The lines in Figure 28, 29, 30 and 31 are the regression lines. The overall coefficient of determination was 0.846

and the adjusted coefficient of determination was 0.845.

Validity and expandability of the regression model

Because the quantitative model was obtained by multiple regression rather than by thermodynamic or specific surface characteristics, the validity of the model under conditions beyond the present study, especially in situations far beyond this research, was not fail-safe. More research should be conducted to accumulate more knowledge of the factors affecting ferrous iron adsorption on lepidocrocite not only on theoretical bases but also in varieties of situations.

The goodness of the model developed in this study was that the Freundlich isotherm data were analyzed by multiple regression techniques. By combining two methods, it would be easy to include the effects of other additive factors. To add the effect of factors of A, B, C, and D, for example, the model can be adjusted as follow:

$$q_e = K\, C^{1/n}[A]^a[B]^b[C]^c[D]^d \qquad \text{(IV-12)}$$

This can be converted to logarithmic form and then, to a multiple regression model:

$$\log q_e = \log K + (1/n) \log C + a \log A + b \log B + c \log C + d \log D \qquad \text{(IV-13)}$$

$$Y = B_0 + B_1X_1 + B_2X_2 + B_3X_3 + B_4X_4 \qquad \text{(IV-14)}$$

The constants of the model can be obtained by multiple regression without using complicated techniques.

Comparison with Tamura et al.'s model

In a study of the catalytic effect of ferric hydroxide on iron oxidation, Tamura et al. (1976b) formulated a model for predicting the adsorption capacity of ferric hydroxide:

$$[Fe^{++}_{ad}]/[Fe^{++}] = K\,[Fe(III)]/[H^+] \qquad \text{(IV-15)}$$

where

$[Fe^{++}_{ad}]$ = amount of ferrous iron adsorbed on ferric hydroxide, mg/l

$[Fe^{++}]$ = equilibrium concentration of ferrous iron in bulk liquid phase, mg/l

$[Fe(III)]$ = amount of ferric hydroxide in a liter of suspension, mg/l

$[H^+]$ = concentration of hydrogen ion, mol/l

K = equilibrium constant

The constant K was measured to be $10^{-9.6}$ mol/mg.

A simple reorganization of the equation leads to the modified Freundlich equation used in the present study. The reorganization was as follows:

$$[Fe^{++}_{ad}]/[Fe^{++}] = K\,[Fe(III)]/[H^+] \qquad \text{(IV-16)}$$

$$[Fe^{++}_{ad}]/[Fe(III)] = K\,[Fe^{++}]/[H^+] \qquad \text{(IV-17)}$$

The left hand side "$[Fe^{++}_{ad}]/[Fe(III)]$" had the same meaning as "q_e" except that it was the amount of adsorbed ferrous iron per milligram of solid whereas "q_e" ia based on adsorbed ferrous iron per gram of solid. The $[Fe^{++}]$ was identical with C in the Freundlich equation. By substituting q_e and C into Tamura et al.'s expression, the

equation becomes:

$$q_e = K' C/[H^+] \qquad \text{(IV-18)}$$

where the constant K' was $10^{-6.6}$ mol/l by compensating for the difference in unit of q_e. As noticed, it was a specific case of the modified Freundlich equation where the power of pH and C were fixed as one.

The predicted values of "q_e" using the two models were calculated for the pH ranges between 6 and 6.75 and ferrous iron concentrations from 2 to 10 mg/l. They are tabulated in Table 7. Because Tamura et al.'s model had steeper slopes for the pH and the equilibrium concentration in the bulk liquid, the predicted values of q_e by Tamura et al.'s techniques increased faster than those by the model of this study, as pH and equilibrium concentration were increased in the bulk suspension. Although they did not agree perfectly, they were in the same order in the examined ranges. In fact, pretty good agreement was obtained if it is considered that Tamura et al.'s model was generalized from data obtained at one pH level with one kind of ferric hydroxide. However, if the environments of pH and ferrous iron concentration are extreme, either high or low, the deviations between the two models can be significant.

Table 7. Comparison of results using different adsorption models

pH	[Fe(II)] (mg/l)	Adsorbed Fe(II) (mg/g) by Eq (IV-18)[a]	by Eq (IV-11)[b]
6.00	2.00	0.502	1.485
6.00	4.00	1.005	2.204
6.00	6.00	1.507	2.777
6.00	8.00	2.010	3.272
6.00	10.00	2.512	3.715
6.25	2.00	0.893	2.171
6.25	4.00	1.787	3.222
6.25	6.00	2.680	4.060
6.25	8.00	3.573	4.784
6.25	10.00	4.467	5.433
6.50	2.00	1.589	3.174
6.50	4.00	3.177	4.712
6.50	6.00	4.766	5.937
6.50	8.00	6.355	6.995
6.50	10.00	7.943	7.943
6.75	2.00	2.825	4.641
6.75	4.00	5.650	6.889
6.75	6.00	8.475	8.681
6.75	8.00	11.300	10.227
6.75	10.00	14.125	11.614

[a]The Eq (IV-18) stands for Tamura et al.'s adsorption model.

[b]The Eq (IV-11) stands for the adsorption model developed in this research.

Crystal Growth of Lepidocrocite

Objective and scope of the experiment

The objective of this experiment was to investigate the morphology of the precipitates resulting from the catalytic oxidation of ferrous iron in the presence of the pre-synthesized lepidocrocite. The precipitates were dried using a freeze drier and identified by X-ray diffractometry. The morphology of the precipitates was investigated by Scanning Electron Microscopy (SEM).

Stepwise procedures

The setup for the oxidation experiment was the same as that for the adsorption tests. The only difference was that air was supplied to the reactor instead of being stripped out.

A 300 mg sample of shattered powder of lepidocrocite from the 3M Co. was added to 2 liters of redistilled water. The suspension was left overnight. Then, 10 ml of 1 M sodium bicarbonate ($NaHCO_3$) were added to the suspension for its buffer capacity. Air was supplied to the reactor for at least 2 hours and carbon dioxide gas was bubbled through the suspension to adjust the pH to 6. The stock ferrous iron solution was introduced into the reactor. The concentration of ferrous iron in the reactor was kept around 5 mg/l. After one hour, a 10 ml aliquot of the

suspension was transferred to the vacuum filter and filtered through a 0.45 μm membrane filter. The filtrate was acidified and the ferrous iron concentration was determined by the 1,10-phenanthroline method. If there was still a considerable amount of iron present, one more hour was allowed for further oxidation. The ferrous iron introduced disappeared from the water within 2 hours, which can not be explained by homogeneous oxidation kinetics. Stock iron solution was injected repeatedly until 100 mg of ferrous iron was oxidized in the suspension. The precipitates were allowed to settle out and then were collected and dried in the freeze drier. The dried precipitates were stored in a desiccator until analysis using X-ray diffractometry and SEM.

Identification of the oxidation product

After the settled products were dried in the freeze drier, their X-ray diffraction pattern was obtained using the copper Kα line with diffracted beam monochromator and pulse height analyzer. The scanned 2θ range was from 2 to 70 degrees by gaining for 2 seconds at every 0.05 degree. The diffraction pattern of the oxidation products is shown in Figure 32 and that of the lepidocrocite before the experiment is also presented in Figure 33 for comparison. The d-spacings and the full width at half maximum intensities of the peaks are also reported in Table 8.

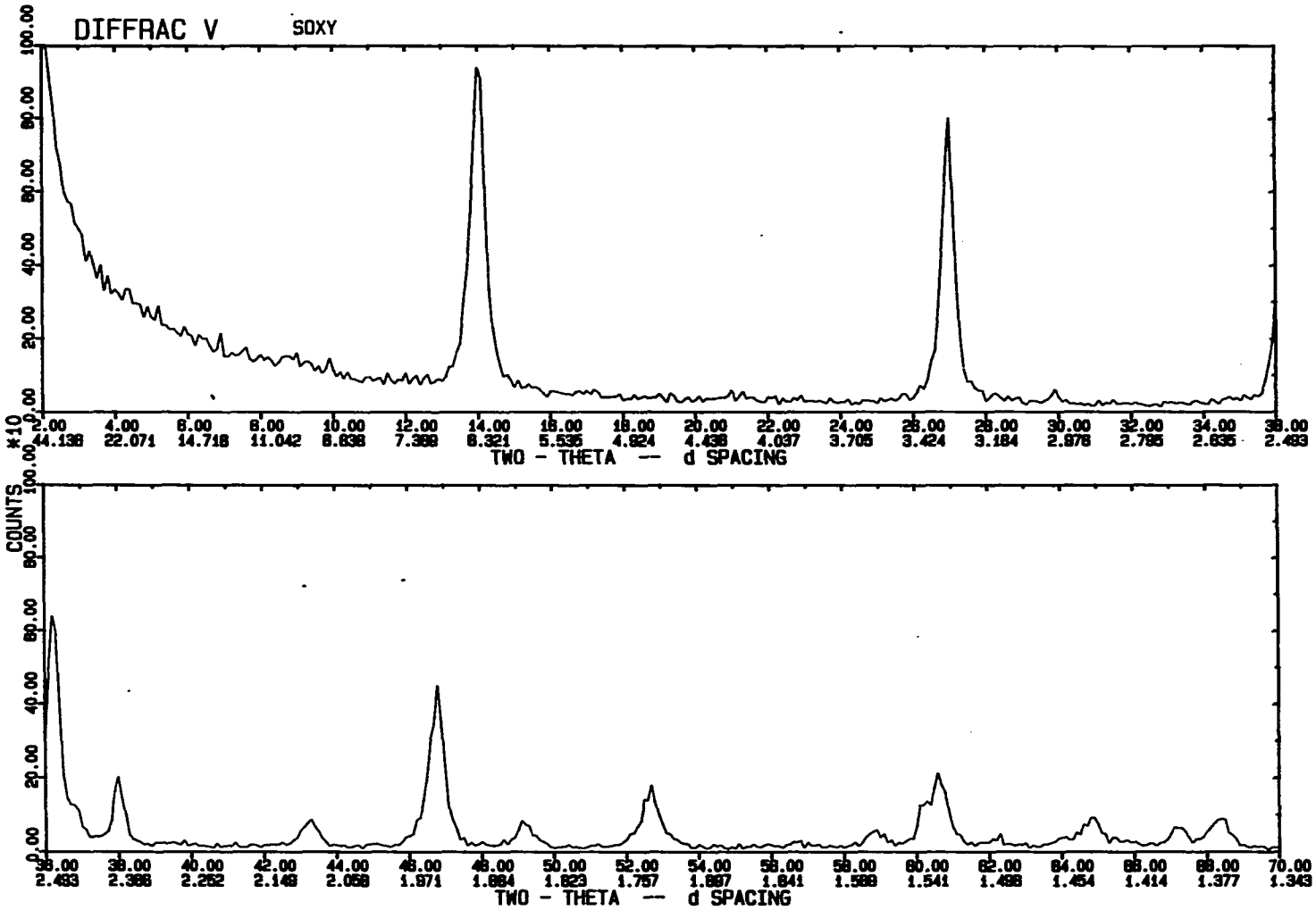

Figure 32. X-ray diffraction pattern of the precipitates after the oxygenation experiments with lepidocrocite-3M. Ferrous iron solution was added continuously into the reactor to be oxidized in the presence of 300 mg of lepidocrocite-3M until 100 mg of ferrous iron was accumulated

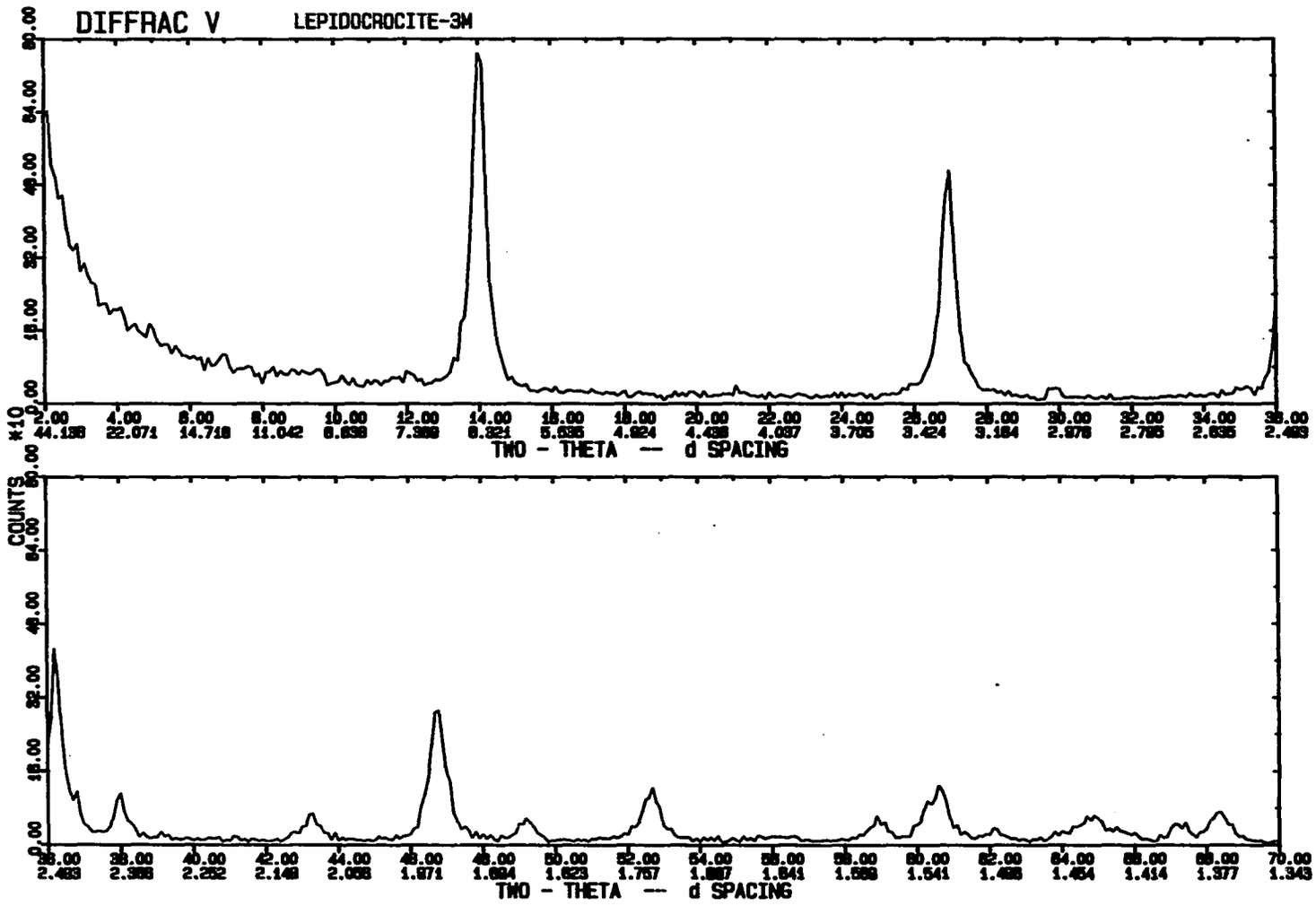

Figure 33. X-ray diffraction pattern of the original lepidocrocite-3M before the oxygenation experiments

Table 8. Peaks of the X-ray diffraction pattern of the oxygenation product

No.	2θ	d-spacing	Integ.I(%)	FWHM	
1	5.829	15.1496	2.2	0.206	
2	14.066	6.2908	100.0	0.535	(0.543)
3	21.314	4.1652	2.0	0.375	
4	27.025	3.2965	79.7	0.509	(0.572)
5	29.926	2.9833	3.3	0.390	(0.351)
6	35.005	2.5612	1.3	0.208	
7	35.148	2.5510	1.5	0.265	
8	36.267	2.4748	70.2	0.532	(0.523)
9	38.022	2.3645	13.8	0.384	(0.408)
10	43.316	2.0870	10.0	0.635	(0.541)
11	46.828	1.9384	51.3	0.579	(0.605)
12	49.186	1.8508	6.9	0.511	(0.498)
13	52.695	1.7355	22.6	0.641	(0.550)
14	58.896	1.5667	6.1	0.671	(0.451)
15	60.671	1.5251	29.2	0.713	(0.829)
16	62.242	1.4903	2.9	0.478	(0.425)
17	64.052	1.4525	1.6	0.284	(0.374)
18	64.920	1.4351	7.8	0.577	(0.682)
19	67.161	1.3926	5.1	0.552	(0.613)
20	68.390	1.3705	10.0	0.628	(0.677)

1. The peaks were detected by the IDENT software provided with SIEMENS X-ray diffractometer.

2. Maximum background slope over one degree = 0.30. The smallest peak relative to the strongest=1.0. 3 points were averaged.

3. The FWHM in parenthesis are those of the lepidocrocite-3M which was the seeded lepidocrocite in the oxygenation experiment. Therefore, comparison of those two FWHMs can reveal the change in line broadening of the oxygenation product.

Morphology of the oxidation product

The oxidation product was dispersed in petroleum ether and shaken in an ultrasonic bath to break down the agglomerates. The powder was then coated with gold to observe the morphology by Scanning Electron Microscopy (SEM). The pictures after the oxidation experiment were taken at 1,000, 10,000, and 30,000 magnification levels and the resulting microphotographs at 10,000 and 30,000 magnification level are shown in Figure 34 through Figure 36. The microphotograph of lepidocrocite-3M before the oxidation experiment was shown in Figure 17.

Analysis of the results

As shown, the change in morphology was quite apparent even though the degrees of change were different. The original lepidocrocite particles from the 3M Co. were covered with the newly oxidized ferrous iron and lost their original acicular shapes. This change in morphology implied that the oxidation of ferrous iron in the presence of lepidocrocite involved the adsorption of the ferrous iron on the lepidocrocite surface followed by its oxidation. The loss of the original shape could be due to the rather rapid oxidation. It seems that, upon further oxidation, the morphology eventually changed to that of the lepidocrocite-K, which is shown in Figure 19.

When the X-ray patterns shown in Figure 32 and 33 were

Figure 34. Microphotograph of the precipitate settled after the oxygenation of ferrous iron in the presence of lepidocrocite-3M. (magnification, X10,000)

Figure 35. Microphotograph of the precipitate settled after the oxygenation of ferrous iron in the presence of lepidocrocite-3M. The original needle shape of lepidocrocite-3M was changed by the adsorption and subsequent oxygenation of ferrous iron. (magnification, X30,000)

Figure 36. Microphotograph of the precipitate settled after the oxygenation of ferrous iron in the presence of lepidocrocite-3M, showing different degree of change compared to Figure 35. (magnification, X30,000)

compared, it was clear that the two patterns agreed very well in terms of the d-spacings, the relative intensities, and the line broadenings of the peaks. Since the peaks in both figures were at the same d-spacings and no extra peaks appeared in Figure 32, it was obvious that the oxidation product was the same compound as the original lepidocrocite from the 3M Co. even though the morphology was different. That conclusion is reasonable when it is considered that 100 mg of ferrous iron were oxygenated in the presence of 300 mg of lepidocrocite. The weight ratio of the oxidation product of ferrous iron to the lepidocrocite is significant. Thus, if the oxidation of ferrous iron in the presence of lepidocrocite could lead to products other than lepidocrocite, their detectable peaks ought to have appeared at different d-spacings.

The relative intensities were almost alike and a slight difference could be expected due to the packing of the samples. However, the fact that there was no significant changes in the line broadening after oxidation aroused curiosity. As shown in Figures 34, 35, and 36, the ferrous iron was adsorbed on the original lepidocrocites and oxygenated there. Because the crystals grew, it was expected that the line broadenings of the peaks in Figure 32 would be sharper than those in Figure 33. A conceivable explanation for the lack of changes in the line broadening

could be the fact that the X-ray diffractometer used could detect the size change only when the size was smaller than 1,000 angstroms. As discussed in the synthesis section, it is still possible that the crystals were bigger than 1,000 angstroms even though the calculated average size nominal to the (020) plane was smaller than the limit.

Several conclusions are possible by combining the results from the SEM and X-ray diffractometry. Ferrous iron was adsorbed and oxidized on the surface of lepidocrocite resulting in crystal growth. Although the morphology of the lepidocrocite changed because of the rapid oxidation, the structure of the compound investigated by X-ray diffraction remained the same, which meant that the oxidation of ferrous iron adsorbed on lepidocrocite resulted in the formation of more lepidocrocite.

CHAPTER V. DISCUSSION

pH Adjustment after Injection of Stock Iron Solution

In many iron oxidation studies, the matrix of stock ferrous iron solution has been a strong acid to prevent ferrous iron from oxidation. Injection of stock iron solution into the reactor resulted in injection of strong acid into the reaction system. Sung and Morgan (1980) showed the variation in pH after addition of stock ferrous iron into a reactor. The pH of the reaction system drops sharply immediately after the introduction of stock iron solution followed by a subsequent increase in pH due to the diffusion of aqueous CO_2 from solution. They claimed that the pH did not recover for about 20 minutes.

In this study, however, the pH variation discussed by Sung and Morgan did not continue for 20 minutes because of the active adjustment of pH using argon gas. The flow rate of argon gas was increased to raise the dropped pH value to the initially designated value. The solution pH recovered to the desired initial value within 5 minutes without difficulty.

Effective pH Range of Heterogeneous Oxidation

After examining the ratio of the homogeneous to the heterogeneous oxidation rates, Sung and Morgan (1980) concluded that autocatalysis was noticeable only for pH

values around 7 to 8. At lower pH regions, the lepidocrocite surface forms slowly and adsorption of ferrous iron is less favorable. In a high pH range, where pH values were higher than 8, the homogeneous oxidation rate dominated. Their conclusion was based on the assumption that there was no lepidocrocite initially in the system.

Assuming that lepidocrocite is seeded or otherwise present in the system, the usefulness of the heterogeneous oxidation mechanism, however, will be greatly enhanced in the low pH regions. In a pH range of 7 to 8, the homogeneous oxidation rate is fast enough to precipitate iron from water with one or two hours of detention. If we use the kinetic constants reported by Tamura et al. (1976b), the ratio of the heterogeneous to the homogeneous oxidation rate was 80 with 100 mg of seeded lepidocrocite per liter at pH 6 and 25 ^{o}C. The calculations are shown in Appendix D. Moreover, the heterogeneous rate depends on the concentration of lepidocrocite in the water, which leads to the conclusion that dissolved iron can be removed fast enough to be practical in low pH regions by providing enough lepidocrocite in the system. Normally, lepidocrocite crystals will remain, to some extent at least, in a filter even after it is backwashed. Thus, a granular media filter used in a home or even a continuous

flow water treatment plant will provide seed lepidocrocite for improving iron oxidation and removal of ferrous iron.

As discussed, the true usefulness of heterogeneous oxidation in engineering practice will be in low pH regions where dissolved iron removal by homogeneous oxidation is not expected.

Change in Oxidation Rate

There is the possibility that the heterogeneous oxidation rate varies as the oxidation proceeds. This expectation becomes evident when the results of oxidation and adsorption experiments are combined. As shown in the oxidation experiments, the morphology of seeded lepidocrocite-3M was changed to a morphology similar to lepidocrocite-K. The change in morphology was due to adsorption of ferrous iron on the surface of lepidocrocite-3M followed by its rapid oxidation. The oxidation rate was too fast for the lepidocrocite-3M to keep its original acicular shape. The adsorption capacity of the newly formed lepidocrocite like lepidocrocite-K was less than that of lepidocrocite-3M because of a suspected narrow pore distribution. Thus, it can be hypothesized that, as oxidation proceeds, the seeded lepidocrocite will be covered with newly oxidized lepidocrocite which may have more narrow pores than the seeded lepidocrocite. Consequently, a more narrow pore distribution will result

in less adsorption capacity which, in turn, may slow down the rate of dissolved iron removal.

Reasonable generalization of the discussion could result in one speculation. As the oxidation of ferrous iron proceeds, there could have been a continuous change in the physical characteristics of the lepidocrocite, e.g., morphology, surface area, etc. Therefore, if the catalytic effect of lepidocrocite on ferrous iron oxidation depends principally on its physical characteristics, the catalytic capability of lepidocrocite would vary continuously.

Effect of Freeze Drying

The effect of the drying procedure on the characteristics of lepidocrocite was examined using freeze drying techniques. As mentioned in the synthesis section, part of the synthesized lepidocrocite-B&A and lepidocrocite-K were dried in a freeze dryer instead of an oven. The vacuum of freeze drying was 200 μm Hg and the temperature in the freezing chamber was -45 ^{o}F. The morphology, surface area per unit weight, and adsorption capacity were investigated to explore the similarity and dissimilarity of freeze-dried lepidocrocites to oven-dried lepidocrocites.

Surface areas were 108.81 m^2/g (with standard deviation of 2.561 m^2/g) and 154.68 m^2/g (with 9.12 m^2/g of standard deviation) for freeze-dried lepidocrocite-B&A and

lepidocrocite-K, respectively. The null hypothesis of no difference between oven dried and freeze-dried lepidocrocite was rejected at the 95 % significance level for lepidocrocite-B&A but was not rejected for lepidocrocite-K. Therefore, the effect of drying method on the surface area of lepidocrocite should be investigated further.

The morphology of freeze-dried lepidocrocites are shown in Figures 37 and 38. Compared with Figures 18 and 19, which were the corresponding lepidocrocites dried in an oven at 60 ^{o}C, no significant difference was noticed.

The adsorption capacity of freeze-dried lepidocrocite-K and lepidocrocite-B&A were examined at pH 6.25 and compared with those of oven-dried lepidocrocites. As shown in Figures 39 and 40, there were no noticeable deviations in the performance between freeze-dried and oven-dried lepidocrocites at pH 6.25. No experiments were conducted at other pH values.

The results of the examination showed that freeze drying did not affect the characteristics of lepidocrocite appreciably even though the t-test indicated a difference in surface areas between oven-dried and freeze-dried lepidocrocite-B&A. However, it does not necessarily mean that the drying method would have no effect on the adsorption capability of lepidocrocite. Because it is

(a) At X10,000 Magnification Level

(b) At X30,000 Magnification Level

Figure 37. Microphotograph of the freeze-dried lepidocrocite-B&A

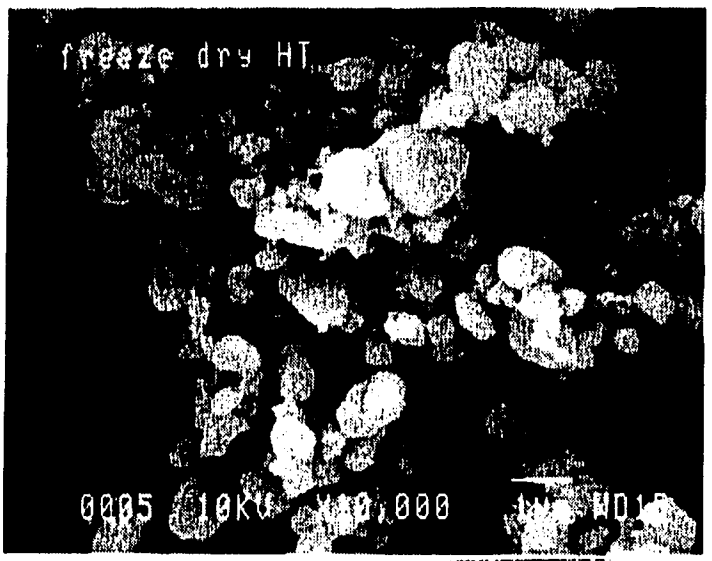

(a) At X10,000 Magnification Level

(b) At X30,000 Magnification Level

Figure 38. Microphotograph of the freeze-dried lepidocrocite-K

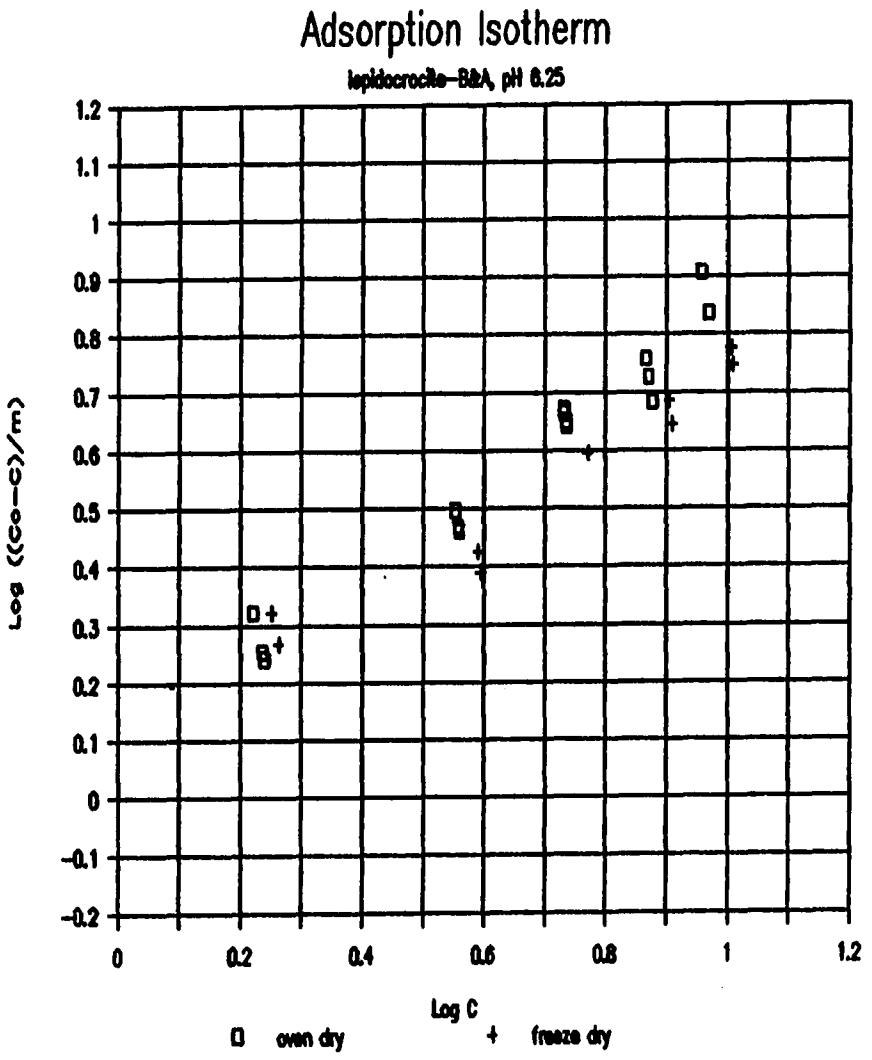

Figure 39. Adsorption isotherm of the freeze-dried and the oven-dried lepidocrocite-B&A at pH 6.25

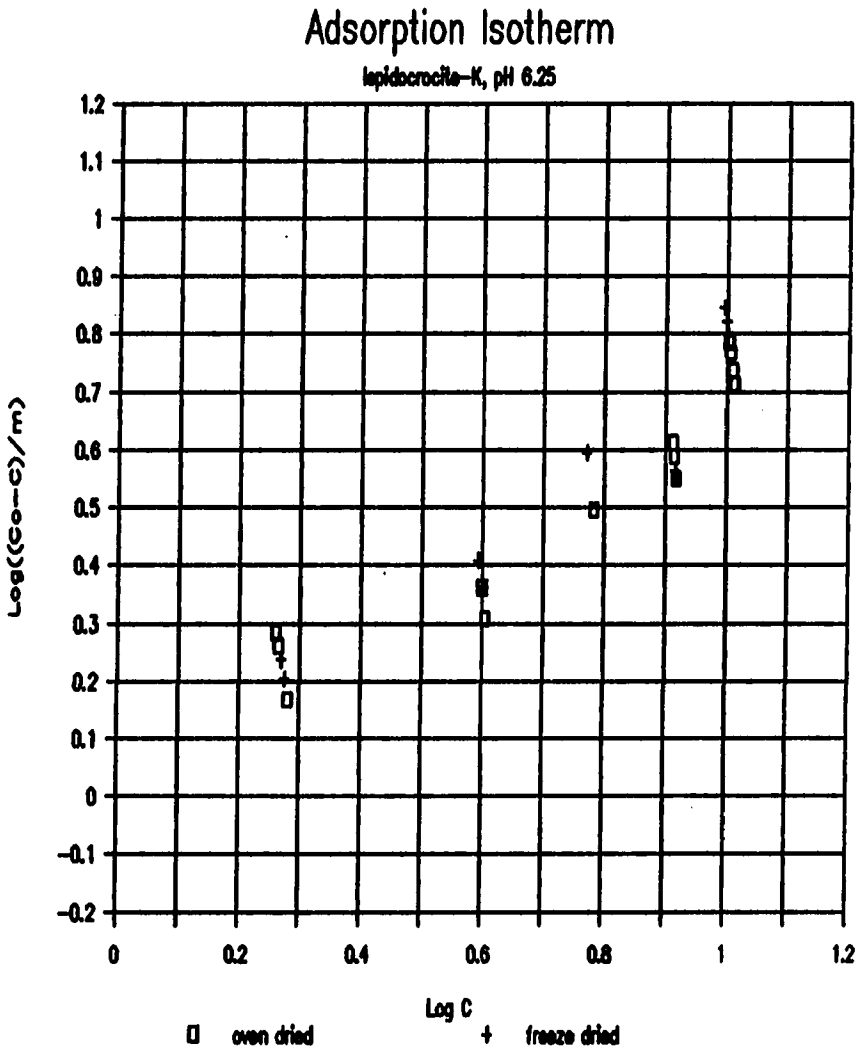

Figure 40. Adsorption isotherm of the freeze-dried and the oven-dried lepidocrocite-K at pH 6.25

suspected that the adsorption capacity of a specific lepidocrocite depends on both surface area and pore size distribution, any drying technique which affects pore size distribution may have an effect on its adsorption capacity. But it could also be speculated that most drying methods might not have a noticeable impact on adsorption behavior of lepidocrocites from the facts that the two somewhat extreme drying techniques did not show any significant difference.

CHAPTER VI. SUMMARY, CONCLUSIONS, AND RECOMMENDATIONS

This study explored the characteristics of synthesized lepidocrocites in terms of their morphology, surface area, ferrous iron adsorption capacity per unit surface area, and the growth of their crystallites. Two kinds of lepidocrocites were synthesized in the laboratory and a third was obtained from the 3M Co. Their morphologies of them were observed using Scanning Electron Microscopy (SEM) and their surface areas were measured by BET isotherm techniques using nitrogen gas at the liquid nitrogen temperature.

The Freundlich isotherm equation was modified to build a model to predict the effect of pH and the concentration of ferrous iron in water on lepidocrocite adsorption capacity. The prediction model is able to integrate the effects of any additive factors in the future. The adsorption capacities of the three distinctive lepidocrocites were measured and the data were processed by multiple regression technique to obtain the constants in the model. Moreover, the correlation between adsorption capacity and surface area was investigated. The role of lepidocrocite in heterogeneous oxidation was investigated by taking microphotographs of the precipitates after oxidation of ferrous iron in the presence of lepidocrocite.

In addition to the determination of the lepidocrocite

surface characteristics, the possibility of applying the heterogeneous oxidation mechanism to engineering practice was tested.

There were lots of observations and discoveries that enhanced our understanding of lepidocrocite and heterogeneous oxidation. Disagreeing data and conflicting reports by previous researchers were integrated and rationalized throughout the experiments. The findings and resulting conclusions are:

1. Dissolved iron at a concentration of 4 to 5 mg/l was reduced to less than 0.3 mg/l while the water was filtered through a sand filter containing previously precipitated iron. Although it was not proven that the removal mechanism involved was entirely depended on the heterogeneous oxidation due to the deposited iron, heterogeneous oxidation was a major removal mechanism at work in the filter.
2. The microphotographs of the lepidocrocites which were pre-identified by their X-ray diffraction patterns revealed that lepidocrocites could have an acicular shape as well as the shape of agglomerated flocs. It was postulated that the shape would vary depending on the environments of their formation, especially on the rate of oxidation. This study, thus, provided an explanation for the various shapes of lepidocrocite

reported.

3. The surface areas of the synthesized lepidocrocites in this study varied widely, from 48.98 m^2/g to 150.28 m^2/g, whereas the surface areas reported by other researchers were from 66 m^2/g to 171 m^2/g. Thus, it was confirmed that lepidocrocite can have a wide variety of surface areas depending primarily on the rate of lepidocrocite formation. The faster the rate of formation, the smaller the crystal size. The smaller the crystallites, the larger the surface area. The ratio of the surface areas of the lepidocrocites were explained quantitatively by the ratio of relative crystal size calculated from X-ray diffraction patterns.

4. It was revealed by the microphotographs of the precipitates taken after oxidation of ferrous iron in the presence of lepidocrocite that the lepidocrocite acted as a seed instead of a catalyst in the heterogeneous oxidation. The microphotographs showed that the adsorbed ferrous iron was oxidized on the surface of the seeded lepidocrocite. The X-ray diffraction pattern of the precipitates was definitely that of lepidocrocite, which leads to the conclusion that the adsorption and subsequent oxidation of ferrous iron on the surface of lepidocrocite formed

additional lepidocrocite. Therefore, heterogeneous oxidation of ferrous iron in the presence of lepidocrocite forms a feed back cycle which consisted of adsorption of ferrous iron on the available sites of the lepidocrocite surface, subsequent oxidation of the adsorbed ferrous iron resulting in the formation of new lepidocrocite and consequent regeneration of the available adsorption sites on the surface.

5. Adsorption capacities of three distinctive lepidocrocites for ferrous iron were investigated at four different pH levels. It was observed that there was no correlation between the surface area based on BET isotherms and adsorption capacity even though adsorption behavior depends strongly on the available surface sites. The sites accessible to nitrogen gas were not available to ferrous iron in water. It was postulated that not only surface area but other physical characteristics, such as pore size distribution, should be taken into account to predict the adsorption capacity of lepidocrocite for ferrous iron.

6. While the adsorption capacity of lepidocrocite for ferrous iron did not have any apparent correlation with surface area, the adsorption capacities per unit weight of the three distinctive lepidocrocites were

close enough to attempt hypothesizing that the adsorption capacity per unit weight of most lepidocrocites would not vary widely.

7. A model based on the Freundlich equation was built to predict the effect of pH and the equilibrium concentration of ferrous iron in water. Multiple regression of data revealed that the amount of ferrous iron adsorbed on the unit weight of lepidocrocite was proportional to the 0.57 power of the concentration of ferrous iron and inversely proportional to the 0.66 power of the hydrogen ion concentration. Tamura et al. (1976b) fixed both powers as unity. The adsorption capacities predicted by both models were in the same order even though the predicted values by Tamura et al.'s model were smaller than those by the model developed in this study. The difference between the two predicted values became larger as the concentration of ferrous iron and pH were lowered.

This study was intended to provide better understanding of lepidocrocite, heterogeneous oxidation, the adsorption capacity of lepidocrocite, the effect of pH and the concentration of ferrous iron in water, and the correlation between adsorption capacity and surface area. This study accomplished these objectives. However, there is a lot more that should be investigated to understand the

applicability of lepidocrocite adsorption and heterogeneous oxidation in removal of dissolved iron in engineering practice. The suggested investigations are as follows:

1. Correlation of pore size distribution of lepidocrocite to its adsorption capacity for ferrous iron.
2. Testing of the adsorption model under various water environments.
3. Evaluation of the applicability of the heterogeneous kinetic equation with an adsorption model should be examined under a variety of situations and in the presence of lepidocrocite levels which may be encountered in engineering practice.
4. The effect of organic matter and silica on the heterogeneous oxidation rate.
5. The role of microorganisms in ground water in affecting dissolved iron removal in the presence of lepidocrocite.

BIBLIOGRAPHY

Abel, E. "Über autoxydation in unbelichteter homogener wäβriger lösung. Mit besonderer berücksichtigung anorganischer systeme." Zeitschrift für Elektrochemie, 59(10):903-906, 1955.

Adamson, A. W. Physical Chemistry of Surfaces. 2nd edition. Interscience Publishers, Inc., New York, 1967.

Bates, R. G. "The modern meaning of pH." Chemical Rubber Company Critical Review in Analytical Chemistry, 10:247-278, 1981.

Baudisch, O. and Albrecht, W. H. "Gamma-ferric oxide hydrate." Journal of the American Chemical Society, 54(3):943-947, 1932.

Bell, G. R. "Removal of soluble iron by filtration." Journal of American Water Work Association, 57:458-471, 1965.

Bernal, J. D., Dasgupta, D. R., and Mackay, A. L. "The oxides and hydroxides of iron and their structure inter-relationships." Clay Minerals Bulletin, 4(21):15-30, 1959.

Berner, R. A. and Morse, J. W. "Dissolution of kinetics of calcium carbonate in seawater-IV. Theory of calcite dissolution." American Journal of Science, 274:108-134, 1974.

Böhm, J. "Röntgenographische untersuchung der mikrokristallinen eisenhydroxydminerale." Zeitschrift für Kristallographie, 68:567-585, 1928.

Breeuwsma, A. and Lyklema, J. "Interfacial electrochemistry of hematite." Discussion of the Faraday Society, 52:324-333, 1971.

Brunauer, S., Emmett, P. H., and Teller, E. "Adsorption of gases in multimolecular layers." Journal of the American Chemical Society, 60:309-319, 1938.

Cher, M. and Davidson, N. "The kinetic of the oxygenation of ferrous iron in phosphoric acid solution." Journal of the American Chemical Society, 77(2):793-798, 1955.

Christensen, H. and Christensen, A. N. "Hydrogen bonds of γ-FeOOH." Physical and Inorganic Chemistry Division, Acta Chemica Scandinavica Series A, 32(1):87-88. 1978.

Clark, L. J. "Iron(II) determination in the presence of iron(III) using 4,7-diphenyl-1,10-phenanthroline." Analytical Chemistry, 34:348-352, 1962.

Cornet, D. and Burwell, R. L., Jr. "Chromium compounds on silica gel." Journal of the American Chemical Society, 90(10):2489-2494, 1968.

CRC Handbook of Chemistry and Physics. 66th edition. Chemical Rubber Company Press, Inc., Boca Raton, Florida, 1985-1986.

Dana, J. D. The System of Mineralogy. 6th ed. John Wiley & Sons, New York, 1900.

Davison, W. "Soluble inorganic ferrous complexes in natural waters." Geochimica et Cosmochimica Acta, 43:1693-1696, 1979.

Davison, W. and Seed, G. "The kinetics of the oxidation of ferrous iron in synthetic and natural waters." Geochimica et Cosmochimica Acta, 47:67-79, 1983.

Dekanel, J. and Morse, J. W. "The chemistry of orthophosphate uptake from seawater onto calcite and aragonite." Geochimica et Cosmochimica Acta, 42:1335-1340, 1978.

Ewing, F. J. "The crystal structure of lepidocrocite." Journal of Chemical Physics, 3(7):420-424, 1935.

Feitknecht, V. W. and Keller, G. "Über die dunkelgrünen hydroxyverbindungen des eisens." Zeitschrift für Anorganische Chemie, 262:61-68, 1950.

Francombe, M. H. and Rooksby, H. P. "Structure transformations effected by the dehydration of diaspore, goethite and delta ferric oxide." Clay Minerals Bulletin, 4(21):1-14, 1959.

Freundlich, H. Colloid and Capillary Chemistry. Methuen and Co., Ltd., London, 1926.

Fricke, R. and Weitbrecht, G. "Dimensionen der primär- und sekundärteilchen bei einigen kristallinen eisen(III)-hydroxyden." Zeitschrift für Anorganische und Allgemeine Chemie, 251:424-428, 1943.

Gadde, R. R. and Laitinen, H. A. "Studies of heavy metal adsorption by hydrous iron and manganese oxides." Anlytical Chemistry, 46(13):2022-2026, 1974.

Gallagher, K. J. and Phillips, D. N. "Proton transfer studies in the ferric oxyhydroxides." Transactions of the Faraday Society, 64:785-795, 1968.

Gallagher, K. J. and Phillips, D. N. "Hydrogen exchange studies and proton transfer in β iron(III) oxyhydroxide." Chimia, 23:465-470, 1969.

Gaudin, A. M. and Fuerstenau, D. W. "Quartz flotation with anionic collectors." Transactions of the American Institute of Mining, Metallurgical and Petroleum Engineers, 202:66-72, 1955.

Ghosh, M. M. Aqueous Environmental Chemistry of Metals. Chapter 5, Ann Arbor Science, Ann Arbor, Michigan, 1974.

Ghosh, M. M., O'Connor, J. T., and Engelbrecht, R. S. "Precipitation of iron in aerated ground waters." Journal of the Sanitary Engineering Division, Proceedings of the American Society of Civil Engineers, 92(SA1):199-213, 1966.

Ghosh, M. M., O'Connor, J. T., and Engelbrecht, R. S. "Bathophenanthroline method for the determination of ferrous iron." Journal of the American Water Works Association, 59:897-905, 1967.

Goto, K., Tamura, H., and Nagayama, M. "The mechanism of oxygenation of ferrous ion in netural solution." Inorganic Chemistry, 9(4):963-964, 1970.

Harned, H. S. and Scholes, S. R., Jr. "The ionization constant of HCO_3^- from 0 to 50^o." Journal of the American Chemical Society, 63:1706-1709, 1941.

Hem, J. D. "Reactions of metal ions at surfaces of hydrous iron oxide." Geochimica et Cosmochimica Acta, 41:527-538, 1977.

primär- und
isen(III)-
und

avy metal
ides."
.

ansfer
sactions of

exchange

tation with
merican
oleum

Metals.
ichigan,

R. S.
ters."
1,
L

R. S.
nation of
er Works

nanism of
ion."

:ation
of the
31.

of hydrous
:a, 41:527-

James, R. O. and Healy, T. W. "Adsorption of hydrolyzable metal ions at the oxide-water interface. III. A thermodynamic model of adsorption." Journal of Colloid and Interface Science, 40(1):65-81, 1972.

James, R. O., Stiglich, P. J., and Healy, T. W. "Analysis of models of adsorption of metal ions at oxide/water interfaces." Faraday Discussions of the Chemical Society, 59:142-156, 1975.

Jobin, R. and Ghosh, M. M. "Effect of buffer intensity and organic matter on the oxygenation of ferrous iron." Journal of American Water Works Association, 64(9):590-595, 1972.

Johnson, G. K. and Bauman, J. E. "Equilibrium constants for the aquated iron(II) cation." Inorganic Chemistry, 17:2774-2779, 1978.

Just, G. "Kinetische untersuchung der autoxydation des in wasser gelösten ferrobicarbonats." Zeitschrift für Physikalische Chemie, 63:385-420, 1908.

Kaneko, K. and Inouye, K. "Electrical properties of ferric oxyhydroxides." Bulletin of the Chemical Society of Japan, 47(5):1139-1142, 1974.

Kaneko, K. and Inouye, K. "Electrical conductivity as a defect property of γ-FeOOH." Journal of the Chemical Society, Faraday Transactions I., 5:1258-1266, 1976.

Kaneko, K. and Inouye, K. "Adsorption of water on FeOOH as studied by electrical conductivity measurements." Bulletin of the Chemical Society of Japan, 52(2):315-320, 1979.

Kaneko, K., Serizawa, M., Ishikawa, T., and Inouye, K. "Dielectric behavior of water molecules adsorbed on iron(III) oxide hydroxides." Bulletin of the Chemical Society of Japan, 48(6):1764-1769, 1975.

Kavanaugh, M. C. and Trussell, R. R. "Design of aeration towers to strip volatile contaminants from drinking water." Journal of American Water Works Association, 72:684-692, 1980.

Kazmierczak, T. F., Tomson, M. B., and Nancollas, G. H. "Crystal growth of calcium carbonate. A controlled composition kinetic study." Journal of Physical Chemistry, 86:103-107, 1982.

Kielland, J. "Individual activity coefficients of ions in aqueous solutions." Journal of American Chemical Society, 59:1675-1678, 1937.

Klug, H. P. and Alexander, L. E. X-ray Diffraction Procedures. 2nd ed. Wiley-Interscience Publication, John Wiley & Sons, New York, 1954.

Kolthoff, I. M. and Moskovitz, B. "Studies on coprecipitation and aging. XI." Journal of Physical Chemistry, 41:629-644, 1937.

Kolthoff, I. M. and Overholser, L. G. "Studies on aging and coprecipitation." Journal of Physical Chemistry, 43:767-780, 1939.

Kozawa, A. "On an ion-exchange property of manganese dioxide." Journal of the Electrochemical Society, 106(1):552-556, 1959.

Kozawa, A. "Ion-exchange adsorption of zinc and copper ions on silica." Journal of Inorganic and Nuclear Chemistry, 21:315-324, 1961.

Langmuir, I. "The adsorption of gases on plane surfaces of glass, mica, and platinum." Journal of the American Chemical Society, 40:1361-1403, 1918.

Liang, Y. J. and Kester, D. R. "Kinetics of ferrous oxygenation in aqueous media." Transactions of American Geophysical Union, 58:1168-1176, 1977.

Linke, K. Solubilities of Inorganic and Metal Organic Compounds. Vol. 2. 4th ed. American Chemical Society, Washington, D.C., 1965.

Loganathan, P. and Burau, R. G. "Sorption of heavy metal ions by a hydrous manganese oxide." Geochimica et Cosmochimica Acta, 37:1277-1293, 1973.

Mackenzie, R. C. and Meldau, R. "The ageing of sesquioxide gels. I. Iron oxide gels." Mineralogical Magazine, 32:153-165, 1959.

MacNaughton, M. G. and James, R. O. "Adsorption of aqueous mercury(II) complexes at the oxide/water interface." Journal of Colloid and Interface Science, 47(2):431-440, 1974.

McClellan, A. L. and Harnsberger, H. F. "Cross-sectional areas of molecules adsorbed on solid surfaces." Journal of Colloid and Interface Science, 23:577-599, 1967.

Misawa, T. "The thermodynamic consideration for Fe-H_2O system at 25°C." Corrosion Science, 13:659-676, 1973.

Misawa, T., Hashimoto, K., and Shimodaira, S. "The mechanism of formation of iron oxide and oxyhydroxides in aqueous solutions at room temperature." Corrosion Science, 14:131-149, 1974.

Morgan, J. J. and Birkner, F. B. Discussion of "Precipitation of iron in aerated groundwaters" by Ghosh, M. M., O'Connor, J. T., and Engelbrecht, R. S. Journal of the Sanitary Engineering Division, Proceedings of the American Society of Civil Engineer, 92(SA6):137-143, 1966.

Morgan, J. J. and Stumm, W. "Colloid-chemical properties of manganese dioxide." Journal of Colloid Science, 19:347-359, 1964.

Nancollas, G. H. "The growth of crystals in solution." Advances in Collide and Interface Science, 10:215-252, 1979.

Nortia, T. and Laitinen, S. "The electonic spectra of some transition metal ions in cation exchange resins. Part I. Nickel(II), cobalt(II), and copper(II) ions in the strongly acidic sulphonate resin DOWEX 50WX8." Suomen Kemistilehti, 41:136-141, 1968.

O'Connor, D. J. and Buchanan, A. S. "Electrokinetic properties of cassiterite." Australian Journal of Chemistry, 6:278-293, 1953.

Okura, T. and Goto, K. "Oxygenation reaction of ferrous ion in natural water." Kogyo Kagaku Zasshi, 58:239-241, 1955.

Olson, L. L. and Twardowski, C. J., Jr. "$FeCO_3$ vs. $Fe(OH)_3$ precipitation in water treatment plants." Journal of the American Water Works Association, 67(5):150-153, 1975.

Onoda, G. Y., Jr., and De Bruyn, P. L. "Proton adsorption at the ferric oxide/aqueous solution interface. I. A kinetic study of adsorption." Surface Science, 4:48-63, 1966.

Oosterhout, G. W. "Morphology of synthetic submicroscopic crystals of α and γ-FeOOH and of γ-Fe_2O_3 prepared from FeOOH." Acta Crystallographica, 13:932-935, 1960.

Parks, G. A. and De Bruyn, P. L. "The zero point of charge of oxide." Journal of Physical Chemistry, 66:967-973, 1962.

Pankow, J. F. and Morgan, J. J. "Kinetics for the aquatic environment." Environmental Science & Technology, 15(10):1155-1164, 1981.

Peacock, M. A. "On goethite and lepidocrocite." Proceedings and Transactions of the Royal Society of Canada, 36(IV):107-119, 1942.

Posnjak, E. and Merwin, H. E. "The hydrated ferric oxides." The American Journal of Science-Fourth Series, 47(281):311-348, 1919.

Postma, D. "Formation of siderite and vivianite and the pore water composition of a recent bog sediment in Denmark." Chemical Geology, 31:225-244, 1981.

Postma, D. "Pyrite and siderite formation in brackish and freshwater swamp sediments." American Journal of Science, 282:1151-1183, 1982.

Robinson, R. B., Demirel, T., and Baumann, E. R. "Identity and character of iron precipitates." Journal of the Environmental Engineering Division, Proceedings of the American Society of Civil Engineers, 107(EE6):1211-1227, 1981.

Schenk, J. E. and Weber, W. J., Jr. "Chemical interactions of dissolved silica with iron(II) and (III)." Journal of American Water works Association, 60:199-212, 1968.

Schwertmann, U. and Taylor, R. M. "The transformation of lepidocrocite to goethite." Clays and Clay Minerals, 20:151-158, 1972.

Schwertmann, U. and Thalmann, H. "The influence of [Fe(II)],[Si], and pH on the formation of lepidocrocite and ferrihydrite during oxidation of aqueous $FeCl_2$ solutions." Clay Minerals, 11:189-200, 1976.

Sears, G. W., Jr. "Determination of specific surface area of colloidal silica by titration with sodium hydroxide." Analytical Chemistry, 28(12):1981-1983, 1956.

Singer, P. C. and Stumm, W. "The solubility of ferrous iron in carbonate-bearing waters." Journal of the American Water Works Association, 62:198-202, 1970.

Standard Methods for the Examination of Water and Wastewater. 16th ed. Greenberg, A. E., Trussel, R. R., Clesceri, L. S., and Franson, M. A. H. eds. American Public Health Association, Washington, D. C., 1985.

Stokes, A. R. and Wilson, A. J. C. "A method of calculating the integral breadths of Debye-Scherrer lines." Proceedings of the Cambridge Philosophical Society, 38:313-322, 1942.

Stumm, W. and Lee, G. F. "Oxygenation of ferrous iron." Industrial and Engineering Chemistry, 53(2):143-146, 1961.

Stumm, W. and Morgan, J. J. Aquatic Chemistry. 2nd edition. Wiley-Interscience, New York, 1970.

Stumm, W. and Singer, P. C. Discussion of "Precipitation of iron in aerated ground waters" by Ghosh, M. M., O'Connor, J. T., and Engelbrecht, R. S. Journal of the Sanitary Engineering Division, Proceedings of the American Society of Civil Engineers, 92(SA5):120-124, 1966.

Sung, W. Discussion of "Identity and character of iron precipitates" by Robinson, R. B., Demirel, T., and Baumann, E. R. Journal of the Environmental Engineering Division, Proceedings of the American Society of Civil Engineer, 109(EE1):269-274, 1983.

Sung, W. Catalytic Effect of the γ-FeOOH Surface on the Oxygenation Removal Kinetics of Fe(II) and Mn(II). Doctoral dissertation, California Institute of Technology, Pasadena, California, 1981.

Sung, W. and Forbes, E. J. "Some considerations on iron removal." Journal of the Environmental Engineering Division, American Society of Civil Engineers, 110(EE6):1048-1061, 1984.

Sung, W. and Morgan, J. J. "Kinetics and product of ferrous iron oxygenation in aqueous systems." Environmental Science & Technology, 14(5):561-568, 1980.

Takai, T. "Studies on the mechanism of catalytic deferrization(I)." Journal of Japanese Water Works Association, 465:27-40, 1973a.

Takai, T. "Studies on the mechanism of catalytic deferrization(II)." Journal of Japanese Water Works Association, 466:22-33, 1973b.

Tamura, H., Goto, K., and Nagayama, M. "Effect of anions on the oxygenation of ferrous ion in neutral solutions." Journal of Inorganic and Nuclear Chemistry, 38:113-117, 1976a.

Tamura, H., Goto, K., and Nagayama, M. "The effect of ferric hydroxide on the oxygenation of ferrous ions in neutral solutions." Corrosion Science, 16:197-207, 1976b.

Tamura, H., Goto, K., Yotsuyanagi, T., and Nagayama, M. "Spectrophotometric determination of iron(II) with 1,10-phenanthroline in the presence of large amount of iron(III)." Talanta, 21:314-318, 1974.

Taylor, R. M. "Influence of chloride on the formation of iron oxides from Fe(II)chloride. II. Effect of [Cl] on the formation of lepidocrocite and its crystallinity." Clays and Clay Minerals, 32:175-180, 1984.

Thornber, M. R. and Nickel, E. H. "Supergene alteration of sulphides-III. The composition of associated carbonates." Chemical Geology, 17:45-72, 1976.

Wajon, J. E., Ho, G., and Murphy, P. J. "Rate of precipitation of ferrous iron and formation of mixed iron-calcium carbonates by naturally occurring carbonate materials." Water Research, 19(7):831-837, 1985.

Weart, J. G. and Margrave, G. E. "Oxidation-reduction potential Measurements applied to iron removal." Journal of American Water Works Association, 49:1223-1233, 1957.

Weiser, H. B. Inorganic Colloid Chemistry; Vol. II, The Hydrous Oxides and Oxyhydroxides. John Wiley and Sons, Inc., New York, NY, 1935.

Weiss, J. "Elektronenübergangsprozesse im mechanismus von oxydations- und reduktionsreaktionen in lösungen." Naturwissenschaften, 23:64-69, 1935.

X-ray Powder Data File. American Society for Testing and Materials, Philadelphia, PA, 1960.

Zasoski, R. J. and Buru, R. G. "A technique for studying the kinetics of adsorption in suspensions." Soil Science Society of American Journal, 42:372-374, 1978.

Zsigmondy, R. and Spear, E. B. Chemistry of Colloids. John Wiley and Sons, Inc., New York, New York, 1917.

ACKNOWLEDGEMENTS

The author gratefully expresses his thanks to the Department of Civil Engineering and the Engineering Research Institute of Iowa State University for their financial support during this research. The author would like to expresses his appreciation to Dr. E. R. Baumann for his valuable guidance and patience during this study. Thanks also go to Dr. C. S. Oulman for his valuable advisements, suggestions and encouragement during hard times. The author express his gratitude to Dr. T. Demirel, Dr. J. L. Cleasby, and Dr. R. C. Seagrave for encouragement and support throughout this study. The author also expresses his thanks to all his colleagues for their friendship and help during the whole school years.

The author wants to express a very special thanks to his son and daughter, Soohoon and Yeon, for their support and patience. Finally, this work is dedicated to Soonhee Choi, wife, mother, and patient supporter throughout and Jumjo Ha, mother in law, whose financial and moral support made my study abroad possible.

APPENDIX A

ALKALINITY AND BUFFER INTENSITY

Buffer intensity values of water is calculated using the following relationship:

$$\beta = 2.3\{[H^+]+[OH^-]+C_T[\alpha_1(\alpha_o+\alpha_2)+4\alpha_2\alpha_o)\} \qquad (A-1)$$

where β = buffer intensity, eq/pH

$C_T = [H_2CO_3] + [HCO_3^-] + [CO_3^{--}]$, mol/l

$\alpha_o = [H_2CO_3]/C_T$

$\alpha_1 = [HCO_3^-]/C_T$

$\alpha_2 = [CO_3^{--}]/C_T$

Alkalinity value is calculated by the following equation:

$$\text{Alk.} = [HCO_3^-] + 2[CO_3^{--}] + [OH^-] - [H^+]$$

$$= C_T(\alpha_1+2\alpha_2) + [OH^-] - [H^+] \qquad (A-2)$$

where Alk.= alkalinity of water

When pH of solution is around 6 or 7 and the buffer intensity is above 4.0×10^{-3} eq/pH, the values of $[H^+]$, $[OH^-]$ and α_2 are negligibly small in the presence of C_T, α_o, and α_1. Therefore, the equations (A-1) and (A-2) can be simplified:

$$\beta = 2.3*C_T*(\alpha_1*\alpha_o) \qquad (A-3)$$

$$\text{Alk.} = \alpha_1*C_T \qquad (A-4)$$

Furthermore, the equations (A-3) and (A-4) can be combined to (A-5) to relate buffer intensity with alkalinity.

$$\beta = 2.3*\alpha_o*\text{Alk.} \qquad (A-5)$$

$K_1 = [H^+][HCO_3^-]/[H_2CO_3]$

$= 10^{-6.42}$ at 15 °C (Stumm and Morgan, 1970) (A-6)

From the (A-6), $[HCO_3^-]=3.801*[H_2CO_3]$ at pH 7. Therefore, by ignoring the value of $[CO_3^{--}]$, $\alpha_o=[H_2CO_3]/([H_2CO_3]+[HCO_3^-]+[CO_3^{--}])$ is 0.208. By substituting 0.208 for α_o in the equation (A-5), alkalinity can be obtained for the buffer intensity of $4.0x10^{-3}$ eq/pH, which is 8.35 m.eq/l or 417 mg/l as $CaCO_3$.

At pH 6, based on the (A-6), $[HCO_3^-]=0.38[H_2CO_3]$. Therefore, $\alpha_o=0.7246$ and $\alpha_1=0.2754$ by ignoring $[CO_3^{--}]$. The alkalinity can be calculated from (A-5) for the water of $4x10^{-3}$ eq/pH buffer intensity, which turned out to be 2.4 m.eq/l or 120 mg/l as $CaCO_3$. By substituting 0.7246 and 0.2754 for α_o and α_1 in the (A-3), the C_T is 0.008715 mol/l for $\beta=4.0x10^{-3}$ eq/pH. Thus, $[H_2CO_3]$, $(C_T*\alpha_o)$, is calculated to be 0.0063 mol/l. To maintain that high $[H_2CO_3]$, the required partial pressure of carbon dioxide is 0.147 atm at 15 °C. The calculation for partial pressure is based on the Henry's law.

$P_A = H_A*X_A$

where P_A = partial pressure of solute A, atm

H_A = Henry's constant for solute A, atm

X_A = molor fraction of solute A

At 15 °C, H_{CO2} = 1296.4 atm (kavanaugh and Trussell, 1980) and X_A = 0.0063 (mol H_2CO_3/l)/55.6 (mol H_2O/l)$=1.133x10^{-4}$.

Therefore, $P_A = 1296.4 \times 1.133 \times 10^{-4} = 0.147$ atm.

APPENDIX B

RATE EQUATION OF HOMOGENEOUS IRON OXIDATION

The rate equation of homogeneous iron oxidation based on the mechanism by Goto et al. (1970) was reported:

$$-d[Fe(II)]/dt = 4k^*K_{(FeOH+)}{}^*K_{(O2OH-)} *\{[Fe(II)]/(1+K_{(FeOH+)}[OH^-]\} *\{[O_2]_{total}/(1+K_{(O2OH-)}[OH^-]\} *[OH^-]^2 \quad (B\text{-}1)$$

where $K_{(FeOH+)}$ = equilibrium constant, $10^{4.5}$ M^{-1}

$K_{(O2OH-)}$ = equilibrium constant whose value is supposed by Goto et al. to lie between $10^{-2.5}$ and $10^{-0.3}$ M^{-1}

The equation (B-1) was simplified by assuming that both "$K_{(FeOH+)}[OH^-]$" and "$K_{(O2OH-)}[OH^-]$" values are much less than 1 at pH's below 7.5. Then, the (B-1) is reduced to a simple form:

$$-d[Fe(II)]/dt = \{4k^*K_{(FeOH+)}{}^*K_{(O2OH-)}\} *Fe(II)]*[O_2]_{total}*[OH^-]^2 \quad (B\text{-}2)$$

The (B-2) is the general rate law of homogeneous iron oxidation where overall rate constant, k_o, was replaced by the term "$\{4k^*K_{(FeOH+)}{}^*K_{(O2OH-)}\}$".

However, the concentration of $[OH^-]$ is $10^{-4.5}$ M at pH 9.5 and 25 ^oC, which, in turn, make the term "$K_{(FeOH+)}[OH^-]$" equal to 1. Then, the rate equation (B-1) becomes:

$$-d[Fe(II)]/dt=\{4k*K_{(FeOH+)}*K_{(O2OH-)}\}/(1+K_{(FeOH+)}[OH^-])$$
$$*Fe(II)]*[O_2]_{total}*[OH^-]^2$$
$$=\{4k*K_{(FeOH+)}*K_{(O2OH-)}\}/(1+1)$$
$$*Fe(II)]*[O_2]_{total}*[OH^-]^2 \qquad (B-3)$$

As shown, the overall rate constant in the (B-3) is half of that in the (B-2).

At pH 11.5 and 25 ^oC, the concentration of $[OH^-]$ becomes $10^{-2.5}$ M making the term "$K_{(FeOH+)}[OH^-]$" much bigger than 1. Therefore, the equation (B-1) becomes:

$$-d[Fe(II)]/dt =\{4k*K_{(FeOH+)}*K_{(O2OH-)}\}/(K_{(FeOH+)}[OH^-])$$
$$*Fe(II)]*[O_2]_{total}*[OH^-]^2$$
$$=\{4k*K_{(O2OH-)}\}$$
$$*Fe(II)]*[O_2]_{total}*[OH^-] \qquad (B-4)$$

The equation (B-4) shows that the oxidation rate is proportional to the first order of concentration of hydroxide.

APPENDIX C

RELATIVE CRYSTAL SIZE OF THREE LEPIDOCROCITES

The Scherrer Equation

$$L = K \lambda/\beta \cos\theta$$

where

L = mean dimension normal to the diffracting plane (Angstroms)

K = constant

λ = wavelength of the X-ray (Angstroms)

β = diffraction line broadening at half maximum intensity (radian)

θ = diffracting angle respect to the plane (degrees)

Crystal sizes normal to the (020) plane was chosen.

Numerical value of each parameter

K = 1, based on Klug and Alexander (1954)

λ = 1.54050 for copper $K\alpha_1$ line

θ : 2θ of (020) plane was 14.069 degrees
Therefore, $\theta = 14.069/2 = 7.035$ degrees

β = FWHM of the (020) plane - Equipment line broadening

The line broadening of mica was used to represent the equipment line broadening and was 0.194 degrees at 2θ of 8.8 degrees . The removal of the copper $K\alpha_2$ was already reflected in FWHMs in the Tables.

Therefore, $\beta_{(\text{lepidocrocite-3M})} = 0.543-0.194 = 0.349$
$\beta_{(\text{lepidocrocite-B\&A})} = 0.756-0.194 = 0.562$

$$\beta_{(\text{lepidocrocite-K})} = 1.063-0.194 = 0.869$$

One degree is $(\pi/180)$ radian.

Therefore, $\beta_{(\text{lepidocrocite-3M})} = 0.349*(\pi/180)$ radian
$\beta_{(\text{lepidocrocite-B\&A})} = 0.562*(\pi/180)$ radian
$\beta_{(\text{lepidocrocite-K})} = 0.869*(\pi/180)$ radian

By substituting numerical values for parameters in the Scherrer Equation, the mean crystal size of lepidocrocite was obtained:

$$L_{(\text{lepidocrocite-3M})} = 1*1.54050/\{0.349*(\pi/180)*\cos(7.035)\}$$
$$= 254.8 \text{ Angstroms}$$

$$L_{(\text{lepidocrocite-B\&A})} = 1*1.54050/\{0.562*(\pi/180)*\cos(7.035)\}$$
$$= 158.24 \text{ Angstroms}$$

$$L_{(\text{lepidocrocite-K})} = 1*1.54050/\{0.869*(\pi/180)*\cos(7.035)\}$$
$$= 102.34 \text{ Angstroms}$$

APPENDIX D

THE RATIO OF THE HETEROGENEOUS OXIDATION RATE TO THE HOMOGENEOUS OXIDATION RATE WITH SEEDED LEPIDOCROCITE

Tamura et al. (1976b) reported the rate equation of oxidation:

$$-d[Fe(II)]/dt = k_o[O_2][OH^-]^2[Fe(II)] + k_{s,o}[O_2]\{K[Fe(III)]/[H^+]\}[Fe(II)] \quad (D\text{-}1)$$

where

k_o = real rate constant for homogeneous oxidation, 2.3×10^{14} $M^{-3}s^{-1}$ at 25 °C

$k_{s,o}$ = real rate constant for heterogeneous oxidation, 73 $M^{-1}s^{-1}$

K = equilibrium constant for the adsorption of Fe(II) on Fe(III) hydroxide, $10^{-9.6}$ mol/mg Fe(III)

[Fe(II)] = concentration of ferrous iron in bulk liquid phase at equilibrium with ferric hydroxide surface, mg/l

[Fe(III)] = concentration of ferric hydroxide, mg/l

$[H^+]$ = concentration of hydrogen ion, mol/l

In the equation, $k_o[O_2][OH^-]^2[Fe(II)]$ represents the homogeneous oxidation rate and $k_{s,o}[O_2]\{K[Fe(III)]/[H^+]\}$ [Fe(II)] reflected the heterogeneous oxidation rate. Therefore, the ratio of hetero to homegeneous oxidation was as follows:

$$\{-d[Fe(II)]/dt\}_{hetero}/\{-d[Fe(II)]/dt\}_{homo}$$

$$=[k_{s,o}[O_2]\{K[Fe(III)]/[H^+]\}[Fe(II)]]/\{k_o[O_2][OH^-]^2[Fe(II)]\}$$

$$=[k_{s,o}\{K[Fe(III)]/[H^+]\}]/\{k_o[OH^-]^2\}$$

$$=[k_{s,o}\ K\ [Fe(III)]]/\{k_o[OH^-]^2[H^+]\} \qquad (D\text{-}2)$$

At 25 ^oC, $[H^+][OH^-]=10^{-14}$ M

By substituting numerical values for the parameters into (D-2), the ratio was calculated:

$$\{-d[Fe(II)]/dt\}_{hetero}/\{-d[Fe(II)]/dt\}_{homo}$$

$$=73*10^{-9.6}*[Fe(III)]/((2.3*10^{14})*10^{-14}*[H^+])$$

$$=31.74*10^{-9.6}[Fe(III)]/[OH^-] \qquad (D\text{-}3)$$

Therefore, the ratio of heterogeneous to homogeneous oxidation rate is proportional to the concentration of ferric iron and is inversely proportional to the concentration of hydroxide ion. The more acidic, the higher the ratio.

At 25 ^oC, pH 6, and 100 mg/l of ferric iron concentration, the ratio was 79.7 based on the (D-3).